Synthesis and Characterization of Graphene oxide by a Novel Approach (Volumetric Titration Method) and Fabrication of GO/rGO-PDMS Nanocomposite for Flexible Sensors

> Submitted By

Gunda Rajitha Reg. No. 10ENPT06

in partial fulfillment of the requirement for the award of the degree of A dissertation submitted to the University of Hyderabad in partial fulfillment of the requirements for the awardof degree

Doctor of Philosophy in Nano Science and Technology

Under supervision of Dr. Raj Kishora Dash



School of Engineering Sciences & Technology University of Hyderabad Prof. C. R. Rao Road, Hyderabad – 500 046



#### **CERTIFICATE**

This is to certify that the thesis entitled "Synthesis and Characterization of Graphene oxide by a Novel Approach (Volumetric Titration Method) and Fabrication of GO/rGO-PDMS nanocomposite for Flexible Sensors" Submitted by Gunda Rajitha bearing registration number 10ENPT06 in partial fulfillment of the requirements for award of Doctor of Philosophy in the School of Engineering Sciences and Technology is a bonafide work carried out by her under my supervision and guidance.

This thesis is free from plagiarism and has not been submitted previously in part or in full to this or any other University or Institution for award of any degree or diploma.

Parts of this thesis have been:

A. published in the following publications:

Raiitha Gunda. Buchi Suresh Madireddv and Raj Kishora Dash, Applied Nanoscience (2018). http://doi.org/10.1007/s13204-018-0663-6.

- B. presented in the following conferences:
  - i. G. Rajitha and R.K.Dash, "International Conference on Nanotechnology: Ideas, Innovations and Initiatives 2017 @ IIT-Roorkee, Roorkee, Delhi.
  - ii. G. Rajitha and R.K.Dash, "International Conference on Materials Science and Nanotechnology – 1<sup>st</sup> - 4<sup>th</sup> March, 2016 @ University of Delhi, Delhi, India.
  - iii. ORAL presentation, National Conference on Advances in Materials Processing and Characterization (NCAMPC-2016)- 4<sup>th</sup>-6<sup>th</sup> January 2016 @ NIT Warangal.
  - iv. 4<sup>th</sup> International Conference on Advanced Nanomaterials and Nanotechnology December 8<sup>th</sup> -12<sup>th</sup>, 2015 @ Indian Institute of Technology Guwahati, Assam, India.
  - International Conference on Nanoscience and Engineering Applications 26<sup>th</sup>, 27<sup>th</sup>& 28<sup>th</sup> June 2014 (Best Poster award) @ JNTU Hyderabad, ICONSEA-2014.

Further, the student has passed the following courses towards fulfillment of coursework requirement for Ph.D.

Course Code		Name	Credits	Pass/Fail	
	NT601	Research Methodology	4	Pass	

and was exempted from doing coursework (recommended by Doctoral Committee) on the basis of the following courses passed during her M.Tech. program (in Int. M.Tech./Ph.D. program) and the M.Tech.degree was awarded:

Course Code	Name	Credits	Pass/Fail
NT401	Phase Transformation and Thermodynamics	4	Pass
NT402	Characterization of Materials	4	Pass
NT403	Seminar	2	Pass
NT404	Design and Selection of Engineering Materials	4	Pass
NT405	Nanomaterials Synthesis and Characterization Laboratory	4	Pass
NT406	Concepts of Nano Science and Technology	4	Pass
NT407	Synthesis and Applications of Nanomaterials	4	Pass
NT451	Nano Biotechnology	4	Pass
NT452	Mechanical Behavior of Nanomaterials	4	Pass
NT453	Modeling and Simulation	4	Pass
NT454	Powder Metallurgy and Ceramics	4	Pass
NT455	Surface Engineering and Advanced Nanofabrication Technologies	4	Pass
NT456	MEMS and NEMS	2	Pass
NT457	Laboratory	4	Pass
NT458	Seminar	2	Pass
NT601	Research Methodology	4	Pass

Dr.RajKishora dash

Supervisor

Prof. M.Ghanashyam Krishna

Dean, SEST, UOH.

## **Declaration**

I hereby declare that the work reported in this Ph.D. dissertation entitled, "Synthesis and Characterization of Graphene oxide by a Novel Approach (Volumetric Titration Method) and Fabrication of GO/rGO-PDMS Nanocomposite for Flexible Sensors" submitted to University of Hyderabad for the award of Doctor of Philosophy in Nano Science and Technology is original and was carried out by me during my tenure as a Ph.D. scholar under the supervision of Dr. Raj Kishora Dash, Assistant Professor at the University of Hyderabad, INDIA. This dissertation has not formed the basis for the award of any degree, diploma, associateship, membership or similar title of any university or institution. Finally, plagiarism of this dissertation has been checked and satisfied the requirements.

Gunda Rajitha

SCHOOL OF ENGINEERING SCIENCES & TECHNOLOGY,

University of Hyderabad,

Hyderabad-500046,

INDIA.

Place: HYDERABAD

Date:

## Acknowledgement

I feel privileged to place before you my research work entitled "Synthesis and Charcterization of Graphene oxide by Volumetric Method and Fabrication of GO/rGO-PDMS Nanocomposite for Flexible Sensors". For the overall completion of this research work I owe its success to numerous diligent personalities.

First and foremost, I wish to place my sincere gratitude to my young, dynamic and inspiring supervisor Dr. Raj Kishora Dash, Assistant Professor, School of Engineering Sciences and Technology, who has provided considerable wealth of resources, opportunities and guidance during my study of research experimental work. His support has been an essential contributing factor towards the completion of this manuscript.

My sincere thanks to my committee members Prof. Ghanashyam Krishna, Dean, School of Engineering Sciences and Technology, for their kind co-operation and guiding spirit I completion of this research work.

I would also like to take this opportunity to thank University Grants Commission, New Delhi, India for the financial support received through University (BBL) Fellowship.

I also thank all the lab assistants for XRD, TEM, FESEM, Raman spectroscopy and UV-visible spectroscopy for their friendship and technical support received.

I would also use this opportunity to convey my thanks to all my group members and fellow students for their co-operation and help received.

Finally, I extend my deep and sense of gratitude and thanks to all the teaching and non-teaching staff for their guidance and kind co-operation in completion of this research work. My stay at University of Hyderabad has been made so unforgettable and enjoyable either directly or indirectly by all the people when I have spent the time with them.

Last but not the least, I would like to thank my parents and family (husband & Kids) for providing an abundance of love, encouragement and support.

#### List of publications and conferences attended

#### **Publications**

- ✓ Rajitha Gunda, Buchi Suresh Madireddy andRaj KishoraDash, Applied Nanoscience (2018). <a href="https://doi.org/10.1007/s13204-018-0663-6">https://doi.org/10.1007/s13204-018-0663-6</a>
- ✓ Rajitha Gunda andRaj KishoraDash, Optically Transparent and High Dielectric Constant Reduced Graphene Oxide (RGO)-PDMS based Flexible Composite for Wearable and Flexible Sensors Journal: Sensors & Actuators: A. Physical (under review)
- ✓ BikashBorha, Rajitha Gunda and Raj KishoraDash, Correlation Between the Thickness and Properties of the Ethanol Treated GO-PDMS based Composite Materials, Journal of Materials Science: Materials in Electronics (submitted and under review).
- ✓ Rajitha Gunda andRaj KishoraDash, Investigation of strain sensing of the fabricated ethanol-treated RGO-PDMS composite for sensors", (Under preparation to submit).

#### Conferences

- ➤ G. Rajitha and R.K.Dash, "International Conference on Nanotechnology: Ideas, Innovations and Initiatives 2017 @ IIT-Roorkee, Roorkee, Delhi.
- G. Rajitha and R.K.Dash, "International Conference on Materials Science and Nanotechnology 1<sup>st</sup> 4<sup>th</sup> March, 2016 @ University of Delhi, Delhi, India.
- ➤ ORAL presentation, National Conference on Advances in Materials Processing and Characterization (NCAMPC-2016)- 4<sup>th</sup>-6<sup>th</sup> January 2016 @ NIT Warangal.
- ➤ 4<sup>th</sup> International Conference on Advanced Nanomaterials and Nanotechnology December 8<sup>th</sup> -12<sup>th</sup>, 2015 @ Indian Institute of Technology Guwahati, Assam, India.
- ➤ International Conference on Nanoscience and Engineering Applications 26<sup>th</sup>-28<sup>th</sup>, June 2014 (Best Poster award) @ JNTU Hyderabad, ICONSEA-2014.

#### **Abstract**

Recently, composite materials are emerging as the new class of materials, which properties can be tuned as per the applications, hence, it has multiple functionalities. Therefore, as per the future demands for the new technologies or devices such as MEMS, Sensors, Micro-fluidic devices, bio-sensors, bio-medical devices and so on, composites and nanocomposites materials may be a potential material, hence, a lot of progress has been going on globally. Out of all these composite materials, polymer-based composites have potential to be used in wearable, flexible sensors and electronic devices because of flexibility, durability and good mechanical properties.

Polymer composites, those are the materials which comprise of two or more different phases of the polymer at least as one of its phase or host material. In order to improve the properties of the host materials, filler materials such as CNTs, nanoparticles, nanorods, nanowire, and graphene are incorporated into the host materials. Recently, graphene, a 2D nanomaterial is known to be the excellent filler material due to their excellent physical, electrical, mechanical and optical properties like very high surface area, high electrical conductivity and thermal conductivity, high strength etc. Therefore, Graphene-polymer composites would be more ideal for making flexible and wearable electronics, MEMS, sensors and biomedical devices.

Graphene oxide(GO) becomes a promising material for several applications and also a source material to produce the reduced Graphene Oxide (rGO), furthermore, the chemical synthesis process is very simple, easy and economical. Furthermore, due to the presence of the different oxygenated functional groups, this material can be utilized for the development of the nanocomposites and other hybrid materials system. In this thesis

work, the first part of the thesis work mainly focus on development of a simple, economical and eco-friendly synthesis of the GO, for this purpose, GO has been prepared by using the different chemical approaches such as Hummers method, modified Hummers method and also by using a novel improved Hummers method which we called as "Volumetric Titration Method". In our chemical approach process to synthesize the GO, we have not employed any toxic chemicals such as NaNO<sub>2</sub> or NaNO<sub>3</sub> and not attained the zero temperature. Thus our process is more cost-effective and eco-friendly.

We have synthesized GO by controlled addition of KMnO<sub>4</sub> by the volumetric method and all the samples were analyzed by XRD, FT-IR, Raman and TEM analysis. Experimental results indicated that 2-3layers of completely oxidized GO were successfully prepared. Furthermore, all the as-obtained GO samples were reduced by using hydrazine hydrate and sodium borohydride. All the analysis results from XRD, FT-IR, Raman, FESEM and TEM confirmed that all the GO's were successfully reduced to reduced graphene oxide (rGO). These samples were applied as nanofiller materials for GO-PDMS and rGO-PDMS nanocomposites.

The second part of the thesis, we have studied the dispersion behavior and stability of the GO synthesized by our approach to fabricate the PDMS based GO/rGO nanocomposites. The PDMS based nanocomposites were prepared by considering three different thicknesses i.e., 500um, 1250um and 2000um by using the mold-casting technique. Two chemical approaches are adopted to investigate the uniformly distributed GO or rGO in the PDMS matrix; firstly, as synthesized RGO was directly employed as filler material and secondly, chemically 1,4,D treated RGO was applied as filler

materials. The structural analysis was carried out by using XRD analysis and the functionality, bonding behavior and molecular structure were studied by using the FT-IR.

From our experimental results, we have concluded that by treating RGO with 1,4,D, more uniform distribution of the RGO in PDMS matrix could be obtained, as a result, 1,4,D treated RGO-PDMS nanocomposite showed almost 88% transparency as compared to the RGO-PDMS nanocomposite and host PDMS. Electrical testing was carried out by four-point probe and results showed that all the samples are insulating in nature due to the lower wt% loading of the filer material. Dielectric measurements were carried out by impedance analyzer and experimental results indicated that the dielectric constant of the 1,4,D chemically treated RGO-PDMS showed higher dielectric constant, which is 16 times more than host material and 1.7 times higher as compared to the RGO-PDMS nanocomposite. Moreover, the thermal stability of the nanocomposite materials is seen to be enhanced by by addition of 1,4,D treated RGO as filler material, which was confirmedby the thermal analysis(TGA) results. The possible mechanisms are also discussed in this thesis work.

Though, electrical conductivity the fabricated 1,4-D-rGO-PDMS nanocomposite is very low, an improvement in the order of 10<sup>5</sup> as compared to host PDMS is achieved. Therefore, our experimental results indicated that 1-4-D chemical treatment solvent dispersion process improves the uniform distribution of the filler-RGO material in the silicon elastomer and also enhances the cross-linking bond between the filler and PDMS matrix. As a result, the thermal stability and dielectric properties of the nanocomposites can be enhanced to higher order even if at very low vol.% of filler when compared to that of host PDMS material. In addition to this, fabricated nanocomposites showed 82%

optical transparency. We believe that our this low cost and facile approach to fabricate these optoelectric nanocomposites can be useful for potential applications in flexible and wearable electronic devices, optical MEMS, sensors, energy storage devices and biomedical devices.

Therefore, we believe that this thesis research work outcomes can be helpful to synthesize smart composite materials having multi-functionalities for MEMS, sensors and biomedical applications. However, more challenges are still required to overcome for utilization of these polymer composites for MEMS, sensors, and electronic applications such as more improvement in electrical properties, flexibility testing, mechanical properties testing and different chemical approaches for the fabrication of the nanocomposites.

## **Thesis Contents**

#### **Chapter-1 Introduction**

- 1.1 Introduction
- 1.2 Overview on Graphene based polymer nanocomposites
- 1.3 Literature review on polymer based nanocomposites
- 1.4 Current Challenges and Issues
- 1.5 Motivation and Objective of the Thesis
- 1.6 Thesis Outline

## Chapter-2 Synthesis of Graphene oxide (GO) by Modified Hummer's method without NaNO2 or NaNO3 (volumetric method)

- 2.1 Introduction
- 2.2 Synthesis of GO by Conventional Hummer's Method
- 2.3 Synthesis of GO by Modified Hummer's Method (MHM)
- 2.4 Synthesis of GO by Volumetric Titration- Modified Hammer's Method (VT-MHM)
- 2.5 Synthesis of GO by Volumetric Titration-MHM with the presence of NaNO<sub>2</sub>
- 2.6 Conclusions

## **Chapter-3 Synthesis of Reduced Graphene oxide**

- 3.1 Introduction
- 3.2 Synthesis of Reduced Graphene Oxide by different Reducing Agents
- 3.2.1. Experimental procedure of reduction process by using Sodium borohydride (NaBH<sub>4</sub>)
- 3.2.2. Experimental procedure of reduction process by using Hydrazinemonohydrate (NH<sub>2</sub>-NH<sub>2</sub>.H<sub>2</sub>O)
- 3.3 Characterization of rGO synthesized from Hummer's method by using NaBH<sub>4</sub>
- 3.4 Reduction of rGO obtained from GO synthesized by Modified Hummer's method
- 3.5 Reduction of GO synthesized by Volumetric Titration-Modified Hummer's method using Hydrazine monohydrate
- 3.6 Conclusions

### Chapter-4Fabrication of PDMS and PDMS-rGO Nanocomposites

- 4.1. Introduction
- 4.2. Fabrication of Flexible PDMS material
- 4.3. Characterization of flexible PDMS substrates
- 4.4. Thickness dependent properties of PDMS-rGO substrates
- 4.5. Fabrication of PDMS-rGO Nanocomposites (without Chemical treatment)
- 4.6. Thickness dependent properties of PDMS-rGO nanocomposite
- 4.7. Conclusions

# Chapter-5Fabrication of Chemically treated PDMS-1,4-D rGONanocomposites

- 5.1. Introduction
- 5.2. Study the dispersion behavior of chemically treated rGO in different solvent system
- 5.3. Fabrication of 1,4-Dioxane chemically treated PDMS-rGO based Nanocomposites
- 5.4. Thickness dependent properties of PDMS-1,4-Dioxane treated rGO nanocomposite
- 5.5. Conclusion

## Chapter-6Comparative study of PDMS-rGO based Nanocomposites (without and with chemical treatment using 1,4-Dioxane)

- 6.1. Introduction
- 6.2. Characterization of rGO-PDMS composite and 1,4-D rGO-PDMS composites
- 6.3. Conclusion

## **Chapter-7Summary and Conclusions**

**Future scope** 

References

#### **ANNEXURE-I**

#### **List of Tables**

Table: 2.2.2. Synthesis of GO preparation by Conventional Hammer's Method

Table: 2.3.1 Synthesis of GO (Vaccum) by Modified Hammer's Method

Table 2.4.1 List of GO synthesis by Volumetric Titration-MHM

Table: 3.3.1. Reduction of Graphene oxide by sodium borohydride (NaBH<sub>4</sub>)

Table: 3.3.2. Reduction of Graphene oxide by Hydrazine monohydrate (NH<sub>2</sub>-NH<sub>2</sub>.H<sub>2</sub>O)

Table: 4.2.1 List of pure PDMS nanocomposite samples of different thickness

Table 4.4.1 List of PDMS-rGO (0.23wt%) nanocomposite samples prepared without chemical treatment.

Table 4.5.1 List of PDMS-rGO (0.23wt%) nanocomposite samples prepared without chemical treatment.

#### **ANNEXURE-II**

#### **List of Figures**

- Fig. 1.1 (Left) Annual number of published literature articles related to carbon nanomaterials from 2004 to 2015. (Right) Annual number of published literature articles related to 'graphene' and 'graphene' with 'polymer' 2016
- Fig. 1.2 Different allotropes of carbon: (a) graphite, (b) graphene, (c)carbon nanotube, (d) C60, (e) C70, (f) C540, (g) amorphous carbon, (h) lonsdaleite, and (i) diamond
- Fig. 1.3 Characterization of graphene samples produced by using melamine as exfoliating agent by using different techniques such as XRD, Raman and Transmission Electron Microscopy
- Fig. 1.4 (a)From left to right: pristine graphite and exfoliated graphene as obtained by tip sonication for 5, 15, 30 and 60 minutes, in o-DCB (b) Photograph of the ½-inch fused silica windows with GO and rGO layers
- Fig.1.5Raman spectrum of graphene. Inset (a): TEM image of graphene (wrinkles in graphene sheets have been marked with arrows). b TEM image of CNTS. Inset (b) evidence of percolation network formation in CNT
- Fig. 1.6 Schematic representation of Ultra capacitor
- Fig. 1.7 represents synthesis of GO by modified Hummer's method and kinetics study
- Fig. 1.8 FT-IR Spectrum of (a) PANI, (b) CuS, (c) PANI/CuS and (d) ZnO/PANI-CuS thin film
- Fig. 1.9 Electrical conductivity of natural rubber (NR) composites as a function of graphene (GE) content
- Fig. 1.10 Overview of silicon applications as reported from literature.
- Fig. 1.11 Photograph of graphene transferred to different flexible substrates. (A) Monolayer graphene transferred to Teflon tape. (B) Multilayer (three layers) graphene on a Teflon filter by transfer three times. (C) Graphene on a CN/CA membrane filter. (D) Multilayer (two layers) graphene on a paraffin film. (E) Graphene on a polycarbonate substrate. (F) Graphene on a PVC substrate. The rulers are scaled in centimeters
- Fig. 1.12 Photographs of graphene on (A) a piece of cloth and (B) regular A4 paper. A drop of PMMA was placed in the center of the cloth, so the edges soaked up more FeCl3

- etchant than the middle, and is therefore darker. In the case of the paper, the entire surface was uniformly coated with PMMA but the graphene offers some protection from the etchant, resulting in more color contrast
- Fig. 1.13 represents the polymer based device applications (a) stretchable 'biostamp' skin sensor and (b) glucose-sensing contact lens
- Fig.1.14 Schematic represents the synthesis of rGO and colloidal dispersion of rGO in different organic solvents
- Fig. 1.15 Schematic represents the dispersion behavior of GO and chemically converted graphene (CCG)
- Fig. 1.16 Schematic represents the dispersion of filler material in the composite matrix
- Fig. 17 Frequency dependence of (a) dielectric constant and (b) loss tangent for PMMA/BaTiO3 nanocomposites
- Fig. 18 Dielectric properties of the composites reported
- Fig. 1.19 Photograph images of normal (A) stretched and (B)bended (C) conductive CNT-graphene-PDMS electrode (D) Microstructure of MWCNT (1D)/Graphene (2D) interconnection in PDMS matrix
- Fig. 1.20 Application in ECG signal (E) Experimental set-up to monitor the ECG signal (F) Photograph of LED operation with a CNT-graphene-PDMS electrode as an interconnection (G) ECG signal measured under the condition of (E)
- Fig. 1.21 Images of graphene EGFETs: (a) 200 mm wafer patterned with 280 transistors
- Fig. 2.2.1 Flow diagram represents the synthesis of GO by Conventional Hammer's Method.
- Fig: 2.2.2 XRD of GO with (a) low KMnO<sub>4</sub> (without vaccum) (b) high KMnO<sub>4</sub> (without vaccum) (c) low KMnO<sub>4</sub> (with vaccum) (d) high KMnO<sub>4</sub> (with vaccum).
- Fig: 2.2.3 FT-IR plots of GO (without vaccum) with low KMnO<sub>4</sub> by conventional Hammer's method.
- Fig: 2.2.4 Raman analysis of GO (a) low KMnO<sub>4</sub> (MH1-01-GO) (b) high KMnO<sub>4</sub> (MH1-02-GO by conventional Hummer's method.
- Fig: 2.2.4 Raman analysis of GO (c) low KMnO<sub>4</sub> (MH1-03-GO) (d) high KMnO<sub>4</sub> (MH1-04-GO) by conventional Hummer's method.

- Fig: 2.2.5 TEM image analysis of GO (a), (b) & (c) low KMnO<sub>4</sub> (without vaccum) and (d), (e), (f) high KMnO<sub>4</sub> (without vaccum) by conventional Hammer's method.
- Fig: 2.2.6 FESEM image analyses of GO (a), (b) & (c) without vacuum by conventional Hammer's method.
- Fig: 2.3.1 Synthesis of GO (Vaccum) by Modified Hammer's Method
- Fig: 2.3.2 XRD analysis of GO with (a) high and (b) low H<sub>2</sub>SO<sub>4</sub> by Modified Hammer's method.
- Fig: 2.3.3 Raman analysis of GO (a) high and (b) low H<sub>2</sub>SO<sub>4</sub> by Modified Hammer's method (MHM).
- Fig: 2.3.4 TEM analysis of GO (a-c) high and (d-f) low H<sub>2</sub>SO<sub>4</sub> by Modified Hammer's method (MHM).
- Fig.2.4.1 Graphical Representation of (a) Volumetric Titration method to synthesize graphene oxide (GO) at room temperature (without any ice-bath or addition of NaNO<sub>3</sub>) (b) schematic for the mechanisms of formation GO by VTM.
- Fig. 2.4.2 XRD analysis of GO synthesis by Volumetric Titration -MHM method (a) MH3-10-GO (b) MH3-11-GO (c) MH3-14-GO (d) MH3-15-GO (e) MH3-16-GO (f) MH3-17-GO.
- Fig. 2.4.3 Raman analysis of GO by Volumetric Titration -MHM method (a) MH3-10-GO (b) MH3-11-GO.
- Fig. 2.4.4 FT-IR analysis of GO by Volumetric Titration -MHM method (a) MH3-10-GO (b) MH3-11-GO (c) MH3-14-GO (d) MH3-15-GO (e) MH3-16-GO (f) MH3-17-GO.
- Fig. 2.4.5 UV-spectroscopy of GO samples aqueous dispersion (a) MH3-10-GO (b) MH3-11-GO (c) MH3-14-GO and (d) MH3-16-GO.
- Fig. 2.4.6 TEM analysis represents MH3-10-rGO-HH (a-c) and (d-f) for MH3-11-rGO-HH samples.
- Fig. 2.5.1 XRD analysis of MH3-10-GO-WN samples with varying oxidation time.
- Fig. 2.5.2 Raman data analysis of MH3-10-GO-WN oxidation time 12Hrs (a) 0.1 NaNO<sub>2</sub>& (b) 0.2NaNO<sub>2</sub>.
- Fig.2.5.3 FT-IR spectral analysis of sample MH3-10-GO-WN with 0.1 and 0.2weight fraction of NaNO<sub>2</sub>.

- Fig. 2.5.4 UV analysis of GO in different solvents (a) MH3-10-GO-WN-EthOH (b) MH3-10-GO-WN-NMP.
- Fig. 2.5.5 TEM analysis of GO with NaNO<sub>2</sub> by using VT-MHM in NMP solvent system.
- Fig. 3.2.1 Flow diagram represents synthesis of RGO by using different reducing agents.
- Fig. 3.3.1 XRD data analysis of RGO under vacuum conditions (a) MH1-03-RGO-NB(V) and (b) MH1-04-RGO-NB(V).
- Fig. 3.3.1 XRD data analysis of RGO under vacuum conditions (a) MH1-03-RGO-NB(V) and (b) MH1-04-RGO-NB(V).
- Fig. 3.3.2 Raman analysis of (a) MH1-01-RGO-NB (b) MH1-02-RGO-NB (c) MH1-03-RGO-NB (V) and (d) MH1-04-RGO-NB (V).
- Fig. 3.3.3 TEM Image analysis of (a) MH1-01-RGO-NB (b) MH1-03-RGO-NB (V) and (c) MH1-04-RGO-NB (V).
- Fig. 3.4.1 XRD data analysis of RGO under vacuum conditions (a) MH1-05-RGO-HH and (b) MH1-06-RGO-HH.
- Fig. 3.4.3 Raman data analysis of (a) MH1-05-RGO-HH (b) MH1-05-RGO-NB (c) MH1-05-RGO-HH and (d) MH1-06-RGO-NB.
- Fig. 3.3.3 TEM Image analysis of (a) MH1-01-RGO-NB (b) MH1-03-RGO-NB (V) and (c) MH1-04-RGO-NB (V).
- Fig. 3.4.1 XRD analysis of rGO (a) MH1-05-RGO-HH and (b) MH1-06-RGO-HH (c) MH1-05-RGO-NB and (d) MH1-06-RGO-NB.
- Fig. 3.4.3 Raman data analysis of (a) MH1-05-RGO-HH (b) MH1-05-RGO-NB (c) MH1-05-RGO-HH and (d) MH1-06-RGO-NB.
- Fig.3.4.4 TEM analysis of (a) MH1-05-RGO-HH and (b) MH1-06-RGO-HH
- Fig.3.4.5 SEM analysis of (a) MH1-05-RGO-HH and (b) MH1-06-RGO-HH
- Fig. 3.5.1 XRD analysis of RGO samples of Volumetric Titration -MHM method (a) MH3-10-RGO-HH (b) MH3-11-RGO-HH (c) MH3-16-RGO-HH (d) MH3-17-RGO-HH.
- Fig. 3.5.2 Raman data of RGO samples by Volumetric Titration-MHM method (a) MH3-10-RGO-HH (b) MH3-11-RGO-HH.
- Fig. 3.5.3 UV-spectroscopy of RGO samples in aqueous dispersion (a) MH3-10-RGO-HH (b) MH3-11-RGO-HH.

- Fig. 4.2.2 Photograph images of pure PDMS based nanocomposites of different thickness of 500μm, 1250μm and 2000μm, and 4000μm respectively.
- Fig. 4.3 Flow diagram used for the fabrication of Flexible PDMS nanocomposites.
- Fig.4.3.1 XRD analysis of pure PDMS samples (a) 500μm (b) 1250 μm and (c) 2000μm.
- Fig.4.3.2 Raman spectroscopy of pure PDMS sample with 2000µm thickness.
- Fig.4.4.1 Comparison plot of *FT-IR* analysis of pure PDMS samples  $500\mu m$ ,  $1250 \mu m$  and  $2000\mu m$ .
- Fig.4.4.2 UV-visible analysis of pure PDMS samples (a)  $500\mu m$  (b)  $1250~\mu m$  and (c)  $2000\mu m$ .
- Fig 4.5.1 Photo image analysis of PDMS-rGO samples with surface cross-sectional area of thickness (a & b) 1250um and (c & d) 2000um.
- Fig.4.5.2.1 XRD analysis of PDMS-rGO nanocomposites with 0.23wt% (a) 500μm (b) 1250 μm and (c) 2000μm.
- Fig.4.5.2.2 XRD analysis of PDMS-rGO nanocomposites with 0.13wt% (a)  $500\mu m$  (b)  $2000\mu m$ .
- Fig.4.5.3 *Raman* analysis of PDMS-rGO nanocomposites with 0.23wt% for (a)  $1250\mu m$  and (b)  $2000 \mu m$  thickness.
- Fig.4.6.1 *FT-IR* analysis with 0.23wt% of varying thickness i.e., 500μm, 1250μm and 2000μm (a) PDMS-rGO nanocomposites and (b) PDMS (pure) & PDMS-rGO nanocomposites samples.
- Fig. 4.6.2 UV-spectroscopy Comparison of Transmittance with different thickness i.e., 500um, 1250um and 2000um (a) PDMS-rGO samples (b) comparison of PDMS (pure) and PDMS-rGO samples.
- Fig. 4.6.3 Comparison plot represents the Dielectric constant of PDMS, PDMS-rGO samples with different thickness i.e., 1250um and 2000um.
- Fig. 5.1.1 Schematic diagram represents the preparation of PDMS-1,4-D- rGO treated nanocomposites.
- Fig. 5.2.1 Schematic represents the dispersion behavior of rGO in different solvent system (a) cyclohexane (b) Diethyl ether (c) NMP (d) 1,4-Dioxane and (e) Ethanol.
- Fig. 5.2.2 UV-spectroscopy represents the dispersion behavior of rGO in solvents (a) 1, 4-Dioxane and (b) NMP.

- Fig. 5.2.3 FT-IR spectroscopy of dispersion rGO NMP and 1,4-Dioxane.
- Fig. 5.3.1 Schematic shows the flow process for the fabrication of PDMS-1,4-D treated rGO based nanocomposites.
- Fig. 5.3.1.1 represents the PDMS-rGO and PDMS-1,4-D-chemically treated rGO nanocomposites
- Fig. 5.3.2 XRD analysis of PDMS-1,4-D-rGO samples with 0.03wt% (a) 500 $\mu$ m (b) 1250  $\mu$ m and (c) 2000 $\mu$ m.
- Fig.5.3.3 Raman analysis comparison plot of PDMS-1,4-D treated rGO nanocomposite with 0.03wt% of 500μm, 1250μm and 2000μm.
- Fig.5.3.4 Scanning electron Microscopy (SEM) analysis (a & b) PDMS and (c) PDMS-rGO nanocomposites.
- Fig.5.4.1 FT-IR analysis comparison of PDMS-1,4-D treated rGO nanocomposite with 0.03wt% of 500μm, 1250μm and 2000μm.
- Fig. 5.4.2 UV-visible spectroscopy of PDMS-1,4-Dioxane chemically treated rGO (a & b) PDMS and (c) PDMS-rGO nanocomposites.
- Fig. 6.2.1 XRD analysis shows comparison plot of PDMS (pure), PDMS-rGO and PDMS-1,4-D-rGO.
- Fig. 6.2.2 Comparison plot of Raman analysis PDMS (pure), PDMS-rGO and PDMS-1,4-D-rGO.
- Fig.6.2.3 FT-IR analysis comparison plot of PDMS (pure), PDMS-rGO and PDMS-1,4-D-rGO.
- Fig. 6.2.4 (a & b) TGA analysis of PDMS-ref, PDMS-rGO and PDMS-1,4-D treated *rGO*nanocomposites.
- Fig. 6.2.5 Comparison plot represents the Dielectric constant of PDMS-rGO and PDMS-1,4-D-rGO samples with a thickness 1250um.
- Fig.6.2.6 IV-analysis shows the (a) PDMS-rGO and (b) PDMS-1,4-Dioxane chemically treated rGO nanocomposites.
- Fig. 6.2.7 Photography images of (a) PDMS-ref (b) PDMS-rGO and (c) PDMS-1,4-D-rGO and (d) UV-visible spectra of PDMS-ref, PDMS-rGO and PDMS-1,4-D-rGOnanocomposites.

## Chapter-1

#### Introduction

#### 1.1 Introduction

Presently, composite materials are emerging as smart materials with multiple functionalities and hence it can be used for several applications such as MEMS, Sensors, Micro-fluidic devices, bio-sensors, bio-medical devices and so on. Out of all these composite materials, polymer-based composites have potential to be used in wearable, flexible sensors and electronic devices because of flexibility, durability and good mechanical properties. Polymer composites, those are the materials which comprise of two or more different phases of the polymer at least as one of its phase or host material. In order to improve the host materials or for the development of new type of materials with multiple functionalities, filler materials are incorporated into the host materials. As compared to the mm or micron filler materials, nanomaterials such as nanoparticles (NP), nanofibres (NF), nanorods (NR), CNT's, graphene etc., are known to be the excellent filler materials due to their distinctive properties like elevated surface area, optical, electrical, mechanical, thermal properties[1]. As compared to their bulk counterpart, hence the host material properties such as electrical, mechanical, optical etc can be finetuned for several applications. For example, the carbon or other polymer-fiber covered, carbon covered rubber, thermoplastic or thermosetting resins, silica or micacoveredresins, polymer blends are the samples of polymer nanocomposites [2-4]. Polymer nanocomposites consisting of nanoparticles (the particle is in the nano dimension range)

are often investigated where the reinforcement of the polymer matrix is achieved [5-7]. Recently, flexible transparent electrodes (FTEs) are showing potential applications in the field of optical and electronics such as flexible solar cells, foldable photo electronics etc.[8, 9].

Moreover, the conductive polymers have got significant noticeas a new class of material contender for electronic and sensors devices as it conduct electricity whereas majority of the polymers are dielectric. Therefore, a wide range of possibilities are existing to apply these materials to develop conductive polymercentered MEMS devices, electrochromic pixel exhibits, biosensors that are made-up with the MEMS fabrication method and the microfabricated touch sensors [10, 11].

Over the past decades, it has been stated that carbonbased materials like carbon black, fullerenes, CNT's and Graphenebased materials (i.e., GO and rGO), are emerging as potential materials and can be used as filler material for the development of nanocomposite materials. The annual publications of articles on GO and rGO based polymer composites are shown in Fig. 1.1. Out of different options for the nanofiller to develop nanocomposite, Graphene, GO and rGO has been very commonly considered in the last decade [12-14]. Therefore, GO and rGO can have the potential to be employed as excellent filler materials for the development of polymer-basednanocomposites.

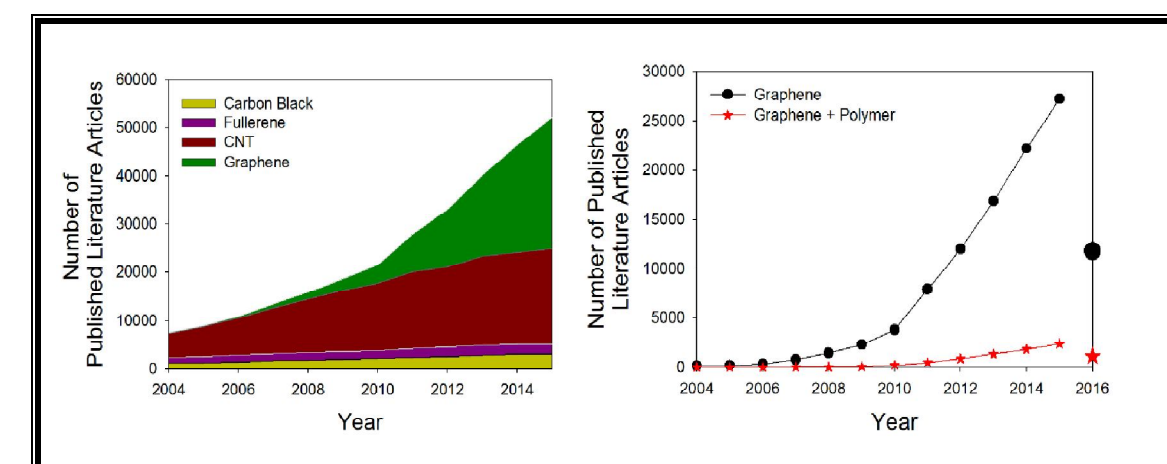


**Fig. 1.1** (Left) Count of published literature articles that are related to carbon nanomaterials during year 2004 - 2015 period. (Right) Count of published literature articles that are related to 'graphene' and 'graphene with polymer' [12].

## 1.2 Overview of Graphene-based Polymer nanocomposites

Graphene is a 2D- hexagonal ring based carbon network that has carbon atoms in a ring construction and it is well-known material for vital applications. Pristinegraphene (a single, virginally sp²-hybridized carbon coating free of heteroatom defects) has been made by numerous methodslike chemical vapor deposition, mechanical exfoliation & cleavage and toughening a single crystal SiC in ultrahigh vacuum [15]. The above procedures have various shortfalls such as with extreme energy necessity, little yield and constraint of the instrument containing growth by chemical vapor deposition (both of agglomerated powders and discrete monolayer onto a substrate), micro mechanical exfoliation of graphite and growth on crystalline silicon carbide[16, 17]Although these methods can fabricate defect-free material with excellent physical properties, present procedures of producing graphene do not return great enough quantities for use as composite fillers [18, 19].

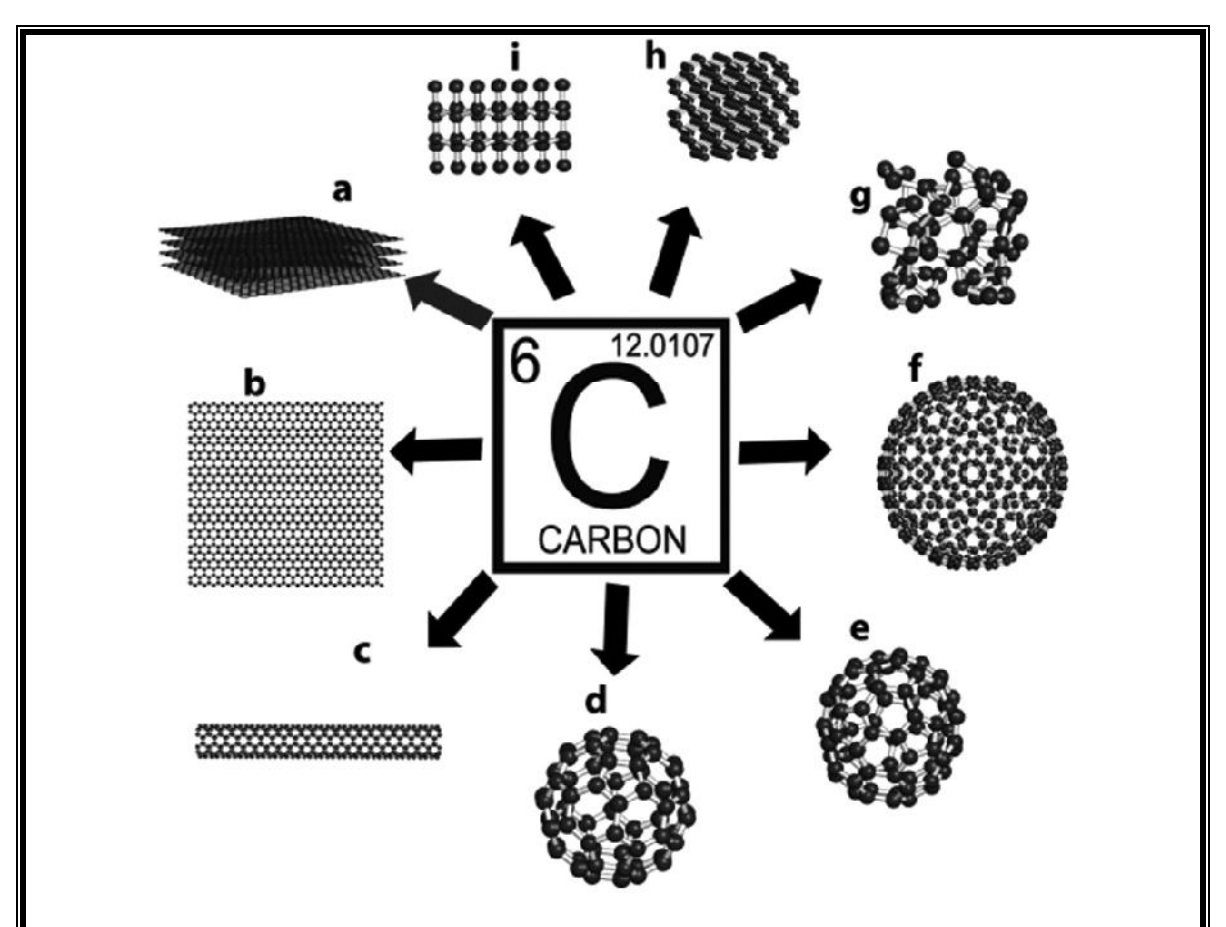


**Fig. 1.2** Various allotropes of carbon: (a) graphite (b) graphene (c) carbon nanotube, (d) C60, (e) C70, (f) C540, (g) amorphous carbon, (h) lonsdaleite and (i) diamond [20].

Out of all those different approaches, the chemical method happens to show a potential route to produce graphene in powder form due to more simple and cost-effective. However, the resultant product might have a large extent of oxygen functional groups and flaws. The chemical process involves three key phases: "graphite oxidation, exfoliation of graphite oxide and reduction of graphene oxide sheets" [21, 22].

**Brodie**has first showed the synthesis of GO in 1859 by accumulating a percentage of potassium chlorate to a slurry of graphite in fuming nitric acid[23]. In 1898, Staudenmaier enhanced this procedure by consuming a combination of strong sulfuric acid and fuming nitric acid tailed by slow adding of chlorate to the reaction

combination[24]. This minor modification in the process has delivered a simple and improved protocol for the fabrication of greatly oxidized GO. In 1958, Hummers stated a different technique for the preparation of grapheme oxide by using KMnO<sub>4</sub> and NaNO<sub>3</sub> in strong H<sub>2</sub>SO<sub>4</sub>. GO made by this process could be used for making big graphitic films[25]. Bonaccorso et al., recently reported that "GO is an atomically thin sheet of carbon covalently bonded with functional groups containing oxygen contain sp<sup>2</sup> and sp<sup>3</sup> hybridized carbon atoms". Generally, it is used like a precursor for the preparation of rGO but lately it has paid notice owing to its optical features. It has been indicated that GO, like rGO, exhibit saturable absorption that makes it fit for passive mode locking of thelaser.Reduced Graphene Oxide (rGO) acquired by means of the usage of benzylamine as lessening and functionalizing mediator, sodium borohydride like decreasing agent. Such grouping of reduction was used in the initial time as reported from the literature [26].

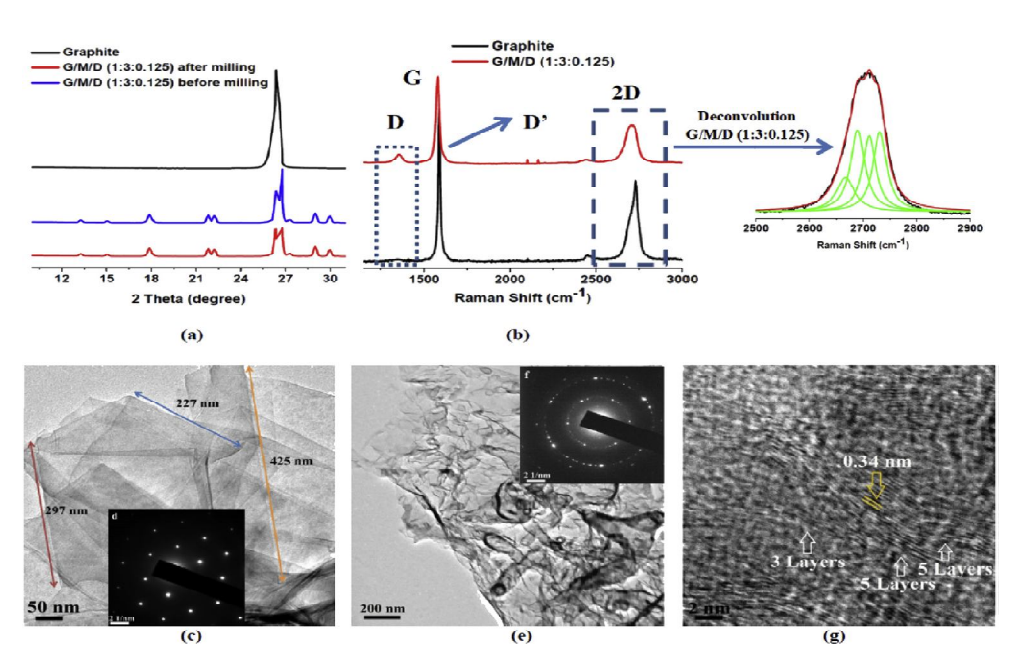


**Fig. 1.3** Characterization of graphene samples produced by using melamine as exfoliating agent by using different techniques such as XRD, Raman and Transmission Electron Microscopy [6].

Graphene has been proved as an "electrode material in electrochemical supercapacitors in electrical/hybrid automobiles" because of their unique with an amazingmixture of properties like "high surface area, lightweight, good electrical conductivity, compatibility with other materials, outstanding flexibility and transparency". Further, it shows excellent mechanical, electrical and thermal properties [27, 28].

A diverse method to obtain graphene sheets in mass quantities is through chemical oxidation of the graphite and following exfoliation in liquid form solvable graphene oxide[29]. However, the final material obtained consists of a diversity of oxygen functionalities, disturbing the prolonged  $\pi$ -conjugated sp<sup>2</sup> network and affects the new electronic features of graphene, thus making it as an insulator[18]. Though drop of graphene oxide produces reduced Graphene Oxide (GO) sheets and maximum of the times, the procedure is inadequate and the physical features of the material formed difficult to achieve pristine graphene[30].



**Fig. 1.4** (a)From left side to right side: pristine graphite and exfoliated graphene as achieved by tip sonication for 5, 15, 30 and 60 minutes, in o-DCB (b) Picture of the ½-inch fused silica windows with GO and rGO coatings [26, 31].

First-class graphene and graphene-based fabrics (Eg: graphene-polymer compounds, graphene intercalated by metallic nanoparticles or other nanostructures such as fullerene and/or CNTs) can be basically achieved beginning from regular graphite.

Graphene is probable nanofiller that can considerably enhance the characteristics of polymer based composites at extremely small loading[32, 33].

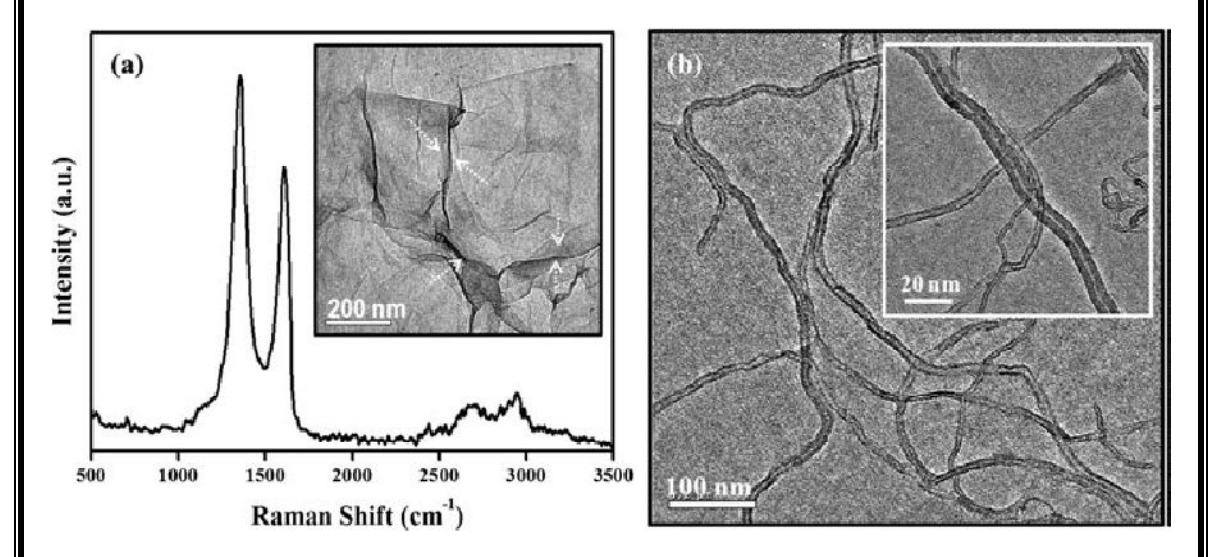


**Fig. 1.5** "Raman spectrum of graphene. Inset (Left): TEM image of graphene (wrinkles in graphenesheets have been marked with arrows). (b) TEM image of CNTS. Inset (Right) evidence of percolation network formation in CNT"[34].

The results till now stated in the literature specify that graphene/polymer compounds show multifunctionality with extensively enhanced tensile power and flexible modulus, electrical and thermal conductivityetc[34]. Despite few challenges and the truth that carbon nanotubes/polymer compounds are occasionally superior in some specific performance, graphene/polymer compounds may have widespread possible applications owing to their exceptional properties and the accessibility of graphene in a big quantity at little charge [35].

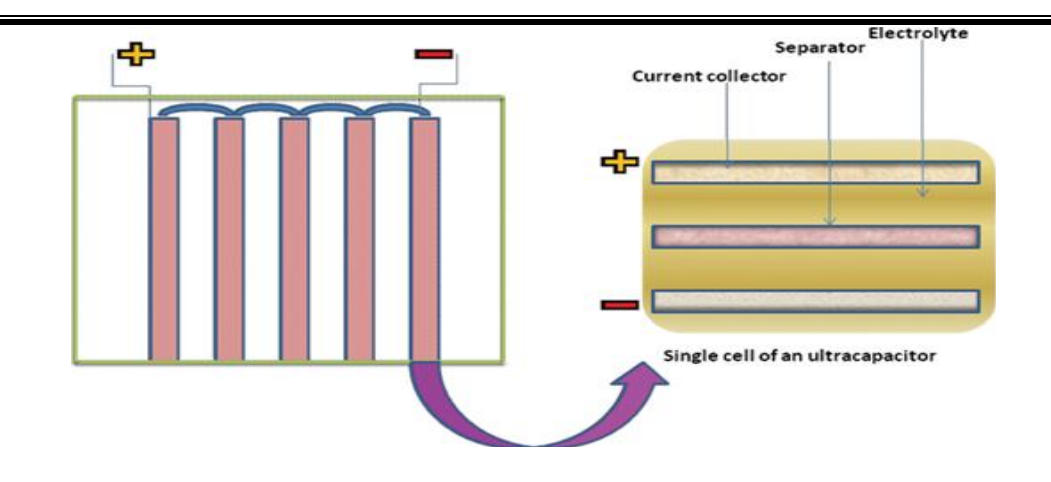
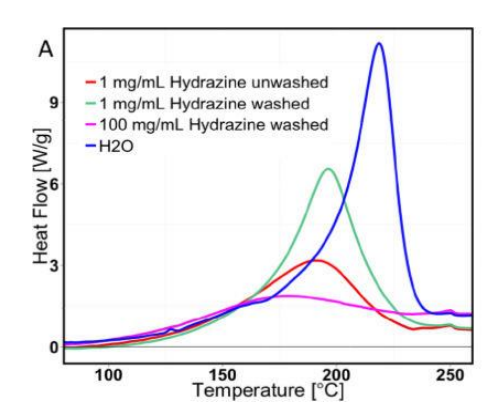


Fig. 1.6 Schematic representation of Ultra capacitor [36].

Recently, another top-down method has been developed to fabricate graphene sheets, involving the exfoliation of graphite in the watery phase by sonication, molecules that overwhelmed the robust van der Waals interaction, supporting the various graphene coatings in graphite[37]. In this context, many liquids have been used to generate steady dispersals of graphenelike surfactants in aqueous media, ionic fluids and organic solvents. Several applications of these graphene sheets obtained by this technique in various energy storage based devices with few examples like capacitors, FETs [30, 38, 39].



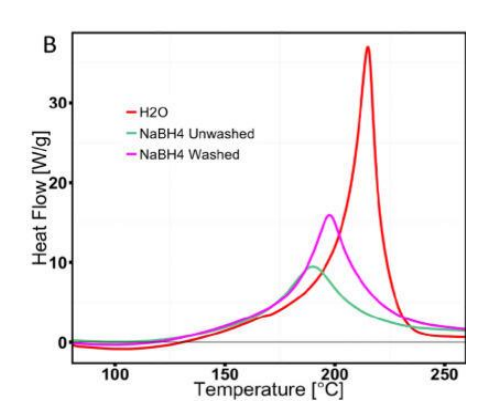


Fig. 1.7 represents synthesis of GO by modified Hummer's method and kinetics study [40].

Yang Qiuet.al,has reported a detailed thermo-chemical and kinetic analysis of GO exothermic decomposition planned to discover the situations and material compositions that prevent explosion during storage and processing of bulk-scale GO synthesis [40]. It is shown that "GO becomes more reactive for thermal decomposition when it is pretreated with OH<sup>-</sup> in suspension and the effect is reversible by back-titration to low pH. This OH<sup>-</sup>effect can lower the decomposition reaction exothermic onset temperature by up to 50°C, causing overlap with common drying operations (100–120°C) and possible self-heating and thermal runaway during processing" [6, 40-43].

### 1.3 Literature Review on polymer-basednanocomposites

The exploration of the nano-world has allowed the integration of nanostructures into polymer matrices with hierarchical architectures. In this way either by compatibilization of nanofillers with different properties or by controlling the collective communication between particles throughout an organized network, it is likely to tailor dielectric, of electrical. mechanical. thermal and magnetic features nanocomposites[3]. "Graphene-polymer nanocomposites have been prepared by three different routes such as Solution mixing[44][?], Melt blending[5]. polymerization[45]". There are several polymers such as PDMS, PANI, PMMA, PS used for the development of novel functional materials with improved performance for different applications. Among other features, elastomers offer decent heat opposition, ease of distortion at ambient temperatures and extraordinary elongation and elasticity before breaking. These features have proven elastomers as outstanding and comparatively lowcost materials for different applications in several areas including automotive, industrial,

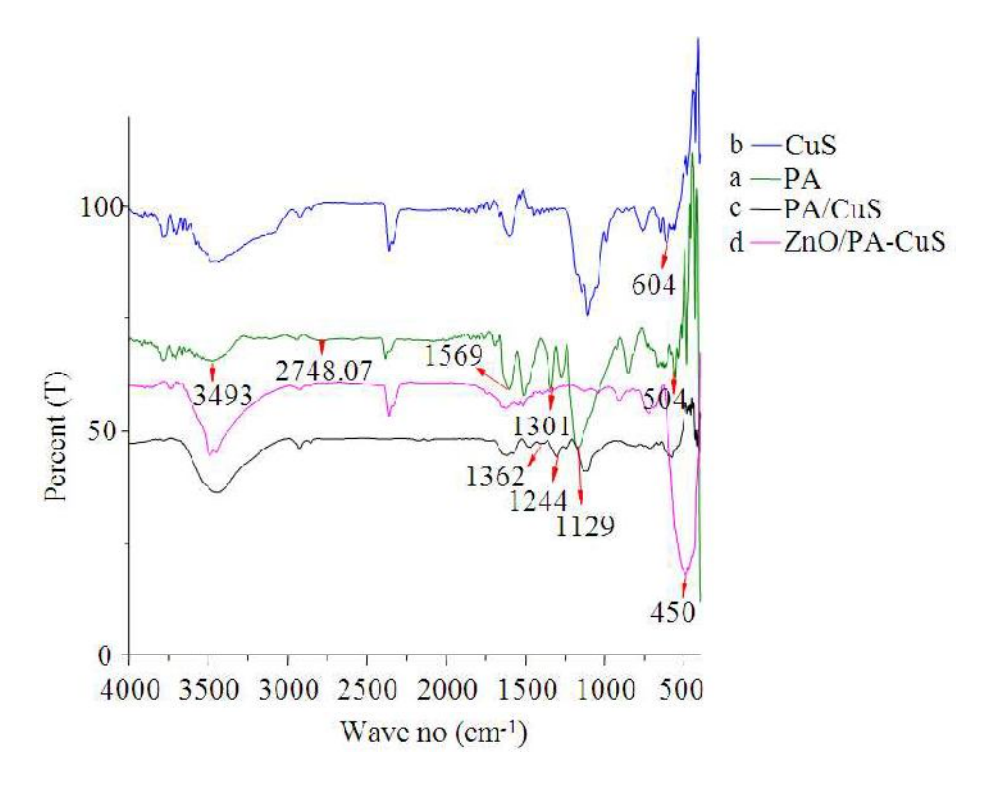
packaging, healthcare etc. "Elastomers can be used effectively as polymeric matrixes and the polymer nanocomposites that are formed exhibit significantly improved properties" [2, 46]. In fact, the design of materials with new properties for specific applications is the key element in the creation of high value-added products in multidisciplinary technological areas such as bioscience, optoelectronics, nano-electronics and nano-photonics. Their general characteristics involve compatibility, ease of fabrication, lightweight, non-corrosive and viscoelastic behavior, a small modulus of flexibility, a high failure strain along with very weak inter-molecular forces [47]. Polymer nanocomposites display considerable property improvements at much lesser loadings than polymer compounds with established micron-scale fillers (like glass or carbon fibers) which finally results in lesser component weight and can streamline processing; moreover, the multifunctional feature improvements made probable with nanocomposites may generate novel applications of polymers [48, 49].

Table 3. Electrical and thermal properties of graphene/polymer nanocomposites.

	Filler	Filler loading (wt% <sup>a</sup> , vol% <sup>b</sup> )		Electrical properties		Thermal properties		
Matrix				Percolation threshold (*-wt%, *b-vol%)	Surface resistance <sup>a</sup> (Ω) / Electrical conductivity <sup>b</sup> (Sm <sup>-1</sup> )	thermal con-	Thermal resistivity <sup>a</sup> (MΩ)/ Thermal Conductivity (W/mK)	Reference
	f-GP <sup>1</sup>	1.5ª	In situ			~25		[53]
-	f-GP1		In situ	0.244 <sup>b</sup>				[52]
Epoxy	CRGO <sup>2</sup>		In situ	0.52 b				[4]
	Graphene	1.0ª	In situ			23.8		[61]
201200	CRGO <sup>2</sup>		In situ	0.62 <sup>b</sup>				[88]
PMMA	f-GO <sup>3</sup>		In situ	0.26 <sup>b</sup>	$2.47 \times 10^{-5b}$			[89]
	TRGO <sup>4</sup>		Solution blending	0.16 <sup>b</sup>				[37]
PE	TRGO <sup>4</sup>	1.0a	Solution blending		$2 \times 10^{8a}$			[36]
	Graphene		In situ	3.8 <sup>b</sup>				[60]
PU	f-GP <sup>1</sup>	0.5	Melt blend. Sol. blend. In situ	>0.5 <sup>b</sup> <0.3 <sup>b</sup> >0.5 <sup>b</sup>				[39]
PVA	f-CRGO <sup>5</sup>	3.0ª	Solution blending	0.37 <sup>b</sup>	$0.9 \times 10^{-26}$			[33]
***************************************	TRGO <sup>4</sup>		Solution blending	4.5ª				[34]
PVDF	TRGO4		Solution blending	0.016 <sup>b</sup>				[90]
PBT	Graphene	0.5 1.0	Solution blending				760 50	[58]
PANI	CRGO <sup>2</sup>	10.0ª	Solution blending		$8.38 \times 10^{-4a}$ $11.92 \times 10^{2b}$			[91]

<sup>&</sup>lt;sup>1</sup>Functionalized graphene, <sup>2</sup>Chemically reduced GO, <sup>3</sup>Functionalized GO, <sup>4</sup>Thermally reduced GO, <sup>5</sup>Functionalized chemically reduced GO

To make polymer electrically conductive, it must mimic the metal, which means that electrons in polymers need to be open to move. "The electrical property of polymeric materials has become an increasingly interesting area of research because these materials possess a great potential for solid state devices" (Xiao *et al.*, 2011; Dong *et al.*, 2011; MacDiarmid, 2001). Conducting polymers (Reda and Al-Ghannam, 2013) are semiconductors and their band-gaps could be adjusted by changing the chemical kind of either the polymer backbone or the side groups existing in the polymeric chain. The overlying of the molecular orbital for the creation of the delocalized molecular wave functions and the partly occupied molecular orbital for a unrestricted movement of electrons throughout the polymeric structure are the essential needs for the polymers to become conductors[50, 51].



**Fig. 1.8** "FT-IR Spectrum of (a) PANI, (b) CuS, (c) PANI/CuS and (d) ZnO/PANI-CuS thin film"[51].

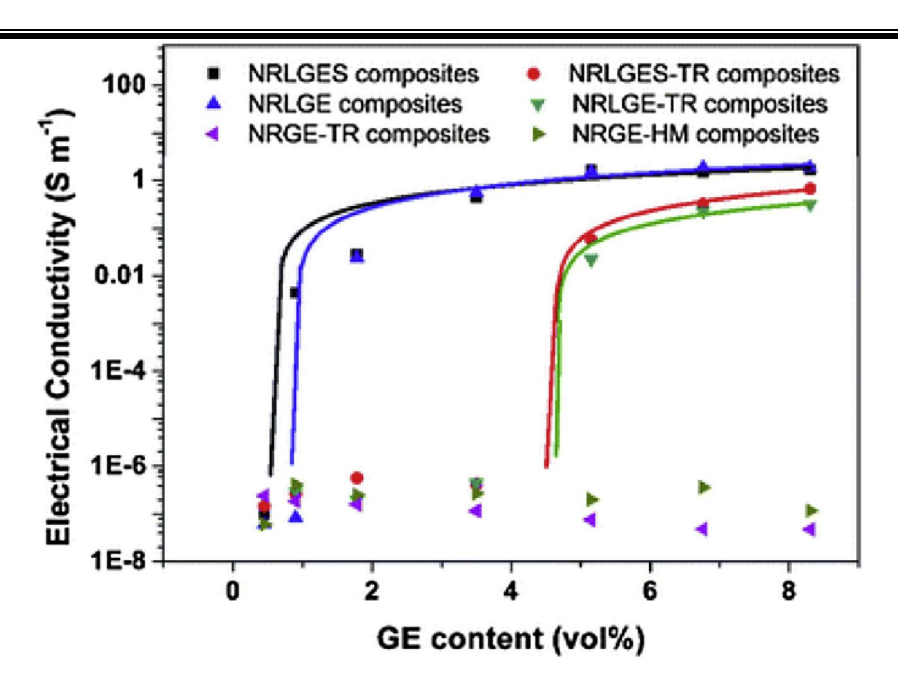


**Fig. 1.9** Electrical conductivity of normal rubber (NR) compounds as a function of graphene (GE) content[52].

## **PDMS (Silicon Elastomers)**

Out of the all elastomeric polymers, "PDMS is a Si-based organic polymer that has found wide applications in MEMS and microfluidic device fabrication, soft lithography, contact lens manufacturing and device encapsulation" [53]. Free-standing, hierarchical reticulate single-walled carbon nanotubes (SWCNT) films are embedded in poly (dimethylsiloxane) (PDMS) to make stretchable conductors (SWCNT/PDMS stretchable conductors).

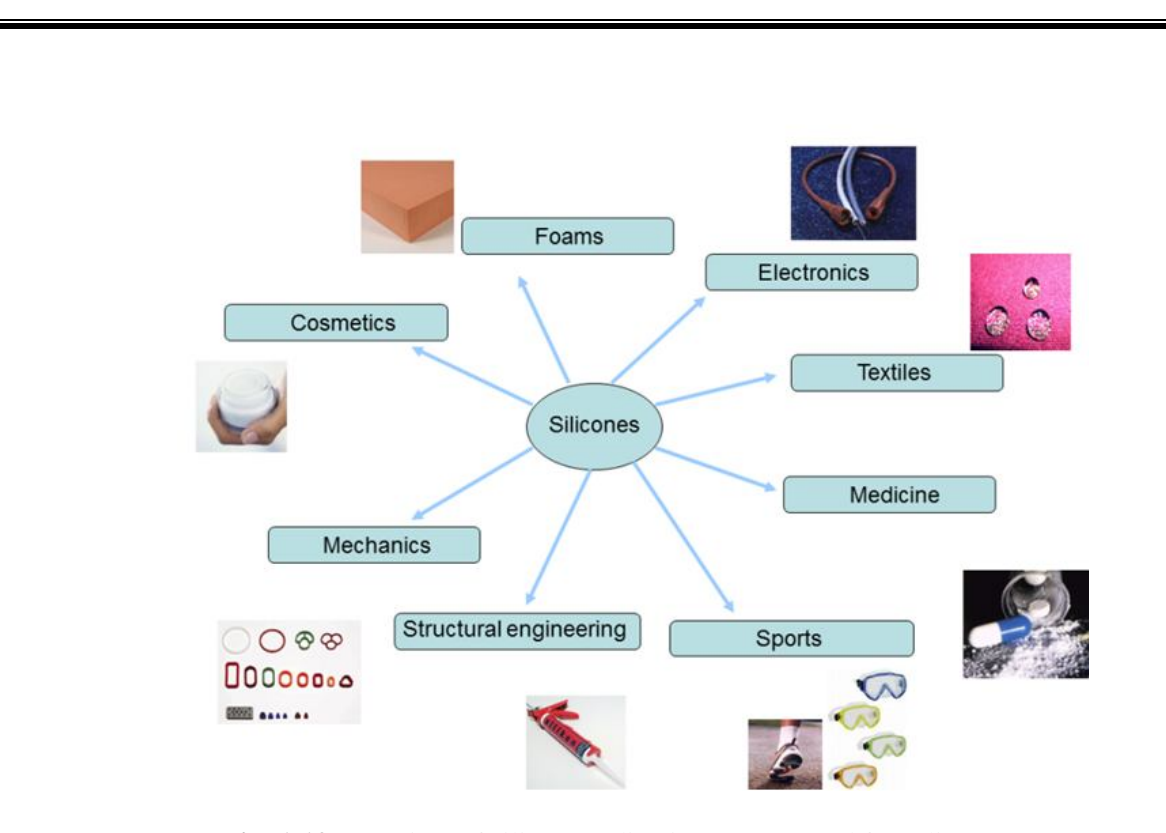


Fig. 1.10 Overview of silicon applications as reported from literature.

The stretchable conductors are very clear in thevisible light area and hold exceptional conductance under big tensile strains. Strain examinations disclose a distinctive strain-history dependence conduct of the resistance and resistance steadiness is succeeded upon repetitive elongating and freeing, implying that the SWCNT/PDMS stretchable conductors can be programmed to be reversibly stretched to a defined strain without confrontation changes. A quantitative explanation of the surge in resistance is determined by adopting the Wei bull distribution. Additionally, a light-emitting diode could be illuminated using a repeatedly prolonged SWCNT/PDMS strip as the connecting wire, exhibiting the utility of the stretchable conductors as interconnects for stretchable electronics. Because of the elevated transparency, extreme conductivity, and exceptional stretchability, in add-on to the facile creation, the SWCNT/PDMS stretchable conductors might be broadly used as interconnects and electrodes for stretchable

intelligent and functional devices[54]. Therefore more research activity is still required to implement this material for several application by employing different nanomaterials as a filler material. Out of those, graphene is emerging as a potential material for fabrication of graphene-PDMS based nanocomposite.

### PDMS (Silicon Elastomers) based Graphenenanocomposites

Graphene-polymer compounds have attracted significant attention because of their great mechanical, electrical and thermal properties[48]. Graphene and its byproducts are extremely effective in strengthening polymers at significant small loadings. The optimal content of graphene, however, changes in different polymer systems. The enhancement in strength is greatly reliant on the integrated quantity of graphene, as it could effect the dispersal, morphology and connections within polymer matrix[55-58].

A Graphene composite which is fabricated by using the functionalization of graphene sheets, in those approaches graphene sheets (rGO) can be dispersed in liquid and organic solvents, that reduce the agglomeration and help to achieve greater loading of graphene in the compounds. Ultra sonication helps to get a consistent dispersion of graphene sheets; however, prolonged exposure to high power sonication induces the deficiencies in graphene, which may degrade the properties of the composites.

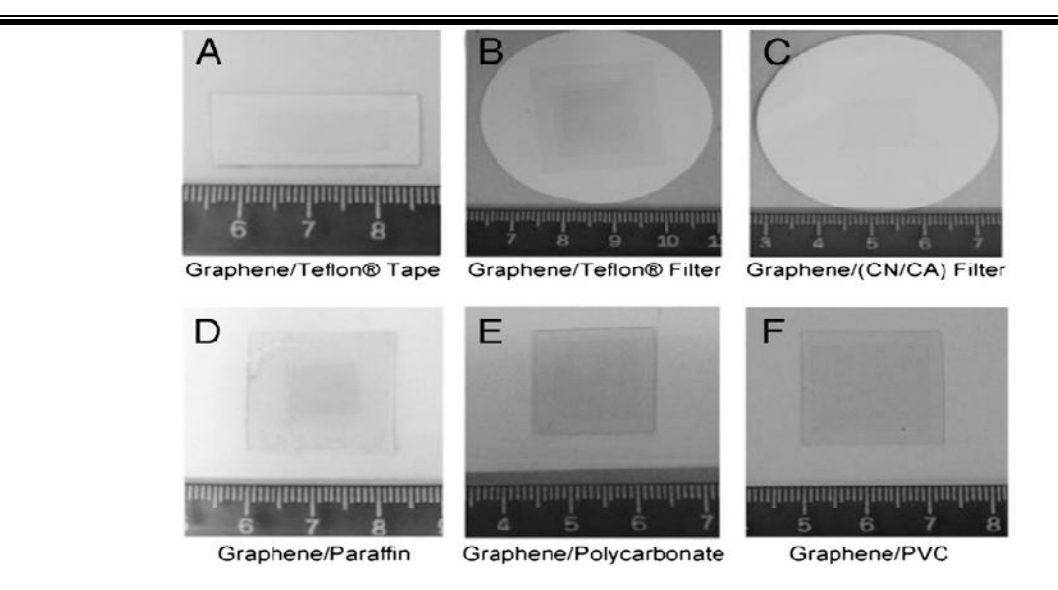


**Fig. 1.11**"Photograph of graphene transferred to different flexible substrates. (A) Monolayer graphene transferred to Teflon tape. (B) Multilayer (three layers) graphene on a Teflon filter by transfer three times. (C) Graphene on a CN/CA membrane filter. (D) Multilayer (two layers) graphene on a paraffin film. (E) Graphene on a polycarbonate substrate. (F) Graphene on a PVC substrate. The rulers are scaled in centimeters"[59].

Dendrite type polymers have been used to functionalize graphene sheets through  $\pi$ - $\pi$  stacking, trailed by deposition of in-situ generated metal nanoparticles, while the poly(N,N-dimethylacrylamide)-b-poly(N-isopropyl acryl amide) block copolymer was intercalated with chemically transformed graphene sheets providing upsurge to a possibly biocompatible hybrid complex[60]. The benefit of the polymernanocomposite is to offer significant additional features thepure polymer without losing its processability, intrinsic mechanical properties and lightweight. Graphene has drawn notice as a assuring candidate to build innovative PNCs owing to its outstanding properties and readily accessibility of its precursor, graphite [44].

**Stankovich** has reported similar to this method and has prepared the GNS/polystyrene nanocomposites. A mild single-step electrochemical approach was used to synthesize functionalized graphene sheets by ionic-liquid-water as solvent precursor which enhance

the properties of functionalized graphenenanosheets in polystyrene compounds by liquidphase blend route exhibit percolation threshold of 0.1vol% electrical conductivity and the polystyrene composite showed the conductivity of 13.84S-m<sup>-1</sup> at 4.19vol% which is 3-15times that of polystyrene composites filled with single-walled CNTs[61, 62].

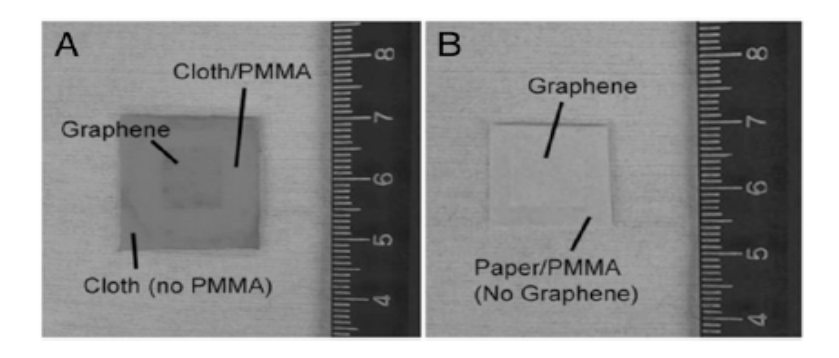


**Fig. 1.12**"Photographs of graphene on (A) a piece of cloth and (B) regular A4 paper. A drop of PMMA was placed in the center of the cloth, so the edges soaked up more FeCl3 etchant than the middle, and is therefore darker. In the case of the paper, the entire surface was uniformly coated with PMMA but the graphene offers some protection from the etchant, resulting in more color contrast"[59].

**Rafiq et al.**have researched the result of FG (oxygenated graphene) content on the breakage durability of nylon-12. They have reported that the highest development (72 %) was attained with the accumulation of 0·6 wt% FG. According to the optical microscopy images as shown in Fig. 1.12, it can be detected that by incorporation of the FG produced a rise in the amount of γ-phase in semicrystalline nylon-12, representing the nucleating ability of the FG. The regular size of nylon crystals reduced in 0·6 wt% FG–incorporated nanocomposite. The reduced crystal size could help the hardiness of nylon-12. However, with the supplement of 1 and 3 wt% FG, the crystal size enlarged, which caused in lesser toughness[14]. Therefore, lower wt% is more effective for preparation of the FG-PMMA nanocomposites.

Presently, scholars in the arena of flexible electronics target to develop materials and patterning processes that upsurge TFT performance while lessening the charge per unit area.

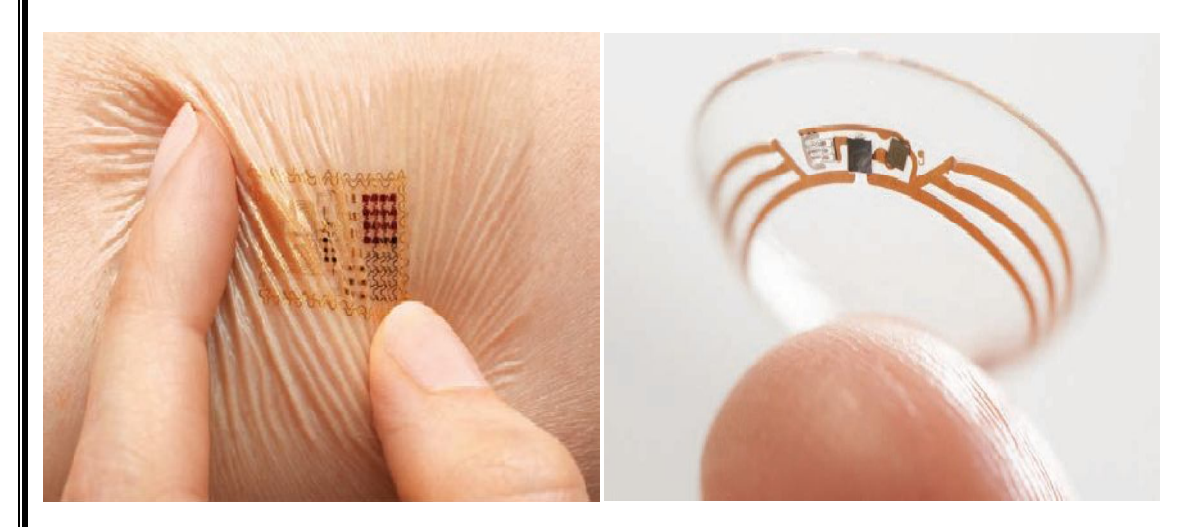


**Fig. 1.13** represents the polymer-based device applications (a) stretchable 'biostamp' skin sensor and (b) glucose-sensing contact lens [62].

Graphene-polymer compounds have the potential to be applied to several products like components of electronic equipment, energy storage media, organic solar cells, heat conduction composites, film packaging and biomimetic devices owing to the amazing properties.

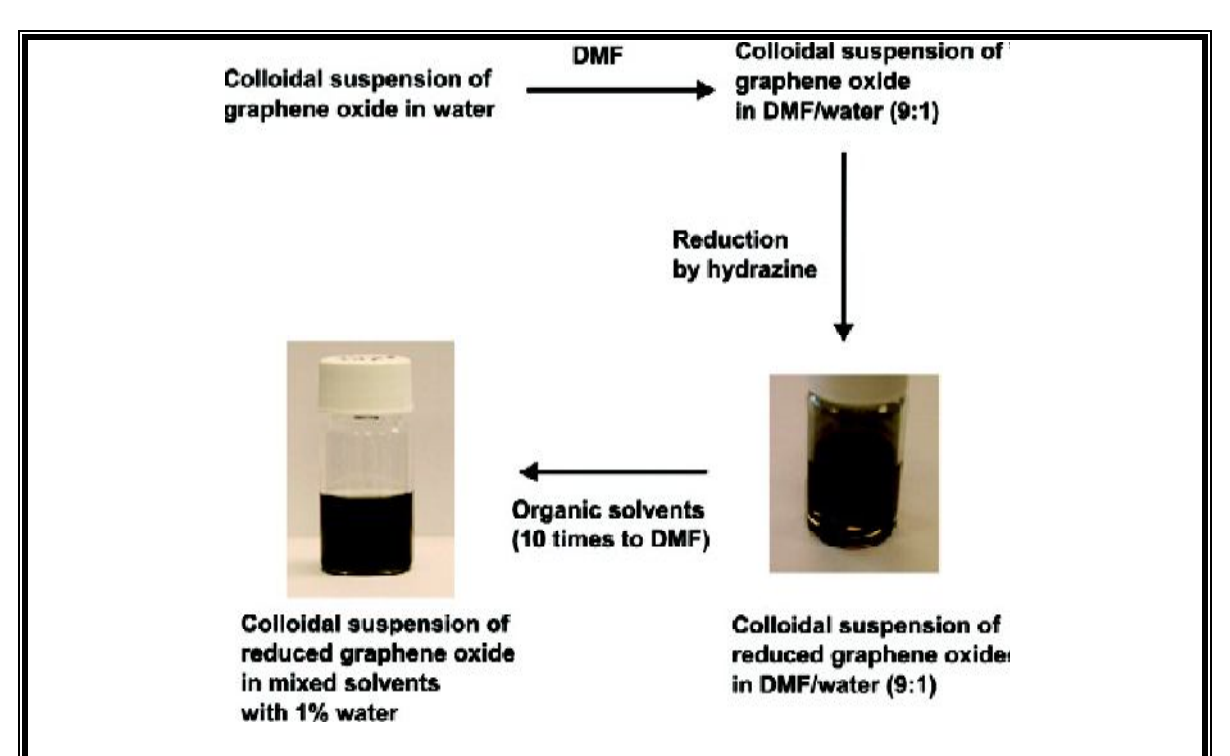


**Fig.1.14** Schematic represents the synthesis of rGO and acolloidal dispersion of rGO in different organic solvents[63].

**Senguptaet.** all have reported, summarized the manufacturing approaches of graphene-based polymer compounds i.e., in-situ polymerization, solution compounding and melt amalgamation. The studies on graphene compounds based on different polymers such as PMMA, polypropylene, PE, PS, polyphenylene sulfide, polyaniline, polyamide, phenyl ethynyl-terminated polyimide etc., has been reported by Kuilla. In-situ polymerization and solution compounding assist to enhance the physical characteristics of composites by improving the dispersal of fillers as stated [57, 64-66].

A big transparent conductive CCG film was readily made-upby a fast, low-budget and simple method using spray deposition of GO-hydrazine dispersal. With this process, the making of the film and decrease of GO to CCG were carriedout concurrently. The prepared CCG films were identical and exhibited a low sheet resistance of 2.2x10<sup>3</sup> ohm-

cm<sup>-1</sup>with84% transparency at a wavelength of 550nm. It is witnessedthat the sheet confrontation of CCG sheets was closely linked to the I(D)/I(G) ratio of Raman data[67].

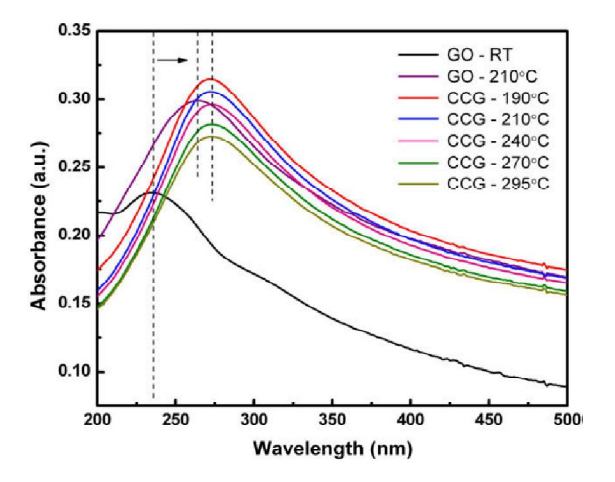


**Fig. 1.15**Schematic represents the dispersion behavior of GO and chemically converted graphene (CCG)[35].

## Study of the Dielectric properties of polymer-basednanocomposites

For the upcoming sensors and great energy density capacitors, it is important to make dielectric materials with an elevated dielectric constant, little loss, great breakdown field, and a low charge. The energy storage capability of the compounds could be improved by the exterior modification of the fillers and from the interface compatibility connecting the fillers and the polymer matrix. The value of energy storing density in a dielectric material is strongly reliant on the dielectric constant ( $\epsilon_r$ ) and breakdown power ( $E_b$ ). However, it is very tough to enhance them synchronously because the improvement of dielectric constant is typically accompanied by a great loss, which may result in small breakdown strength. Inorganic dielectrics (i.e. ferroelectric ceramics) show relatively great dielectric constants, but they also have small breakdown strength and deprived processability. Polymers own a high breakdown strength and good processability, but their dielectric

constant is comparatively low (usually smaller than 5). Therefore, "dielectric composites combining ceramics and polymers have been widely studied due to their excellent dielectric properties, good mechanical flexibility, and easy of fabrication" [22]. To obtain great performance dielectric composites, it is very important to disperse ceramic nanoparticles into the polymer matrix consistently and to get good quality dielectric composites with an identical microstructure.

Recent studies have shown that the simple mixing and solution casting of a filler in a polymer matrix normally resulted in deprived film quality and inhomogeneity because by introducing the high surface energy ceramic particles into a low surface energy polymer it sources extremely inhomogeneous electric fields at the interfaces, that may conduct charges owing to the incorrect and non-uniform dispersal. Thus, it decreases the dielectric breakdown power of the compounds. Therefore, the appropriate organic amendment of the surface of the particles may be an applicable way to prevent the agglomeration of the nanoparticles and improve the uniform dispersals [56, 68, 69].

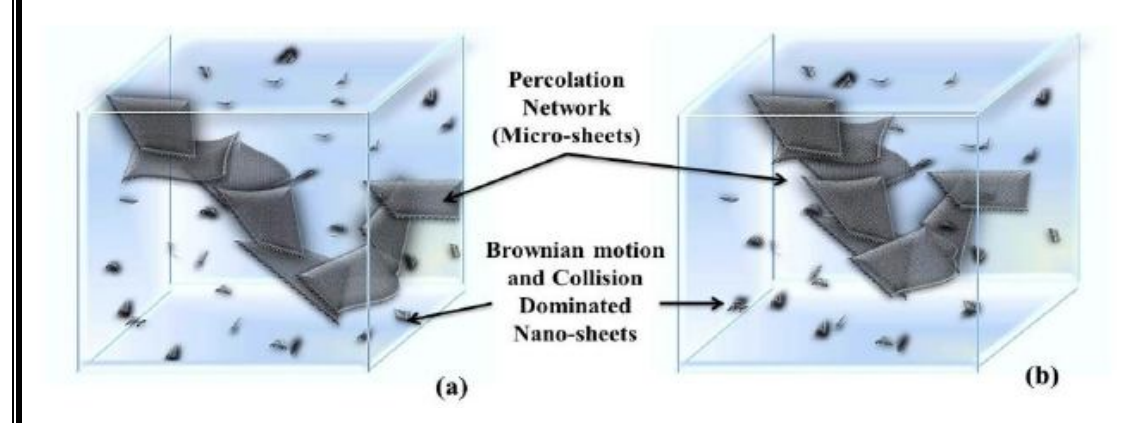


**Fig. 1.16** Schematic represents the dispersion of filler material in the composite matrix [32].

Surfactants like phosphate sulfonate, silane, and carboxylate based surface modifiers or coupling agents are added to the polymer nanocomposites for improving the dispersal and also to upsurge the dielectric breakdown. It is trusted that the bridge-linked

action of the coupling agent can also enhance the composite uniformity and enhance the dielectric reaction of the composite. The selection of the coupling agent is therefore an important design thought, which influences the polymer matrix, surface characteristics of the filler, and polarization losses at the interface.

**Shail K. Gupta et. al**have prepared the PMMA/BaTiO<sub>3</sub> nanocomposite sheets prepared by using solution processing method and the nanoparticles are homogeneously dispersed in the PMMA polymer matrix. They have reported that there is a surge in the dielectric constant with a rise in the BaTiO<sub>3</sub> filler content in the polymer matrix as shown in Fig. 1.17 and the dissipation factor  $(\tan \delta)$  decreases with an increase in the frequency[70].

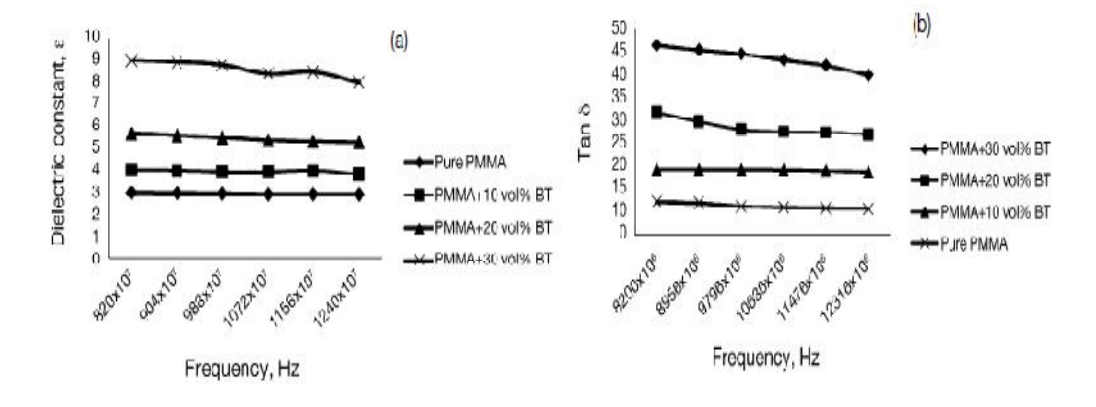


**Fig.1.17** Frequency dependence of (a) dielectric constant and (b) loss tangent for PMMA/BaTiO3 nanocomposites[70].

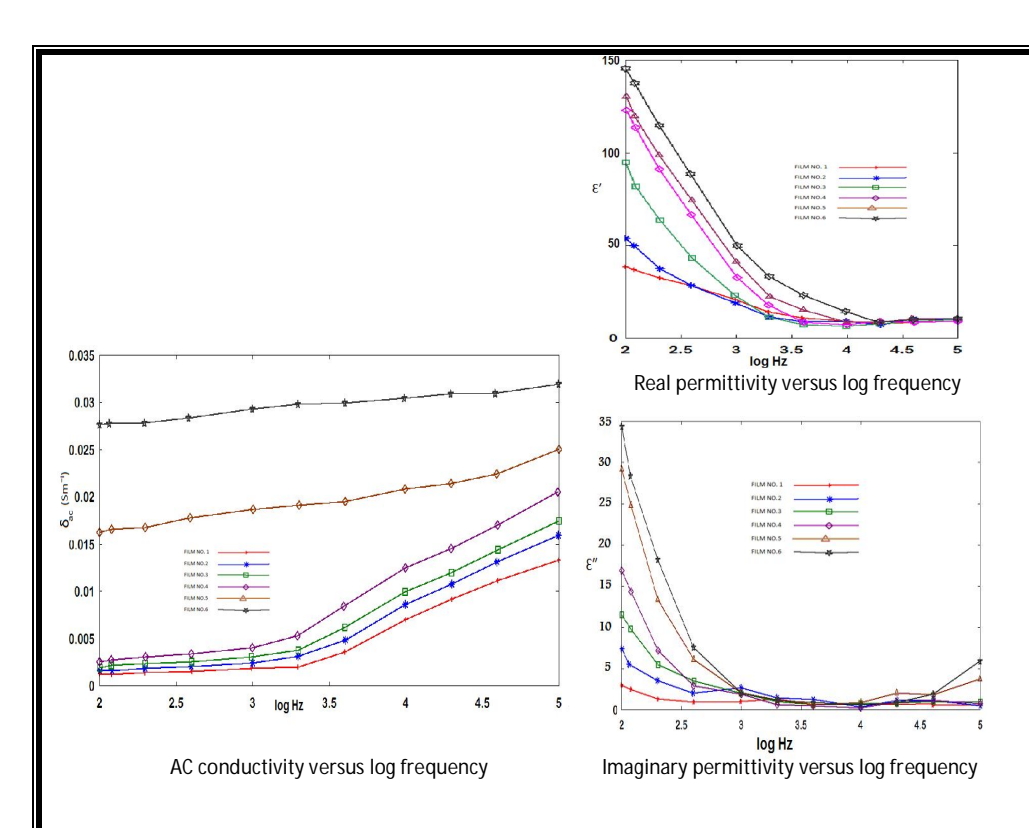
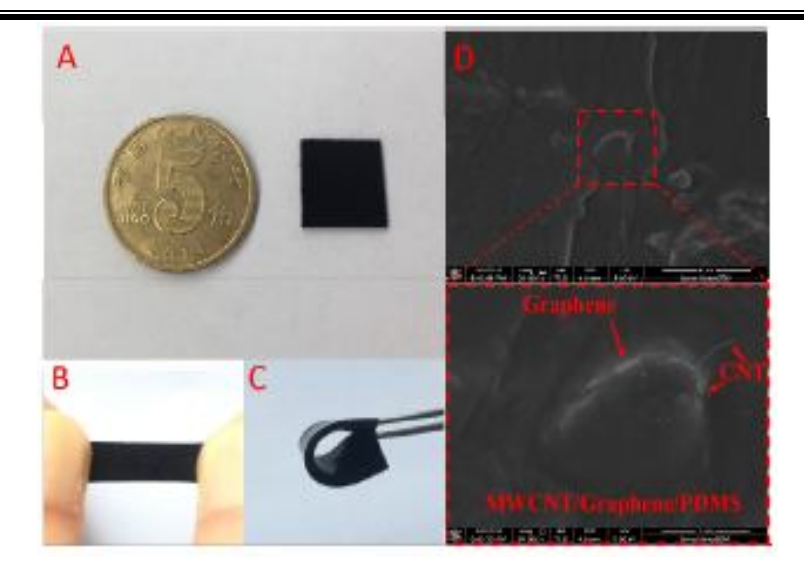


Fig.1.18 Dielectric properties of the composites reported [71].

#### 1.4 Flexible Sensors

Strain sensors with anelevated elastic limit, extreme sensitivity are necessary to assemble the growing requirement for wearable electronics and sensors. The rising demand for the wearable electronics such as skin-surface mountable sensors and implanted sensors, strain sensors (also termed 'strain gauges') capable of relatively high sensitivity 14 and high elastic limit have attracted attention globally. Highly sensitive and stretchable sensors have great potential for broad applications such as flexible displays, robotics, health-monitoring devices, and sports (e.g. performance monitoring and novice training)[72-76].



**Fig. 1.19** Images of normal (A) stretched and (B)bended (C) conductive CNT-graphene-PDMS electrode (D) Microstructure of MWCNT (1D)/Graphene (2D) interconnection in PDMS matrix [54].

Strain sensors have a broad range of uses in engineering, medicine and industry for measuring various quantities like stress, pressure, torque and vibration. Despite their outstanding features, conservative strain sensors like semiconductor-based strain gauges, show some limitations like measurement range, little sensitivity, complications to be embedded in material structures, low exhaustion life and sensitivity to environmental situations and influencing effects. Therefore, a new class of smart materials is need to overcome these shortfalls [34].

An elevated strain measurement sensitivity can be touched at the percolation threshold. "The percolation threshold depends on different factors such as CNT aspect ratio, CNT type, shell quality, dispersion degree and the functionalization of the CNTs"[77]. Commonly, CNT networks with functionalized CNTs have greater percolation thresholds than non-functionalized CNTs. Analyses have indicated that percolation threshold and conductivity intensely depends on the type of polymer, fabrication factors, uniform

spatial distribution of individual CNTs and degree of alignment. Therefore, percolation thresholds ranging from less than 0.5wt% to over 10wt% of CNTs loading have been

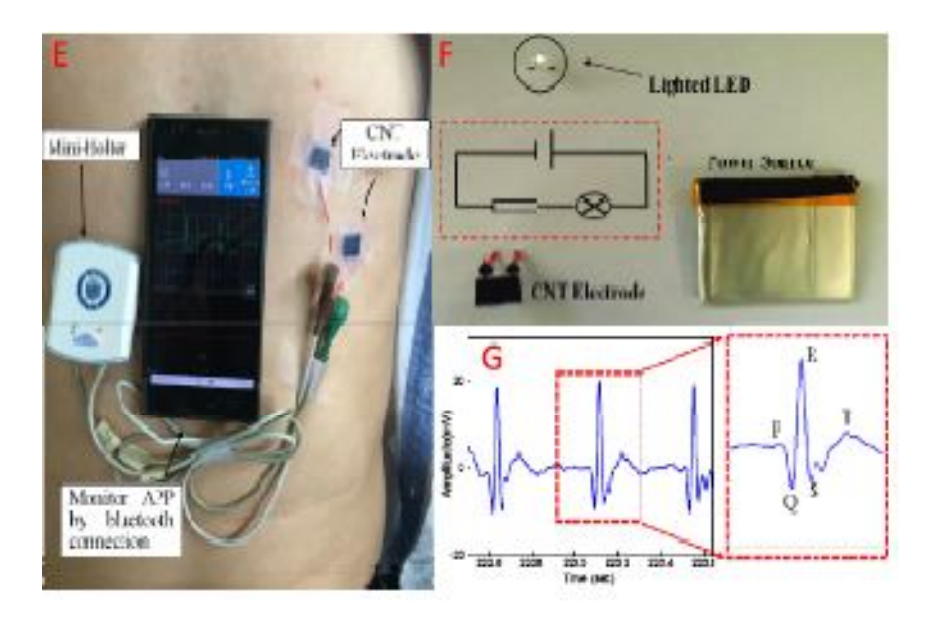


**Fig. 1.20** Application in ECG signal (E) Experimental set-up to observe the ECG signal (F) Image of LED procedure with a CNT-graphene-PDMS electrode as an interconnection (G) ECG signal measured under the condition of (E) [54].

reported. It is anticipated that the accumulation of CNTs to a polymer considerably improves the conductivity of the composite [34]. Latest improvements in strain sensors built on CNT thin films and CNT/polymer compounds by considering the effect of the fabrication factors, kind of CNTs and polymers on the strain sensor conduct and reproducibility. A strain sensor has been created with PEDOT: PSS according to the piezoelectric function that contains the variations in the electric resistance to the applied pressure [78, 79].

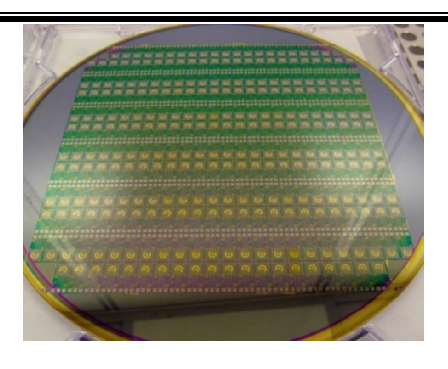


Fig. 1.21 Pictures of graphene EGFETs: (a) 200 mm wafer patterned with 280 transistors[80].

As reported from the current literature, several groups are working globally in the fabrication of graphene-based devices for several purposes. However, with new applications come ever-growing demands for new classes of polysiloxane materials with enhanced, better and even novel materials properties [68, 81, 82].

# 1.5 Current Challenges and Issues

Recent literature has been focused on the polymer-basedgraphenenanocomposites because of the excellent properties of the 2D honeycombgraphene. The current research activities on the facile synthesis of graphene and GO to develop novel hybrid materials for various applications. The chemical approaches to prepare the Go and RGO from the graphite is a favorable route for producing a large-scale production of graphene. There is great attention to the preparation method of GO-based material composites. Graphene, however, has a major drawback of low dispersibility in water since low surface area as reported from the literature and hence, limits the applications. There exists a lot of chemical methods i.e., Hummer's method and modified Hummer's method, CVD, mechanical exfoliation but limits the applications because of their structure, morphology and defects/disordered characteristics obtained from different synthesis methods. The solution processing requires more time for drying and usually results in the restacking of graphene through the drying procedure. The superior quality of graphene is usually produced using method named Chemical Vapor Deposition (CVD), mechanical peeling and Carbonization from solid sources. These approaches are not appropriate for the mass synthesis of graphene used as the filler. The liquid exfoliation and drop of graphene oxide to fabricate Chemically Converted Graphene (CCG) in big quantities used for the fabrication of polymer-basedgraphenenanocomposites.

Current status of the polymer-basednanocomposites in the near future plays a major role in the fields of Micro-Electronic Mechanical Systems (MEMS), Opto-electronic system, Flexible Electronic systems and so on. Development of these polymer nanocomposites by

facile methods to enhance the electrical, thermal, optical and mechanical properties is a current challenging issue. As per current literature, it has been seen that that one of the main issues in preparing the good polymer-basednanocomposite is the good dispersal of the graphene in a polymer host matrix. The solvent rapport of the polymer and the filler plays animportant role in getting decent dispersion. However, restocking happens regularly during addition with the polymer matrix owing to robust van der Waals forces between the graphene fillers and sources cracks, pores, and pin holes in the compound. These flaws drop the valuable properties of the graphene-polymer compounds. Good dispersal is vital for getting the preferred improvement in the ultimate physical and chemical properties of the compounds [83]. One of the main tasks is to achieve the decent dispersion of the graphene in a polymer matrix is to eliminate the agglomeration of polymer host material due to the intrinsic vander Waals forces and  $\pi$ - $\pi$  stacking. Moreover, Graphene is also hydrophobic nature. There are different methods have been developed for the preparation of these nanocomposite structures, including solution mingling, melt mixing and in-situ polymerization [84-86]. Another main issue is that for refining the electrical conductivity of the polymer nanocomposites, higherVol% or Wt% filler materials are incorporated that degrade the mechanical durability and flexibility and hence, to develop the polymer-basednanocomposites with improved flexibility with low Vol/Wt (%) of filler materials in the polymer matrix. To enhance the optical transparency with a low percentage (%) by Volume or weight (%) since as found from the literature, optical transparency varies with an increase in weight of fillers in the polymer matrix. Obtaining a uniform or homogenous dispersion of the filler material in the polymer matrix with enhanced properties is a challenging issue. Furthermore, more research

activities are still needed to obtain a zero defect nanocomposite with an identical microstructure, elevated dielectric constant, great dielectric strength, and little dielectric loss [38, 68, 87-89].

## 1.6The Motivation and Objective of the Thesis

The main objective of this thesis work is divided into two parts, the first objective is to synthesize graphene oxide by using a novel chemical approach (volumetric method) without applying of NaNO2/NaNO3 or attending zero temperature requirement for obtaining a 2-3 layer fully oxidized GO in a simple, economical and eco-friendly approach. The second goal of this thesis work is to cultivate a uniformly distributed reduced graphene oxide (rGO) based PDMS nanocomposite and to investigate the optical, thermal and dielectric properties for future applications in transparent flexible and wearable sensors.

#### 1.7 The Thesis Outline

chapter deals with the introduction of nanomaterials, basednanocomposites and Literature review. The second chapter of the thesis involves the synthesis and characterization of graphene oxide by using Conventional Hummer's, Modified Hummer's, method and our novel volumetric approach (without the addition of NaNO<sub>2</sub> or NaNO<sub>3</sub>). The third Chapter of this thesis describes the chemical decrease of graphene oxide to reduced Graphene Oxide by the chemical reduction process. Chapter-4 deals with the fabrication and Characterization of neat PDMS and rGO-PDMS composite without any chemical treatment of the NGO. Chapter 5 involves the fabrication and characterization of 1,4-Dioxane chemically treated rGO-PDMS nanocomposites. Also, the optical, thermal, dielectric and electrical properties are studied. Chapter 6 deals with the comparative study of the structural, bonding, thermal, optical, dielectric and flexibility of rGO-PDMS and 1,4-D-chemically treated rGO-PDMS nanocomposites. Ultimately, the summary and conclusions are outlined in Chapter 7.

# **Chapter-2**

# Synthesis of Graphene Oxide (GO) by Modified Hummer's method without NaNO<sub>2</sub> or NaNO<sub>3</sub> (Volumetric method)

#### 2.1 Introduction

This chapter deals with the synthesis and characterization of graphene oxide (GO) by using Conventional Hummer's method and a novel controlled process called volumetric titration process. The structure, morphology, bonding and molecular structure are investigated by using XRD, TEM, FESEM, FT-IR, Raman and UV-spectroscopy.

#### 2.2 Synthesis of GO by Conventional Modified Hummer's Method

#### 2.2.1 Preparation

Initially, sulphuric acid 23ml was taken in a glass beaker kept in ice-bath for 45minutes and maintained the temperature <0°C. Then graphite powder and NaNO<sub>3</sub> crystals were added and subjected to constant stirring for 45min in an ice-bath for the thorough mixing of the chemical reaction. Follow by the addition of KMnO<sub>4</sub> slowly to the above solution. The solution color changes to greenish black from black color and maintained the temperature (<20°C) during the reaction and the solution attained the room temperature was subjected to oil-bath with constant stirring. Further addition of 10ml H<sub>2</sub>O<sub>2</sub> and 140ml of DI H<sub>2</sub>O the color changes to brown and with continuous stirring for 15min graphene oxide (GO) settled out was filtered and neutralized the pH by using 5% HCl, DI water and methanol. Vacuum conditions: Graphite precursor heated in an oven at 50°C for 24hrs under vacuum of 720mm of Hg. GO synthesized from graphite precursor treated under vacuum by a conventional method.

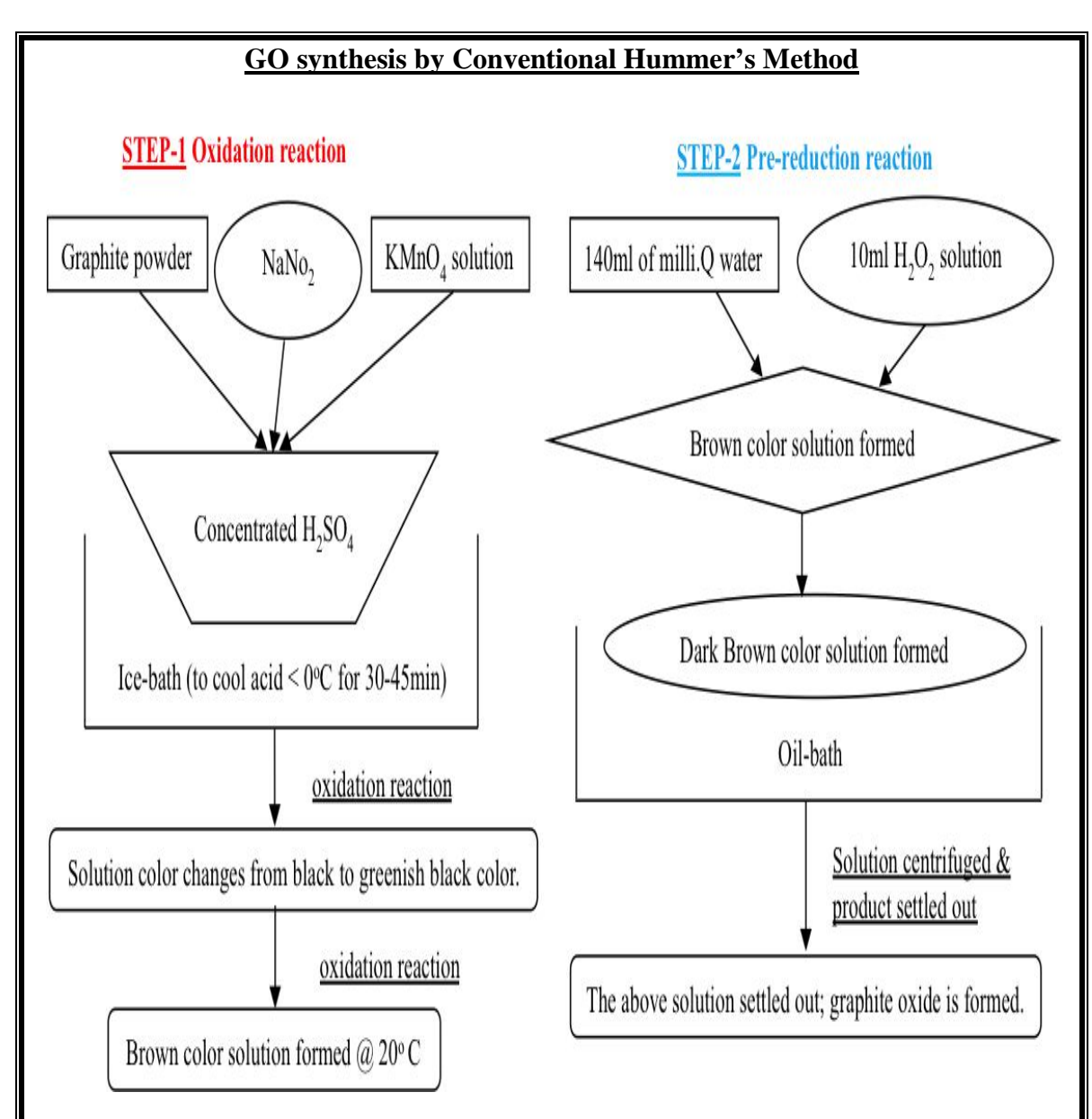


Fig. 2.2.1 Flow diagram represents the synthesis of GO by Conventional Hummer's Method.

Fig. 2.2.1 represents the block diagram of GO synthesized by conventional Hummer's Method as reported from the literature. The synthesis stepwise process in brief is represented in Fig. 2.2.1.

Table: 2.2.1. Synthesis of GO preparation by Conventional Hummer's Method

Sl. No.	Sample ID	Graphite (gms)	H <sub>2</sub> SO <sub>4</sub> (ml)	KMnO <sub>4</sub> (gms)	NaNO <sub>3</sub> / NaNO <sub>2</sub>	H <sub>2</sub> O <sub>2</sub> (ml)	H <sub>2</sub> O (ml)

					(gms)		
1.	MH1-01-GO	1.00803	23	3.00201	0.50108	10	140
2.	MH1-02-GO	1.00199	23	3.2411	0.50001	10	140
3.	MH1-03-GO	1.0072	23	3.00078	0.50018	10	140
4.	MH1-04-GO	0.99820	23	3.21750	0.49731	10	140

From the Table 2.2.1, the parameters are used to synthesize GO by Conventional Hummer's method with thelow and high amount of potassium permanganate i.e., theoxidizing agent used in the process. GO synthesis was carried out with graphite precursor without vacuum and under vacuum conditions i.e., 720mm of Hg in order to remove the traces of moisture content from the precursor material.

#### 2.2.2 Structural analysis by XRD

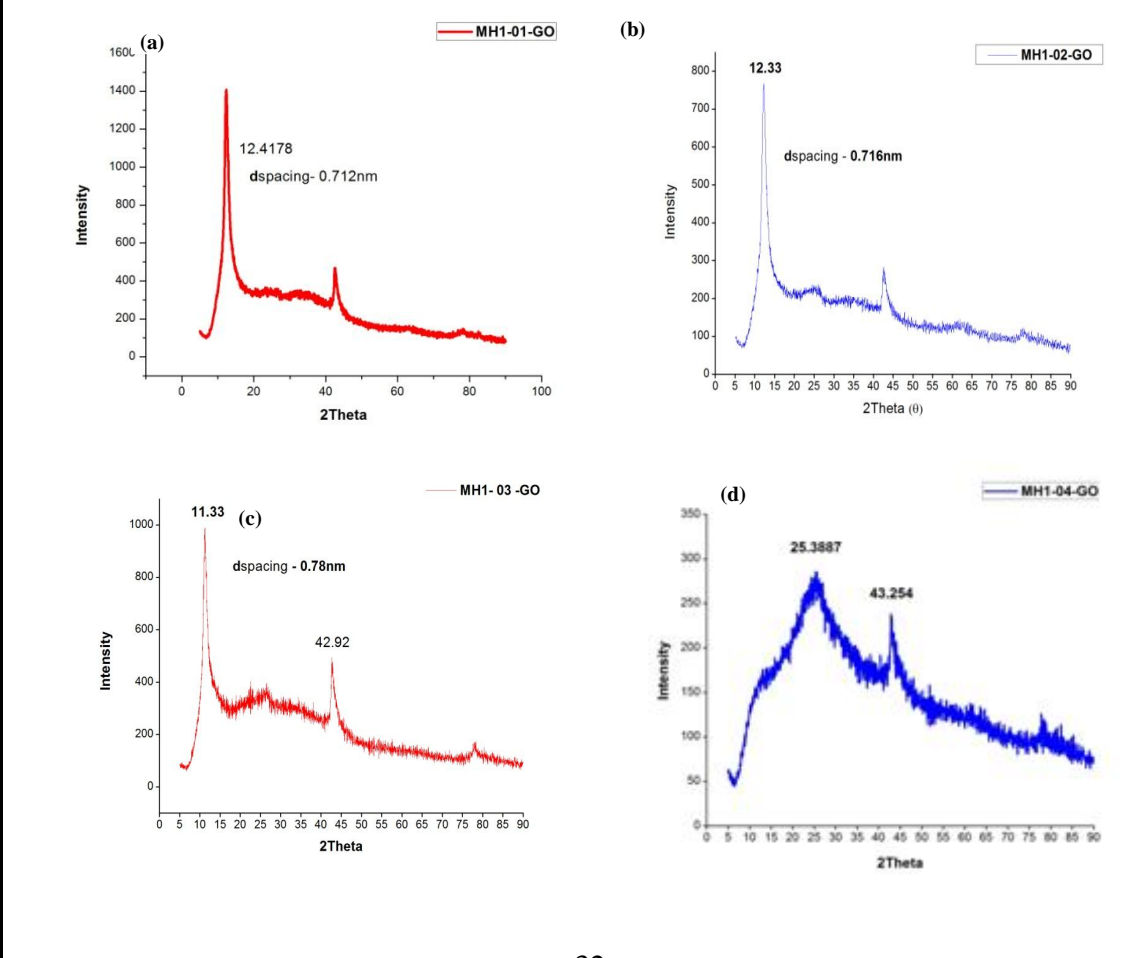


**Fig: 2.2.2** XRD patterns of GO with (a) low KMnO<sub>4</sub> (without vaccum) (b) high KMnO<sub>4</sub> (without vaccum) (c) low KMnO<sub>4</sub> (with vaccum) (d) high KMnO<sub>4</sub> (with vaccum).

Fig. 2.2.2 shows the XRD analysis of GO synthesized from Conventional Hummer's Method without vacuum and under vacuum conditions. From Fig. 2.2.2 (a) and 2.2.2 (b), 2□ peak appears at 12.42°& 12.33° for the samples MH1-01-GO and MH1-02-GO respectively with lower and higher amount of KMnO₄. The peak around 42.9° as sown in the Fig. 2.2.2 (a-d) obtained from the precursor graphite powder used in the process. From the Fig. 2.2.2 (b), there is an increase in the inter-planar spacing of 0.716nm when compared to low concentrations of the oxidizing agent, it is observed with d-spacing 0.712nm. From the Fig. 2.2.2 (c), the oxidation of the graphite pre-treated in vacuum to GO results with an increase in inter-planar distance of 0.78nm when compared with MH1-01-GO and MH1-02-GO. The crystallite size of GO by Conventional Hummer's Method is found to be 0.09nm and 0.1nm for MH1-01-GO & MH1-02-GO and MH1-03-GO & MH1-04-GO with 0.115nm & 0.05nm respectively. XRD analysis indicates that complete oxidation of graphite to graphene oxide with a slight shift in peak towards the right with an increase in KMnO₄.

#### 2.2.3 Bonding characteristics by FT-IR spectroscopy

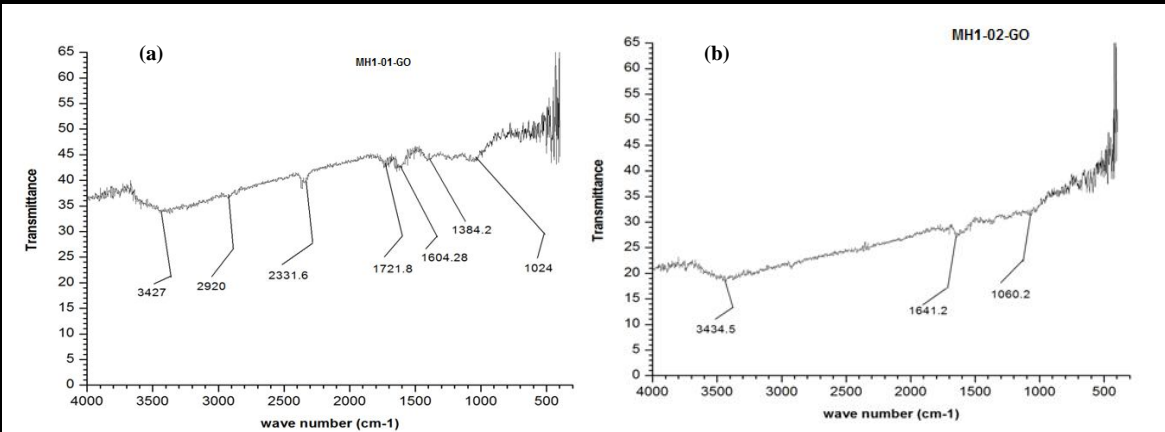


**Fig: 2.2.3** FT-IR plots of GO (without vacuum) with (a) low and (b) high KMnO<sub>4</sub> by conventional Hammer's method.

Fig. 2.2.3 (a) & (b) shows the FT-IR analysis of the GO samples MH1-01-GO and MH1-02-GO respectively with low and high KMnO<sub>4</sub> without vacuum. Oxidation of graphite by conventional Hummer's method from FTIR analysis observed the presence of different functional groups 3427cm<sup>-1</sup> due to the hydroxyl (-OH) groups, carbonyl (C=O) at 1384.2cm<sup>-1</sup>& 1024cm<sup>-1</sup> and carboxyl (-COOH) groups.

#### 2.2.4 Raman analysis

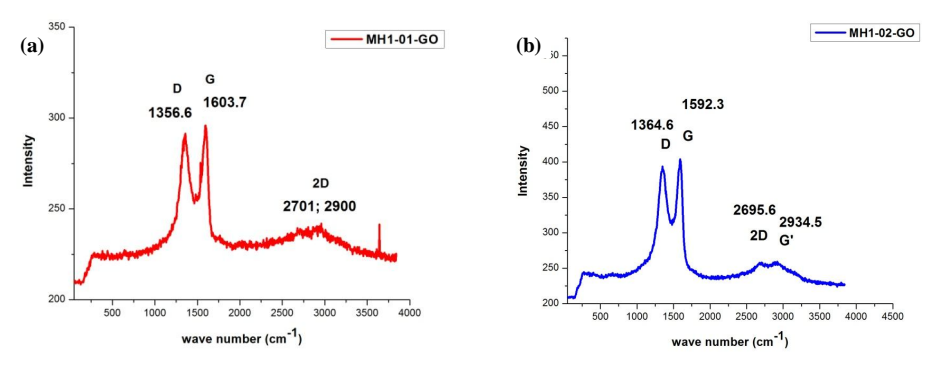


**Fig: 2.2.4** Raman analysis of GO (a) low KMnO<sub>4</sub> (MH1-01-GO) (b) high KMnO<sub>4</sub> (MH1-02-GO by conventional Hummer's method.

Fig. 2.2.4 (a) and (b) shows Raman analysis of GO (without vacuum) samples with low and high concentrations of oxidizing agent i.e.,  $KMnO_4$  where D-band at 1356.6cm<sup>-1</sup> and G-band 1603.7cm<sup>-1</sup> with the 2D-band at 2701cm<sup>-1</sup>& 2900cm<sup>-1</sup>. It is observed that the D-peak shifts towards right higher wave numbers because the formation of defects and  $I_D/I_G$ 

ratios are found to be 0.978 & 0.976 for the samples MH1-01-GO and MH1-02-GO respectively.

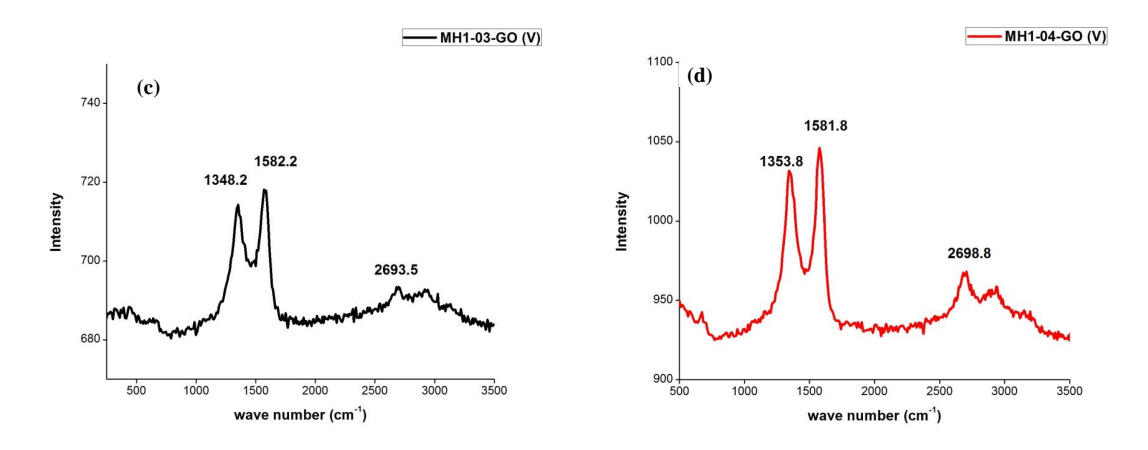


**Fig: 2.2.4** Raman analysis of GO (c) low KMnO<sub>4</sub> (MH1-03-GO) (d) high KMnO<sub>4</sub> (MH1-04-GO) by conventional Hummer's method.

Fig. 2.2.4 (c) & 22..4 (d) shows there is no much difference in a shift of D- peak wrt graphite structure when compared with the samples MH1-03-GO and MH1-04-GO respectively. There is a rise in the D and G band intensities with an increase in the KMnO<sub>4</sub>.

## 2.2.5. Morphology analysis by TEM

**TEM sample preparation:** GO of 0.5mg taken in 50ml of water and ultrasonication carried out for 10-15min.

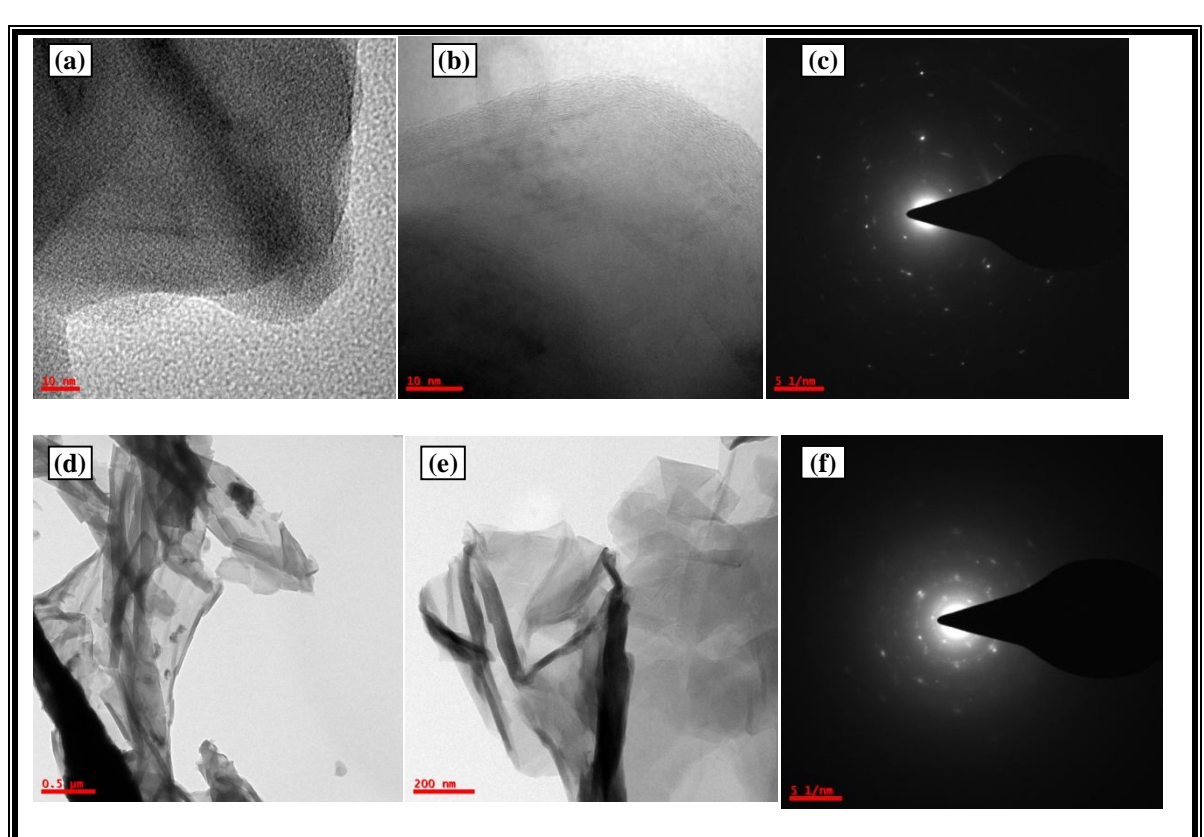


**Fig: 2.2.5** TEM image analysis of GO (a), (b) & (c) low KMnO<sub>4</sub> (without vaccum) and (d), (e), (f) high KMnO<sub>4</sub> (without vaccum) by conventional Hammer's method.

From Fig. 2.2.5 (a-c) shows the TEM analysis of GO samples MH1-01-GO & Fig. 2.2.5 (d-f) for MH1-02-GO with low and high amounts of oxidizing agent. We can observe that GO with thick sheets and multilayered structure from fig. 2.2.5 (a-c) from HR-TEM image analysis and the SED pattern shows the incomplete oxidation of graphite because of the low amount of KMnO<sub>4</sub>. From fig. 2.2.5 (d-f), we can see more transparent graphene oxidized sheets because there is an increase in oxidation with an increase in the KMnO<sub>4</sub>. We can infer from the fig. 2.2.5 (d) & 2.2.5 (e) that GO with a layered structure, transparent, wrinkles and presence of multi-layered graphene sheets.

#### 2.2.6. FESEM analysis



**Fig: 2.2.6** FESEM image analyses of GO (a), (b) & (c) without vacuum by conventional Hummer's method.

Fig. 2.2.6 shows the graphene oxide synthesized by conventional Hummer's method shows the FESEM image analysis of MH1-02-GO. We observed the oxidized GO wrinkle formation and thin sheets with layered structure morphology.

## 2.3. Synthesis of GO by Modified Hummer's Method (MHM)

#### 2.3.1 Preparation

A glass-beaker containing sulphuric acid was placed in an ice-bath maintained at low temperature (i.e., below 0°C). The graphite powder uniformly dispersed in the above solution by continuous magnetic mixing for 1hr 30min to obtain a uniform reaction mixture. Then potassium permanganate was slowly added and the color of the solution changed to dark greenish and after 15min sodium nitrite (NaNO<sub>2</sub>) added slowly in 2-3steps. The solution color still in dark green after constant stirring for 30min and then turned to brown upon addition of H<sub>2</sub>O<sub>2</sub> slowly drop by drop with a boiling solution and a sudden rise in temperature of 160°C. The rise in temperature slowed down by using 140ml of DI water to maintain room temperature (i.e., 25°C) and the solution

continuously stirred for 1hour 30min and allowed to stay the whole night, separated the settled product by filtration and neutralized to pH 7.

Table: 2.3.1 Synthesis of GO (Vaccum) by Modified Hummer's Method

S.No.	Graphite (gms)	H <sub>2</sub> SO <sub>4</sub> (ml)	KMnO <sub>4</sub> (gms)	NaNO <sub>2</sub> (gms)	H <sub>2</sub> O <sub>2</sub> (ml)	H <sub>2</sub> O (ml)
1.	0.3689	23	1.18931	0.18479	10	140
2.	0.3078	7.0794	0.99372	X	5	70

Table 2.3.1 shows the GO synthesis with higher and lower amounts of  $H_2SO_4$  (ml),  $H_2O_2$  (ml) and  $H_2O$  (ml) keeping the conventional ratio of graphite to KMnO<sub>4</sub> (1:3) constant. GO synthesized by using the Modified Hummer's Method (MHM) were studied by XRD, Raman, TEM and FT-IR.

#### Block diagram of GO synthesis by Modified Hummer's Method

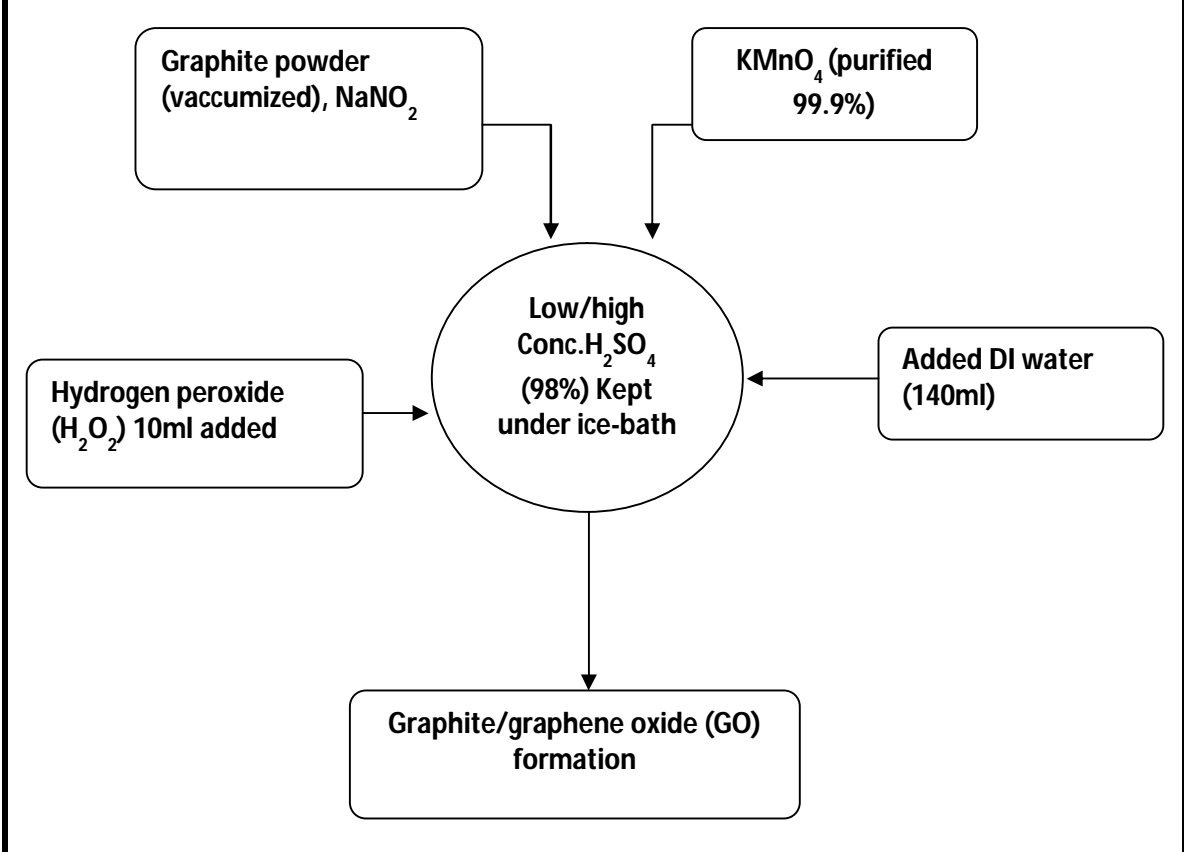


Fig: 2.3.1 Synthesis of GO (Vaccum) by Modified Hummer's Method.

Fig. 2.3.1 represents the block diagram of GO synthesized by using Modified Hammer's method where thelow and high amount of sulphuric acid (H<sub>2</sub>SO<sub>4</sub>) used during the GO synthesis.

#### 2.3.2. XRD analysis

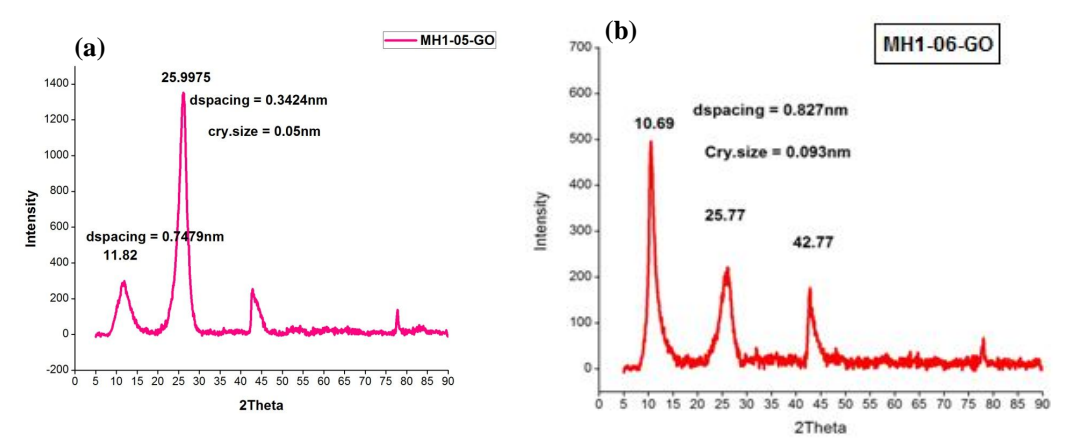
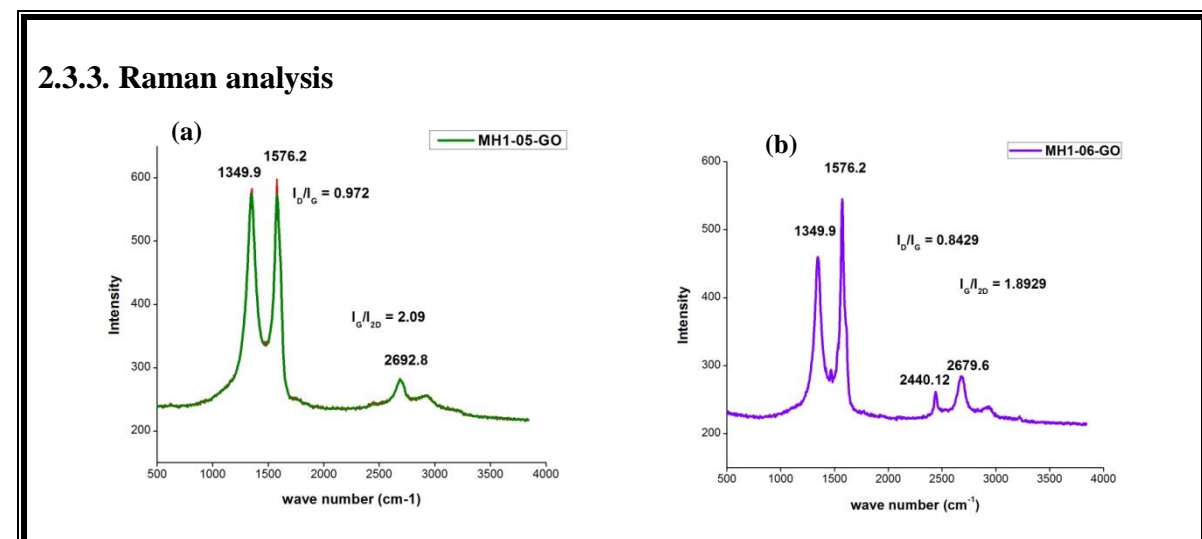


Fig: 2.3.2 XRD analysis of GO with (a) high and (b) low H<sub>2</sub>SO<sub>4</sub> by Modified Hummer's method.

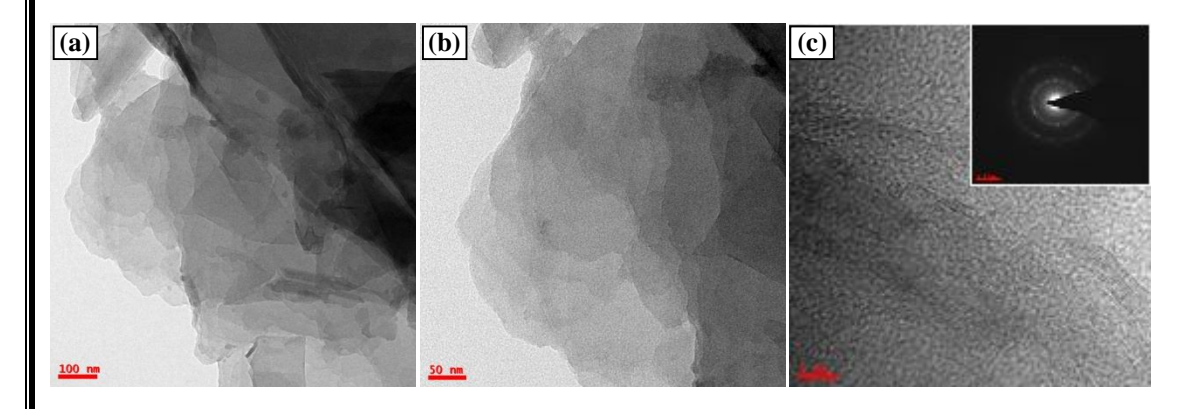
Fig. 2.3.2 shows the MH1-05-GO and MH1-06-GO samples with the high and low amount of  $H_2SO_4$ . Fig. 2.3.2 (a), XRD analysis observed oxidation of graphite with a higher amount of sulphuric acid with 1:3 ratio of graphite to KMnO<sub>4</sub>. It is observed the two peaks from fig. 2.3.2 (a) possess  $2\Box$  positioned at  $11.8^{\circ}$  partially oxidized &25.9° from the XRD peak obtained due to the incomplete oxidation with d-spacing values 0.75nm and 0.34nm respectively. From fig. 2.3.2 (b), it is inferred that the oxidation of the graphite to GO with a lower amount of  $H_2SO_4$  with  $10.69^{\circ}$  obtained MH1-06-GO with an increase in interplanar spacing of 0.827nm when compared to MH1-05-GO.



**Fig: 2.3.3** Raman analysis of GO (a) high and (b) low H<sub>2</sub>SO<sub>4</sub> by Modified Hummer's method (MHM).

Fig. 2.3.3 shows the Raman analysis of MH1-05-GO (high  $H_2SO_4$ ) and MH1-06-GO (low  $H_2SO_4$ ) by MHM method. It is observed the rise in D-intensity with  $I_D/I_G$  is 0.972 because of increase in the defects due to the oxidation of graphite to obtain MH1-05-GO and the sample from fig. 2.3.3(b) observed that D-band intensity is low and  $I_D/I_G$  value is 0.8429 when compared with MH1-05-GO. There is no such shift in the D & G-band intensities for the samples MH1-05-GO & MH1-06-GO whereas the 2D-band intensities are at 2693cm<sup>-1</sup> and 2440cm<sup>-1</sup>& 2680cm<sup>-1</sup> with an increase in the  $I_G/I_{2D}$  ratios are 2.09 and 1.89 respectively.

# 2.3.4. TEM analysis



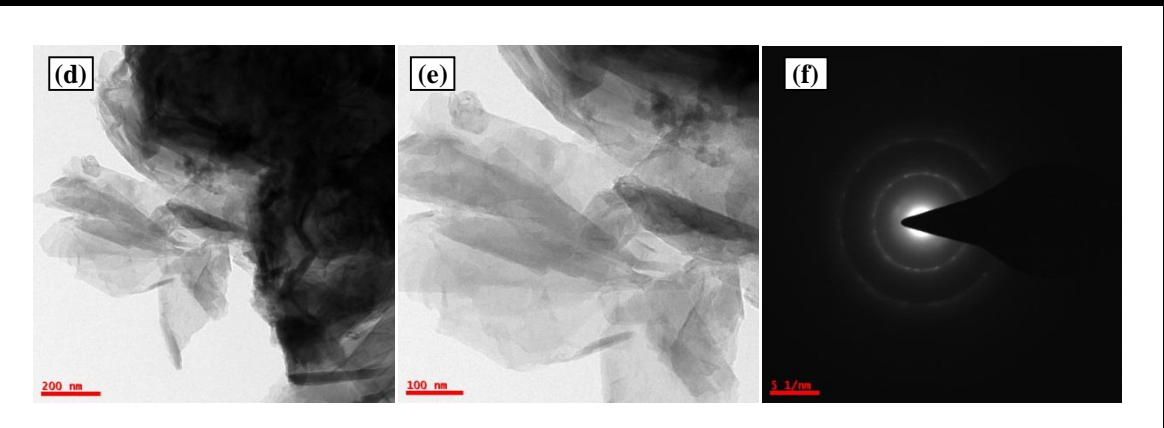


**Fig: 2.3.4** TEM analysis of GO (a-c) high and (d-f) low H<sub>2</sub>SO<sub>4</sub> by Modified Hummer's method (MHM).

Fig. 2.3.4 shows the structure and morphology of TEM analysis. As shown in the Fig. 2.3.4 (a-c), for the sample MH1-05-GO and fig. 2.3.4 (d-f) MH1-06-GO respectively. We can observe the sample with thick graphene sheets from fig. 2.3.4 (a & b) and the 2.3.4 (c) infers the sample MH1-05-GO with multi and few-layered structures from HR-TEM image analysis and the SED observed that the GO obtained from the synthesis with ahigh amount of H<sub>2</sub>SO<sub>4</sub> is amorphous in nature. From the fig. 2.3.4 (d-f), GO obtained with allow amount of sulphuric acid are more transparent with very thin graphene oxide sheets with amorphous SED pattern are afew-layered structure from HR-TEM image analysis.

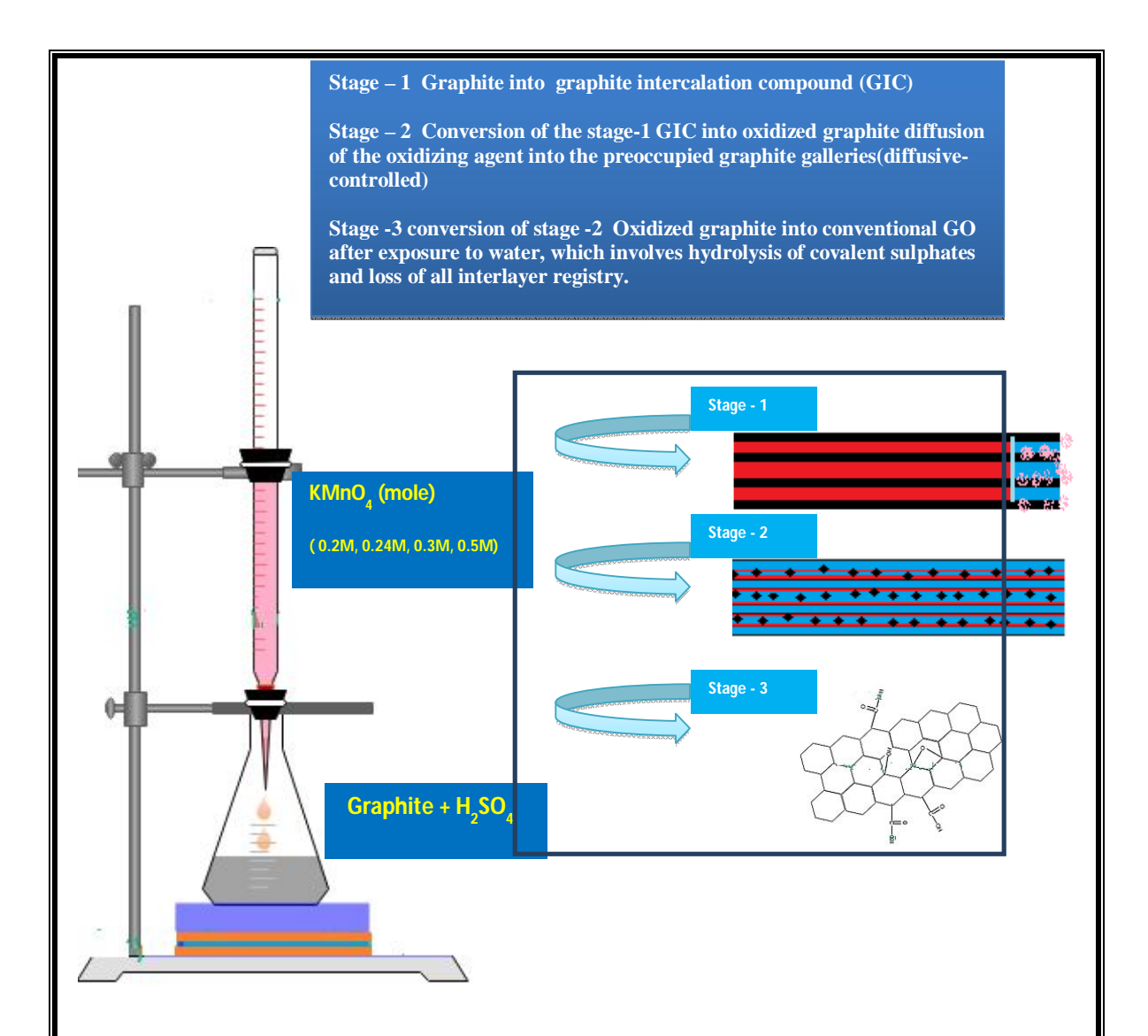
# **2.4.** Synthesis of GO by Volumetric Titration- Modified Hummer's Method (VT-MHM)

#### 2.4.1. Synthesis of GO in the absence of GO

#### **Preparation**

Graphite powder of 0.3161gms in 10ml of sulphuric acid was taken in a 250ml of glass beaker constantly stirred for 1hour and then potassium permanganate (0.25M) solution of 8ml was added slowly for 20min by using volumetric titration process as

shown in Fig. 2.4.1. The color of the solution changed from black to dark greenish and continuous stirring for 1hour then followed by the addition of 5ml hydrogen peroxide. Then, 70ml of DI water was added and subjected to magnetic stirring at 30°C temperature for 1hour. It was allowed to settle down GO whole night and then filtered the product by filtration using a Wittmann paper (45micron). Finally, the sample was collected and neutralized with 5%HCl, DI water and methanol. The sample dried on hot-plate and placed in an oven @ 50°C for 24hrs to remove traces of moisture content. In this process NaNO<sub>2</sub>/NaNO<sub>3</sub> was not added during synthesis. The complete oxidation of the graphite was carried out from the controlled addition of KMnO<sub>4</sub> by using volumetric titration approach. Hence, our method is completely the modified form of existing Hummer's method.

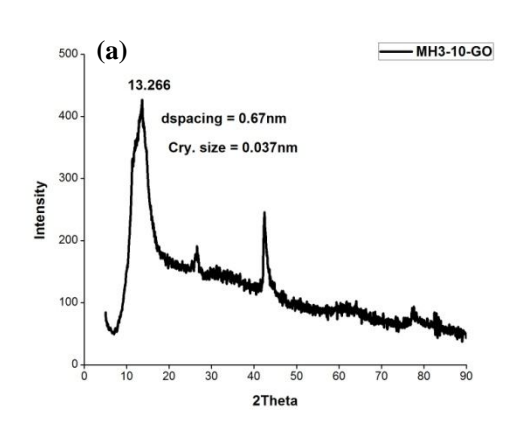


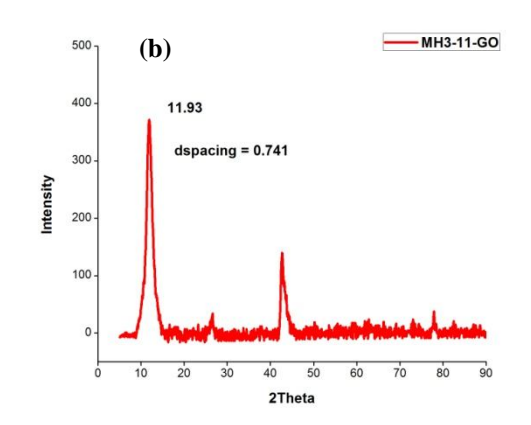
**Fig.2.4.1**Graphical representation of (a) Volumetric Titration method to synthesize graphene oxide (GO) at room temperature (without any ice-bath or addition of NaNO<sub>3</sub>) (b) schematic for the mechanisms of formation GO by VTM.

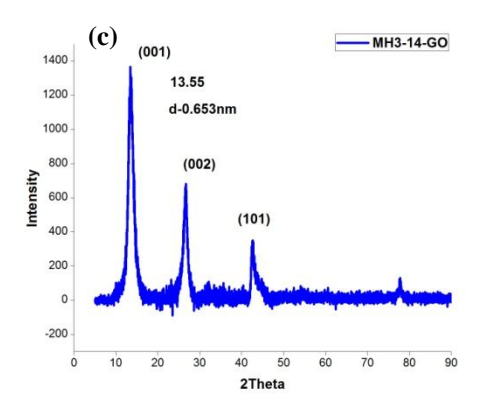
Table 2.4.1 shows the list of synthesis parameters that were used for different GO samples prepared by volumetric titration approach.

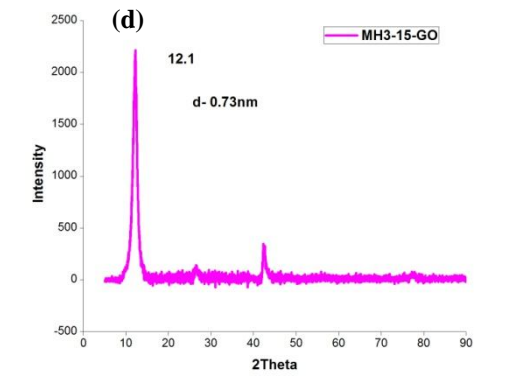
Table 2.4.1 List of GO synthesis by Volumetric Titration-MHM							
S.No.	Sample ID	Graphite (gms)	H <sub>2</sub> SO <sub>4</sub> (ml)	Volume of KMnO <sub>4</sub> (ml)	H <sub>2</sub> O <sub>2</sub> (ml)	H <sub>2</sub> O (ml)	
1.	MH3-10-GO	0.17302	10	8.0	5	70	
2.	MH3-11-GO	0.1764	11	9.5	5	70	
3.	MH3-14-GO	0.3717	10	22	5	50	
4.	MH3-15-GO	0.3714	21	36	5	50	
5.	MH3-16-GO	0.1762	10	15	5	50	
6.	MH3-17-GO	0.1789	20	15	5	50	

# 2.4.2 XRD structural analysis









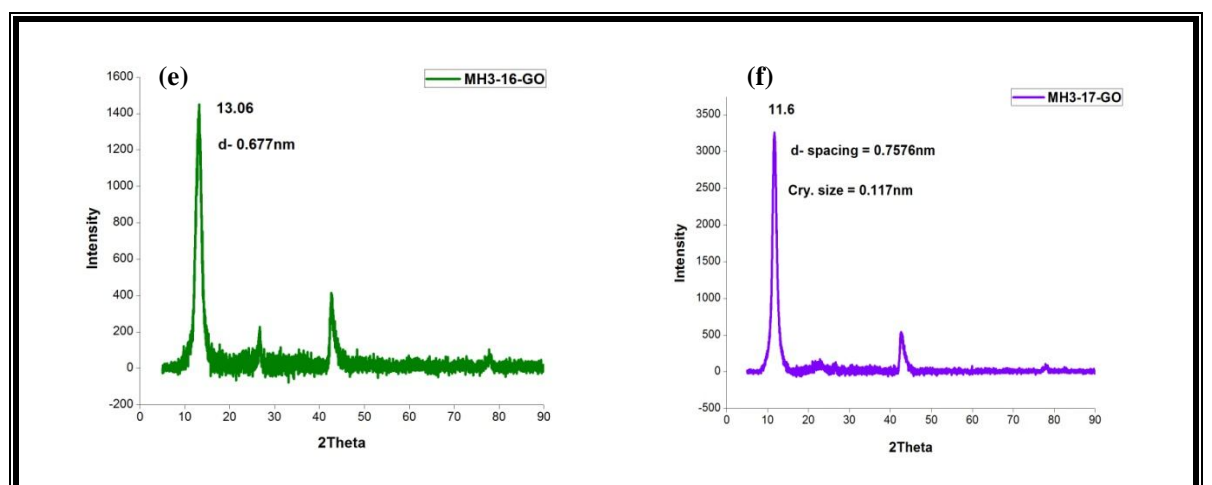


**Fig. 2.4.2** XRD analysis of the GO synthesis by Volumetric Titration -MHM method (a) MH3-10-GO (b) MH3-11-GO (c) MH3-14-GO (d) MH3-15-GO (e) MH3-16-GO (f) MH3-17-GO.

Fig. 2.4.2 shows the XRD analysis of GO samples obtained from Volumetric Titration – Modified Hummer's Method (VT-MHM). From the above XRD analysis we observe the effect of d-spacing with varying the ratio of KMnO<sub>4</sub> and  $H_2SO_4$  during the reaction process. The samples when compared withthe Table 2.4.1, MH3-10-GO and MH3-11-GO we observe the increase in d-spacing with an increase in oxidizing agent. Further, when the samples MH3-14-GO & MH3-15-GO are compared keeping the amount of graphite precursor constant, we confirm that there is an increase in inter-planar distance with partial oxidation at 13.55° with d-spacing of 0.653nm from the sample MH3-14-GO and complete oxidation with  $2\Box = 12.1$ ° and d-spacing is 0.73nm from Table 2.4.1. From Fig. 2.4.2 (e) and Fig. 2.4.2 (f), we confirm that complete oxidation of the samples with  $2\Box$  at 13.06° & 11.6° and inter-planar spacing i.e., d-spacing values are 0.677nm & 0.757nm respectively.

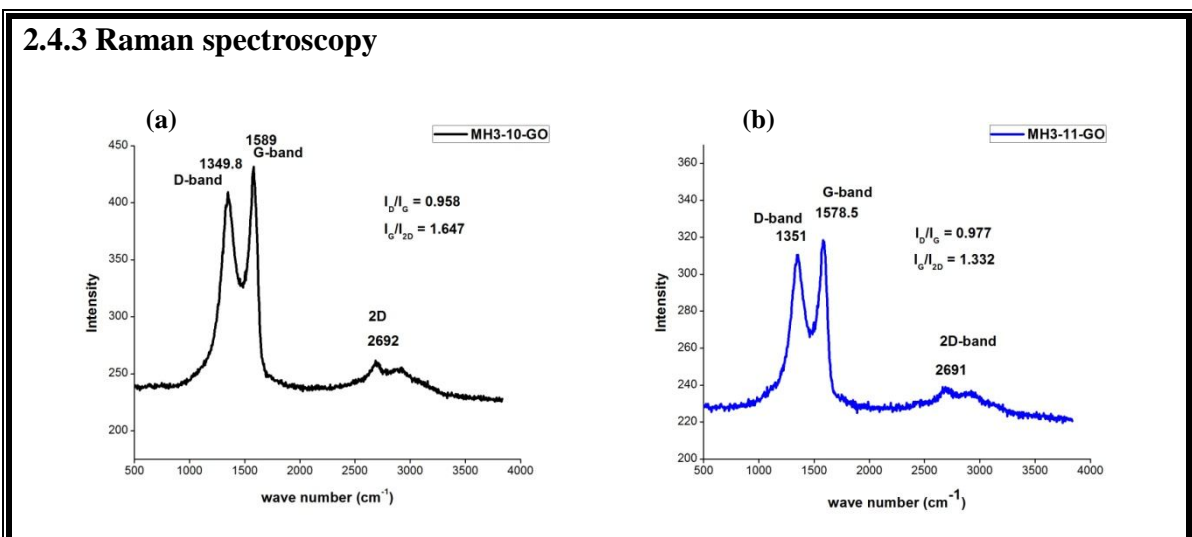


**Fig. 2.4.3** Ramananalysis of GO by Volumetric Titration -MHM method (a) MH3-10-GO (b) MH3-11-GO.

Fig. 2.4.3 shows the Raman spectroscopy data analysis of samples MH3-10-GO and MH3-11-GO. The GO samples obtained by volumetric titration- MHM observed with decrease in D-band intensity of MH3-10-GO when compared with MH3-11-GO and the shift in D-peak towards left positioned at 1349.8cm<sup>-1</sup> and G-peak to higher wave numbers of 1589cm<sup>-1</sup> and we can infer that retain in graphitic structure with the rise in 2D-peak at 2692cm<sup>-1</sup>. We observe from fig. 2.4.3 (b) with D & G bands at 1351cm<sup>-1</sup> & 1578.5cm<sup>-1</sup> where there is a minor move in peak and rise in 2D-peak at 2691cm<sup>-1</sup> and we can observe the increase in defects with an increase in oxidizing agent.

#### 2.4.4 FT-IR analysis MH3-11GO-(b) MH3-14-GO-(c) MH3-15GO-(d) 80 MH3-16-GO-(e) MH3-17-GO-(f) 75 1385.6 1044 1629 Transmittance (%) 70 3426 65 (d) (c) 55 4000 3500 3000 2500 2000 1500 1000 Wavenumber (cm-1)

**Fig. 2.4.4** FT-IRstudyof GO by Volumetric Titration -MHM method (a) MH3-10-GO (b) MH3-11-GO (c) MH3-14-GO (d) MH3-15-GO (e) MH3-16-GO (f) MH3-17-GO.

Fig. 2.4.4 shows the FT-IR analysis of GO samples obtained by Volumetric Titration-Modified Hummer's method. We observe the functional groups attached due to the oxidation with anincrease in the oxidizing agent. The GO samples obtained characterized by ft-IR analysis from the above fig. 2.4.4, we infer GO obtained possess 77% transmittance for the sample MH3-10-GO whereas the samples from Fig. 2.4.4 (b-e) observed with decrease in %transmittance with an increase in the KMnO<sub>4</sub>. GO obtained with hydroxyl (–OH) functional groups at 3426cm<sup>-1</sup>, carbonyl (C=O) at 1385.6cm<sup>-1</sup> and 1629cm<sup>-1</sup> due to the C-C aromatic structure of the samples.

# 2.4.5 UV-spectroscopy

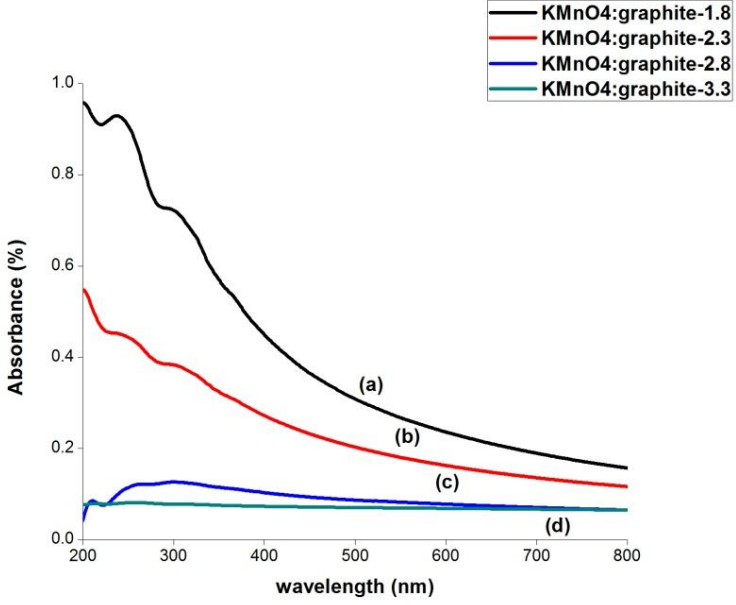


**Fig. 2.4.5** UV-spectroscopy of GO samples aqueous dispersion (a) MH3-10-GO (b) MH3-11-GO (c) MH3-14-GO and (d) MH3-16-GO.

UV-visible spectroscopic examination of graphene oxide exhibits two characteristic peaks at 231nm & shoulder peak ~300nm which are associated with  $\pi$  to  $\pi^*$  transitions of aromatic C-C and n to  $\pi^*$  transition of C=O bonds respectively. GO aqueous dispersions results the effect of KMnO<sub>4</sub> with lower concentrations undergoes the rearrangement reaction. UV analysis shows the partial re-conjugation of  $\pi$ -network during oxidation and GO is observed to be more stable may be due to the formation of epoxide and ether functional groups confirmed from the *ft-IR* analysis. With an increase in KMnO<sub>4</sub> (mol%), the absorbance (%) decreases. The GO synthesized with higher mole (%) of KMnO<sub>4</sub> i.e., samples S3 & S4 confirmed the increase in extent of oxidation with the different functional groups such as -OH, C=O, -COOH, C-O-C and -COOR etc., whereas the GO with highly unstable as observed from the UV- spectroscopic analysis.

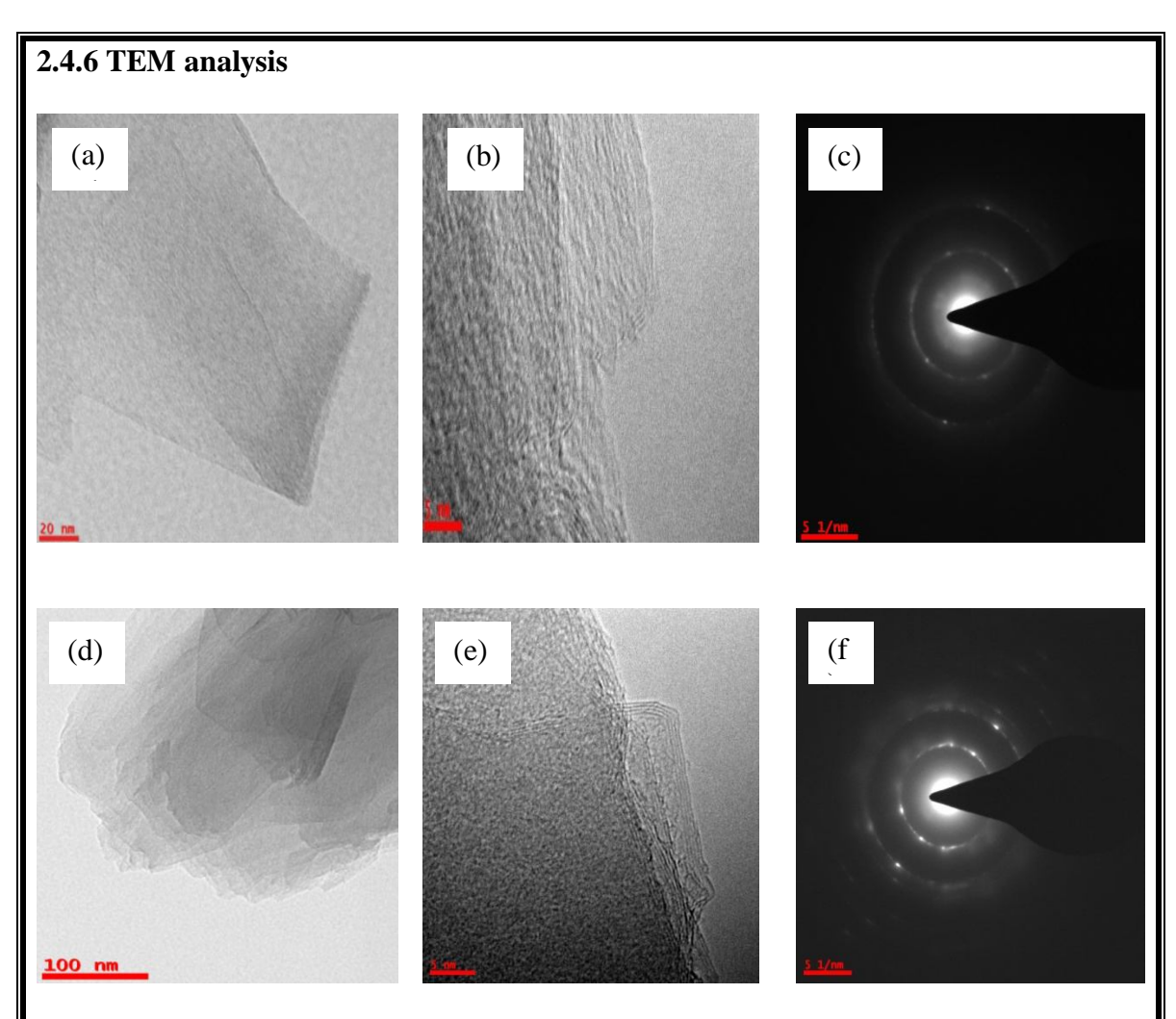


Fig. 2.4.6 TEM analysis represents MH3-10-rGO-HH (a-c) and (d-f) for MH3-11-rGO-HH samples.

From the above TEM analysis, Fig. 2.4.6 (a) shows the flat transparent layered large-sizegraphene sheets and the sample Fig. 2.4.6 (b) observed with 2-3 layered structure from HR-TEM images and the SED pattern with semi-crystalline rGOnanosheets from the Fig. 2.4.6 (c), (a) and (b) observed with transparent graphene sheets and few-layeredgraphene sheets respectively and the SED pattern is crystalline as seen from Fig. 2.4.6 (c).

# 2.5 Synthesis of GO by Volumetric Titration-MHM (VT-MHM) with the presence of $NaNO_2$

#### **Preparation**

Initially 10ml of sulphuric-acid was taken in a conical flask maintained at room temperature. Then graphite powder was added followed by the addition of sodium nitrite (NaNO<sub>2</sub>) and continuously stirred for an hour then the temperature was ~35°C. After the complete uniform dispersion then KMnO<sub>4</sub> (0.25M) was added slowly by using volumetric titration approach as shown in Fig. 2.4.1. The temperature was slowly raised to  $58^{\circ}$ C- $60^{\circ}$ C and further addition of KMnO<sub>4</sub> slowly decreased the temperature to  $40^{\circ}$ C and stirred for 2hrs continuously at this temperature. Then 5ml of H<sub>2</sub>O<sub>2</sub> solution ( $30_{\text{V}/\text{V}}\%$ ) was added slowly we observed there is a rise in temperature of 5-10C° and 70ml of water with constant stirring for 1hour GO was formed and allowed to settle for overnight and separated the product, filtered, dried on hot-plate and heated in oven @50°C under vacuum for 24hrs.

#### 2.5.1 X-ray Diffraction analysis

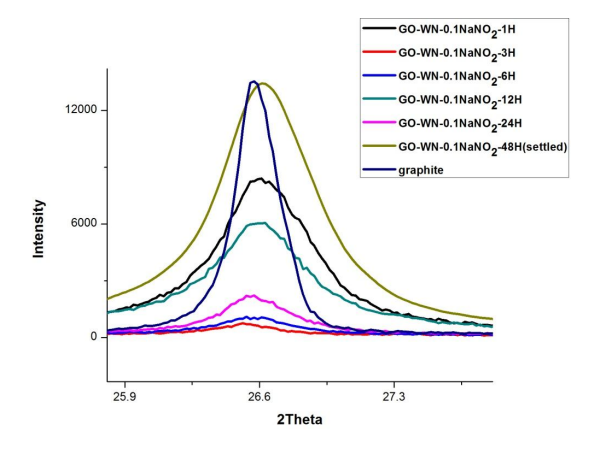
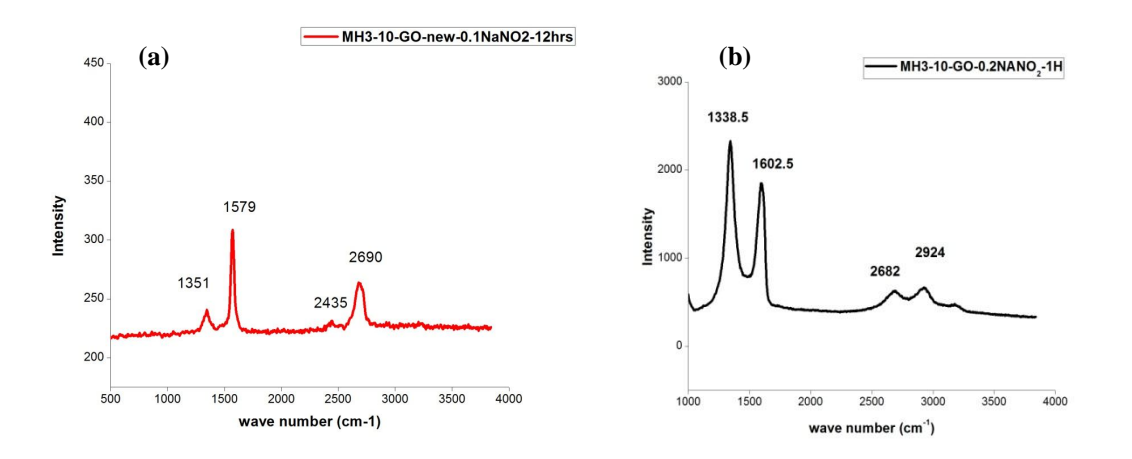


Fig. 2.5.1 XRD analysis of MH3-10-GO-WN samples with varying oxidation time.

From the Fig. 2.5.1, XRD analysis shows GO obtained in the presence of NaNO<sub>2</sub> from VT-MHM with different oxidation time. GO formed on the surface of solution mixture was collected after an hour was subjected to characterization for XRD analysis. From the Fig.2.5.1, we observe the exfoliation of graphite with different oxidation time i.e., 1H, 3H, 6H, 12H and 24H and 48Hrs. We observe that there is no change in the position of  $2\Box$  but as the oxidation time is increased, the peak broadened is found implies the number of layers decreases and very thin sheets of graphene layers is obtained.

#### 2.5.2 Raman spectroscopy



**Fig. 2.5.2** Raman data analysis of MH3-10-GO-WN oxidation time 12Hrs (a) 0.1 NaNO<sub>2</sub>& (b) 0.2NaNO<sub>2</sub>.

From Fig.2.5.2 Raman analysis, the sample MH3-10-WN-12Hrs shows D, G and 2D-bands are at 1351cm<sup>-1</sup>, 1579cm<sup>-1</sup> and 2435 & 2690 cm<sup>-1</sup> respectively. We observe from Fig.2.5.2 that there is no rise in D-band intensity which shows minimum defects and rise in G-band observed favors graphitic structure. Fig.2.5.2. (a) & (b) shows the rise in D-band and fall in G-band intensities infers generation of defects with an increase in the amount of NaNO<sub>2</sub> during the synthesis process. The decrease in graphitic structure G-

band towards right at 1602.5cm<sup>-1</sup> and rise in 2D, G`-bands are at 2682cm<sup>-1</sup>, 2924cm<sup>-1</sup> respectively found with change in structure and morphology due to the sudden rise in temperature in the presence of NaNO<sub>2</sub>which enhance therate of reaction. Hence, it is possible that more defects/disordered are formed in this process.

#### 2.5.3 FT-IR analysis

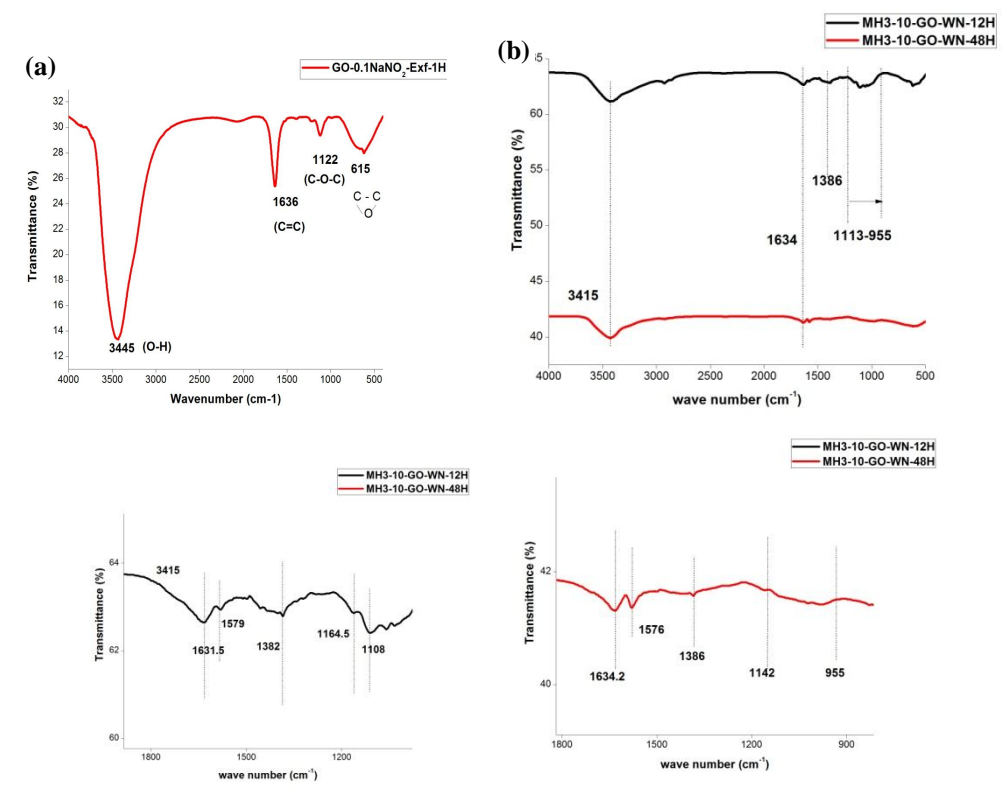


**Fig.2.5.3** FT-IR spectral analysis of sample MH3-10-GO-WN with 0.1 and 0.2weight fraction of NaNO<sub>2</sub>.

FT-IR analysis of MH3-10-GO-WN with 0.1NaNO<sub>2</sub> shows the GO with functional groups such as major with hydroxyl (–OH), carbonyl (C-O-C) and (C=O) and minor with aromatic structure C=C i.e., sp<sup>2</sup> bonded structure. As the oxidation time is increased there is a decrease in the extent of oxygen functional groups of the GO sample in the presence

of NaNO<sub>2</sub> and the transmittance of the bulk sample is decreased when compared to the exfoliated sample.

#### 2.5.4 UV-spectroscopy

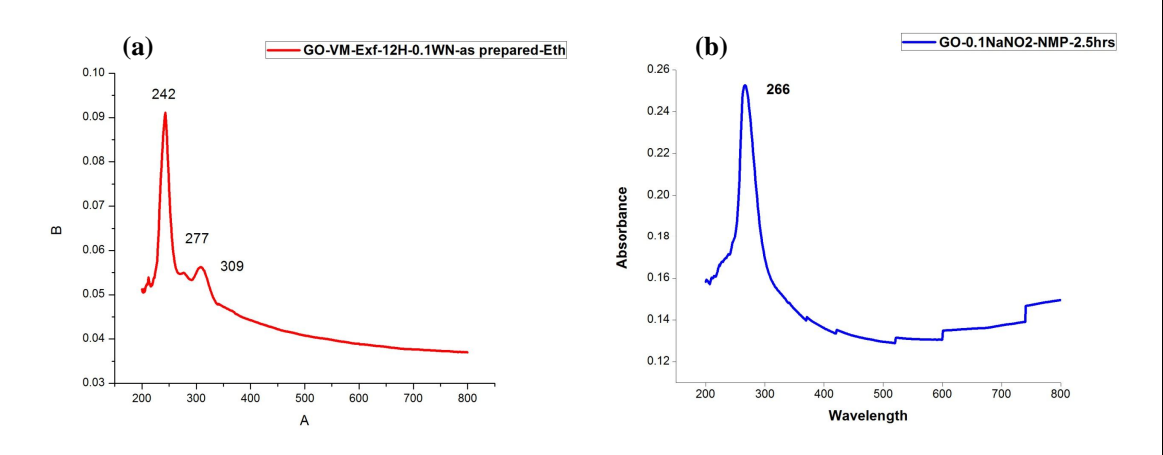


**Fig. 2.5.4** UV analysis of GO in different solvents (a) MH3-10-GO-WN-EthOH (b) MH3-10-GO-WN-NMP.

The above Fig. 2.5.4 shows the UV-spectroscopy analysis of the samples MH3-10-GO-WN-EthOH and MH3-10-GO-WN-NMP. We observe from Fig. 2.5.4 (a) that two characteristic peaks obtained in which excitation of n to  $\pi$  transitions at 242cm<sup>-1</sup> and277cm<sup>-1</sup> because of the presence of hydroxyl (OH) groups as confirmed from Fig. 2.5.3 (a) *ft-IR* analysis whereas  $\pi$  to  $\pi$ \* transitions corresponds to the peak at 309cm<sup>-1</sup> is obtained due to the partial reduction in ethanol dispersion by ultrasonication. The sample Fig. 2.5.4 (b) shows the single peak at 266cm<sup>-1</sup> because of  $\pi$  to  $\pi$ \* transitions from the sample MH3-10-GO-WN by complete reduction in NMP dispersions.

#### 2.5.5 Transmission Electron Microscopy (TEM)

Sample preparation: GO sample in the presence of NaNO<sub>2</sub> taken in NMP solvent and sonicated by using ultrasonication bath for homogenous exfoliated GO sheets dispersion.

The sample prepared by drop casting on si/glass substrate and evaporated the solvent at 50°C on hot-plate.

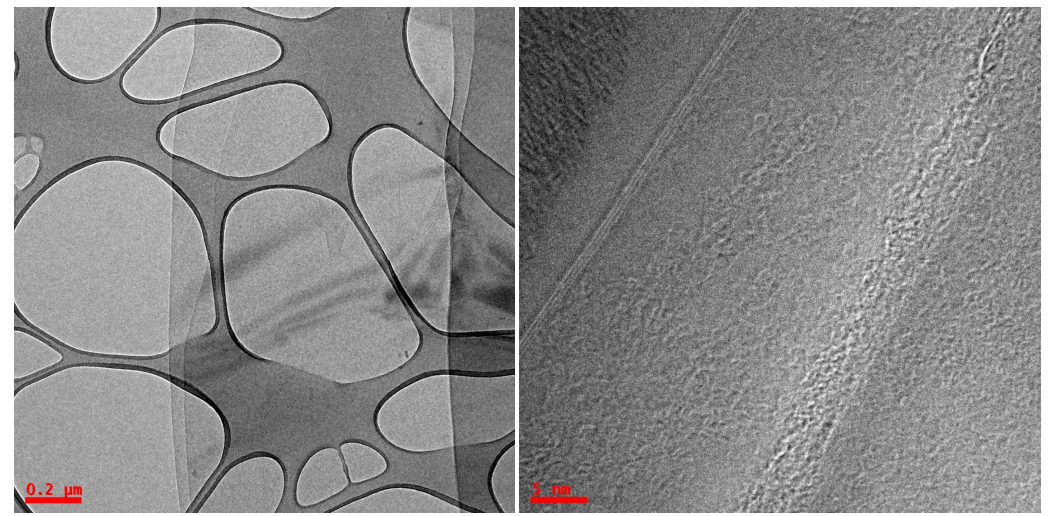


Fig. 2.5.5 TEM analysis of GO with NaNO<sub>2</sub> by using VT-MHM in NMP solvent system.

From the above Fig. 2.5.5 TEM image analysis, GO synthesized in presence of sodium nitrite shows the exfoliated large graphene sheets with highly transparent with bi, tri or few-layered nanostructure from the HR-TEM image analysis.

#### 2.6 Conclusions

Graphene oxide synthesized by different chemical methods using Conventional Hummer's method and Modified Hummer's method by varying the amount of oxidizing agent i.e., potassium permanganate &sulphuric acid and studied the effect of structure and morphology by XRD analysis, defects by Raman analysis, functionality by FT-IR analysis with low and high amount of oxidizing agent. The effect of anincrease in the oxidizing agent increase the extent of oxidation and increase in the defects formation with the layered morphology as observed from SEM,transparent wrinkled morphology, thick sheets may be due to un-oxidized GO synthesis as confirmed from the TEM

analysis and highly unstable by UV-spectroscopy. In order to minimize the disorder or defects in the GO synthesis, we have developed a novel approach of GO synthesis process without usingNaNO<sub>2</sub>/NaNO<sub>3</sub> during the oxidation reaction which evolves the toxic gases such as NO2 and N2O4 and also our process was carried out without maintaining zero temperature. The effect of KMnO<sub>4</sub> on the extent of oxidation was investigated by using different mole ratios of KMnO<sub>4</sub> (0.25M) solution. XRD analysis reveals that increase in oxidation with an increase in the oxidizing agent alters the spacing and an increase in inter-planar spacing are observed for the sample with 0.24mole ratio having spacing value of 0.74nm and decrease in interlayer distance further addition of KMnO<sub>4</sub> solution. The characterization techniques used for the study of the samples by using FT-IR, Raman, SEM, TEM, UV-spectroscopy analysis. Further studied the effect of NaNO<sub>2</sub> during the synthesis of GO by using VT-MHM and analyzed by different characterization techniques and the TEM analysis shows highly transparent large graphene sheets are obtained utilized for various applications. Hence, the synthesis of GO in the absence of toxic gases during synthesis with high transparency was observed from the FT-IR analysis and highly stable material from UV-analysis and minimum defects/disordered structure from Raman and transparent graphene sheets from TEM image analysis is a commercially viable and economical way of a synthesis route for many industrial applications. Therefore, the GO synthesis by using volumetric titration method in the absence of GO with fewer defects/disordered structure is a facile and commercially viable method useful for wide applications.

## Chapter-3

## **Synthesis of Reduced Graphene Oxide (GO)**

## 3.1. Introduction

This chapter deals with the reduction of GO by using different reducing agents such as hydrazine hydrate (NH<sub>2</sub>-NH<sub>2</sub>.H<sub>2</sub>O) and sodium borohydride (NaBH<sub>4</sub>). The as-obtainedrGO samples were investigated by XRD, FT-IR, Raman, SEM, TEM and UV-spectroscopy. Here, we discussed the reduction process of the GO samples obtained from Hummer's, modified Hummer's and our novel approach volumetric titration method and characterization of the corresponding reduced graphene oxide (rGO) samples obtained by the reduction process.

## 3.2. Synthesis of reduced Graphene Oxide (rGO) by different Reducing **Agents** GO sample MHM-1 & MHM-2 DI water Ultrasonication Bath Reducing agents $NH_2 = NH_2$ (or) NaBH<sub>4</sub> (or) NH<sub>3</sub> GO/DI water based sample added Condensation process with the reducing agent **Parameters** 1. Temperature - 85 C Slowly the black ppt. cooling time - 120min Settles out Sonication-80min Filtrate collected by centrifugation 1st Step 2<sup>nd</sup> step **Final** DI water **HCl** Methanol Vacuum drying 10min & hot plate

Fig. 3.2.1 Flow diagram represents a synthesis of RGO by using different reducing agents.

# 3.2.1. The experimental procedure of reduction process by using Sodium borohydride ( $NaBH_4$ )

**Table: 3.2.1.** Reduction of Graphene oxide by sodium borohydride (NaBH<sub>4</sub>)

Sl.No	Sample code	Amount of GO (gms)	Sodium borohydride (gms)	DI water (ml)	Temperatur e (°C)
1	MH1-01-RGO-NB	9.375	0.075	9.4	80
1.	WIIII-UI-KUU-ND	9.373	0.073	9.4	80
2.	MH1-02-RGO-NB	9.375	0.075	9.4	80
3.	MH1-03-RGO-NB (V)	0.1507	0.76	150	70
			· · · · · · · · · · · · · · · · · · ·		
4.	MH1-04-RGO-NB (V)	0.15171	0.77	150	70

The GO (MH1-01-GO and MH1-02-GO) powder in gms was taken in a round bottom flask contains DI water such that GO:DI water are in the ratio of 1:1 and subjected to ultrasonication for homogeneous dispersion by using BRANSON 450 sonicatorfor an hour. A clear brown color solution was obtained and then adjusted the pH to 11 by using 5% sodium carbonate (Na<sub>2</sub>CO<sub>3</sub>) solution. Then 0.00075gms of sodium borohydride in 1.875ml of DI water prepared and added to the above solution which was maintained the pH value at 11. Now, the solution kept in an oil-bath @80°C and continuously stirred for 1.5hr. Then after the black color of the solution obtained and subjected to centrifugation, neutralized to pH 7 by using 5% HCl, water and methanol. Finally, the product dried on hot-plate and in an oven @50°C for 24hrs to remove traces of moisture content.

# 3.2.2. Experimental procedure of reduction process by using Hydrazine monohydrate ( $NH_2$ - $NH_2$ - $H_2$ O)

**Table: 3.2.2.** Reduction of Graphene oxide by Hydrazine monohydrate (NH<sub>2</sub>-NH<sub>2</sub>.H<sub>2</sub>O)

Sl.No.	Sample code	Amount of GO (gms)	Hydrazine monohydrate (ml)	DI water (ml)	Temperature (°C)
1.	MH1-01-RGO-HH	0.06225	0.31125	16	90
2.	MH1-02-RGO-HH	0.0245	0.1225	6.2	90
3.	MH1-03-RGO-HH	0.20437	1.0	50	90
4.	MH1-04-RGO-HH	0.2	1.0	50	90

(Assumption: GO:HH = 1:5)

GO samples (i.e.,MH1-01-GO& MH1-02-GO)of 0.06225gms was taken in a round bottom flask which contains 0.31125ml of reducing agent hydrazine monohydrate(78-82%) was added then subjected to 30min ultrasonication and placed in an oil-bath on hot-plate maintained at 90°C under condenser mantle for 24hrs for cooling and a black color reduced graphene oxide solution was obtained. Finally, the black product reduced graphene oxide settled out filtered by centrifugation (3500rpm, 15min), by using vacuum filtration unit, neutralized to pH 7 and dried the sample at 50°C on hot-plate.

# 3.3. Characterization of rGO by using sodium borohydride and hydrazine monohydrate

GO synthesized from Hummer's method subjected to reduction by using sodium borohydride. The list of samples is shown in the above Table 3.2.2.

#### 3.3.1. XRD analysis

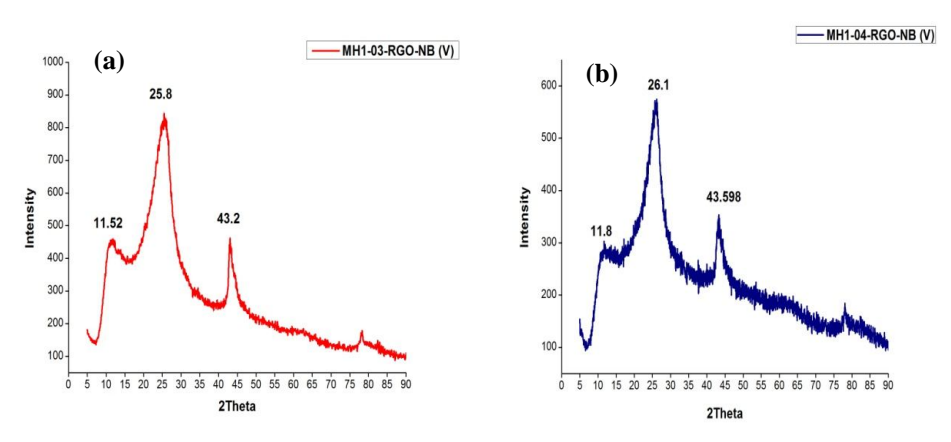


**Fig. 3.3.1** XRD pattern of rGO under vacuum conditions (a) MH1-03-RGO-NB(V) and (b) MH1-04-RGO-NB(V).

Fig. 3.3.1 (a) shows the XRD analysis of reduced graphene oxide (RGO) of MH1-03-RGO-NB(V) and MH1-04-RGO-NB(V) obtained GO from Hummer's method under vacuum conditions. From the Fig. 3.3.1 (a), the peak at 25.8 from MH1-03-GO and Fig. 3.3.1 (b) shows the reduced peak with  $2\Box$  at 26.1° of the sample MH1-04-GO are obtained due to the reduction by using sodium borohydride as a reducing agent.

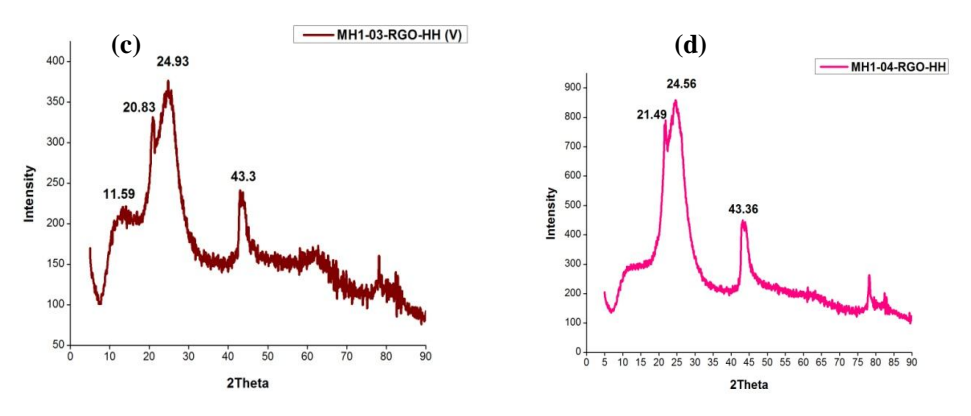


**Fig. 3.3.1** XRD data analysis of RGO under vacuum conditions (c) MH1-03-RGO-HH (V) and (d) MH1-04-RGO-HH.

The Fig. 3.3.1 (c) and (d) shows of MH1-03-RGO-HH and MH1-04-RGO-HH partially reduced graphene oxide by hydrazine monohydrate with the peaks positioned at 24.93° & 20.83° and 24.93° & 24.56° respectively are obtained.

#### 3.3.2. Raman analysis

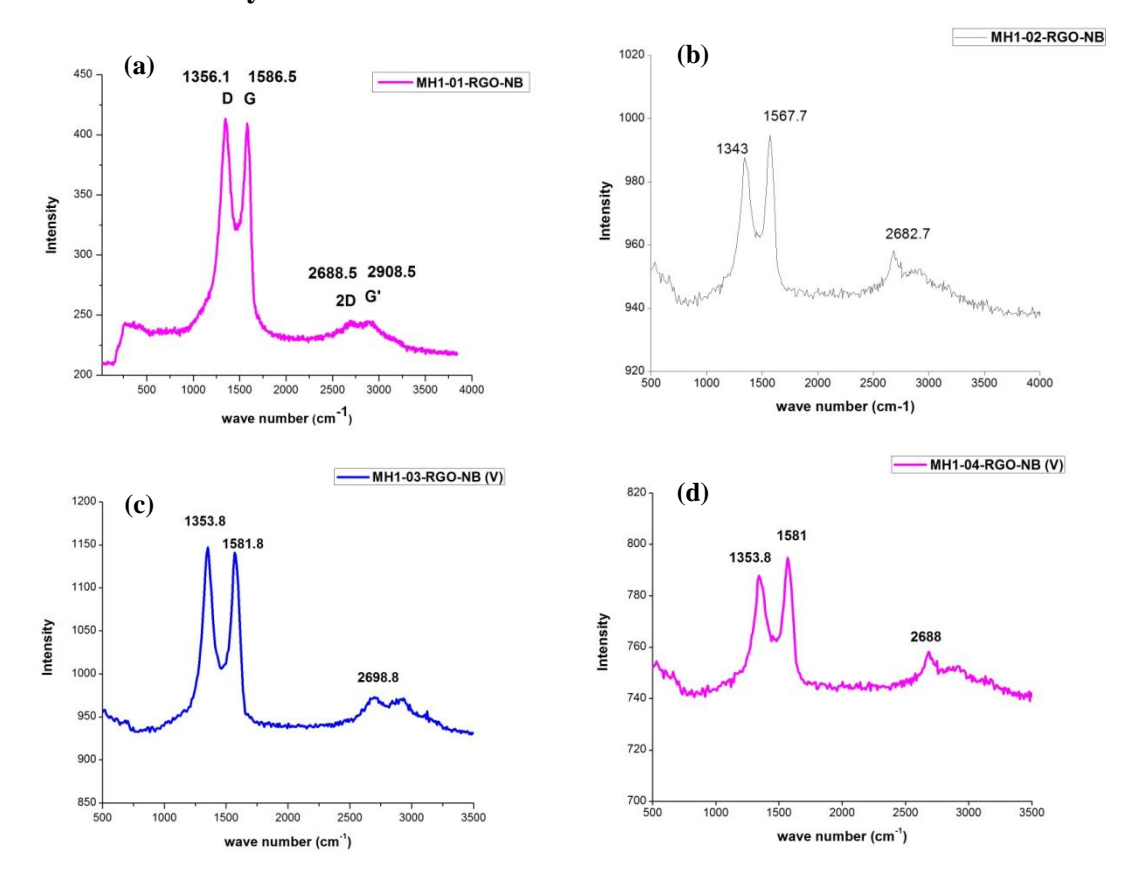
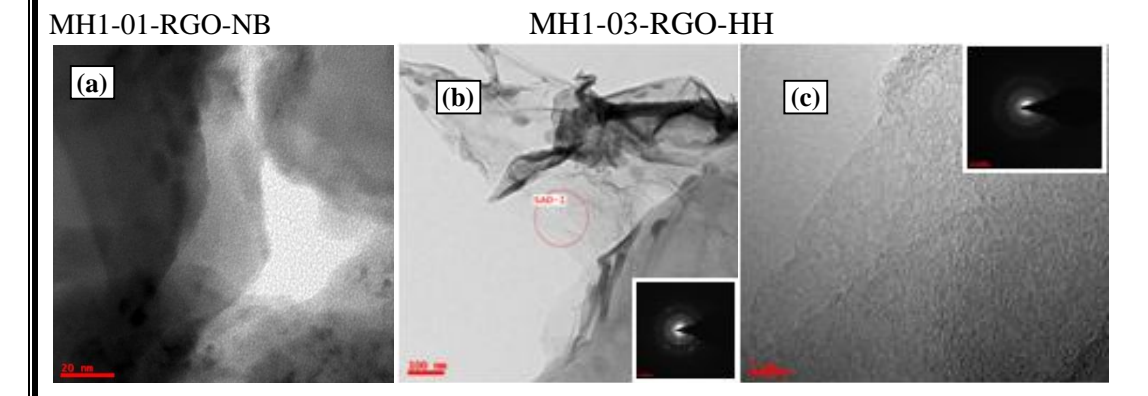


**Fig. 3.3.2** Raman analysis of (a) MH1-01-RGO-NB (b) MH1-02-RGO-NB (c) MH1-03-RGO-NB (V) and (d) MH1-04-RGO-NB (V).

Raman analysis from the Fig. 3.3.2 shows reduced graphene oxide samples obtained from GO synthesized by Hummer's method without vacuum and under vacuum conditions. We can infer from the above results that there is a rise in the D and G-band intensities such that with allow amount of oxidizing agent upon reduction increase the smaller  $sp^2$  domain with an increase in the  $I_D/I_G$  ratio. Furthermore with ahigher amount

of KMnO<sub>4</sub> during the synthesis of GO upon reduction with sodium borohydride results with low  $I_D/I_G$  ratios with a rise in a2D-band peak at 2682cm<sup>-1</sup> and 2688cm<sup>-1</sup> respectively from the Fig. 3.3.2 (b) and (d) analysis.

#### 3.3.3. TEM analysis





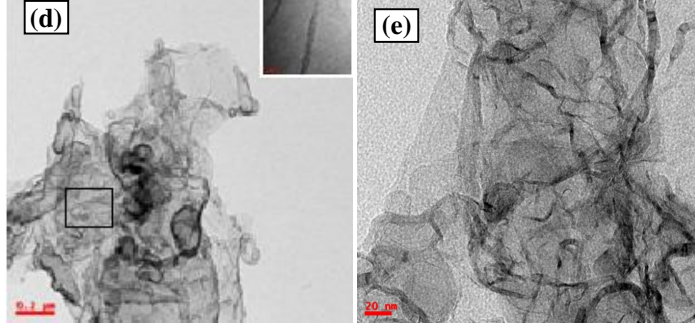


**Fig. 3.3.3** TEM Image analysis of (a) MH1-01-RGO-NB (b, c) MH1-03-RGO-NB (V) and (d, e) MH1-04-RGO-NB (V).

From the above TEM image analysis of the reduced graphene oxide obtained by the reduction using the reducing agents of sodium borohydride (NaBH<sub>4</sub>) and hydrazine monohydrate (NH<sub>2</sub>-NH<sub>2</sub>.H<sub>2</sub>O). We can infer from the above analysis such that the reduction of samples by hydrazine hydrate are highly transparent wrinkled structure and morphology with multi to few layered graphene sheets are obtained. Hence, the samples of fig. 3.3.3 (a-e) found with multilayered structure from HR-TEM images and amorphous from SED pattern were observed.

# **3.4.** Characterization of rGO obtained from GO synthesized by Modified Hummer's method

The samples obtained by the reduction process of GO synthesized from modified Hummer's method were analyzed by different characterization techniques and discussed.

#### 3.4.1. Structural analysis by XRD

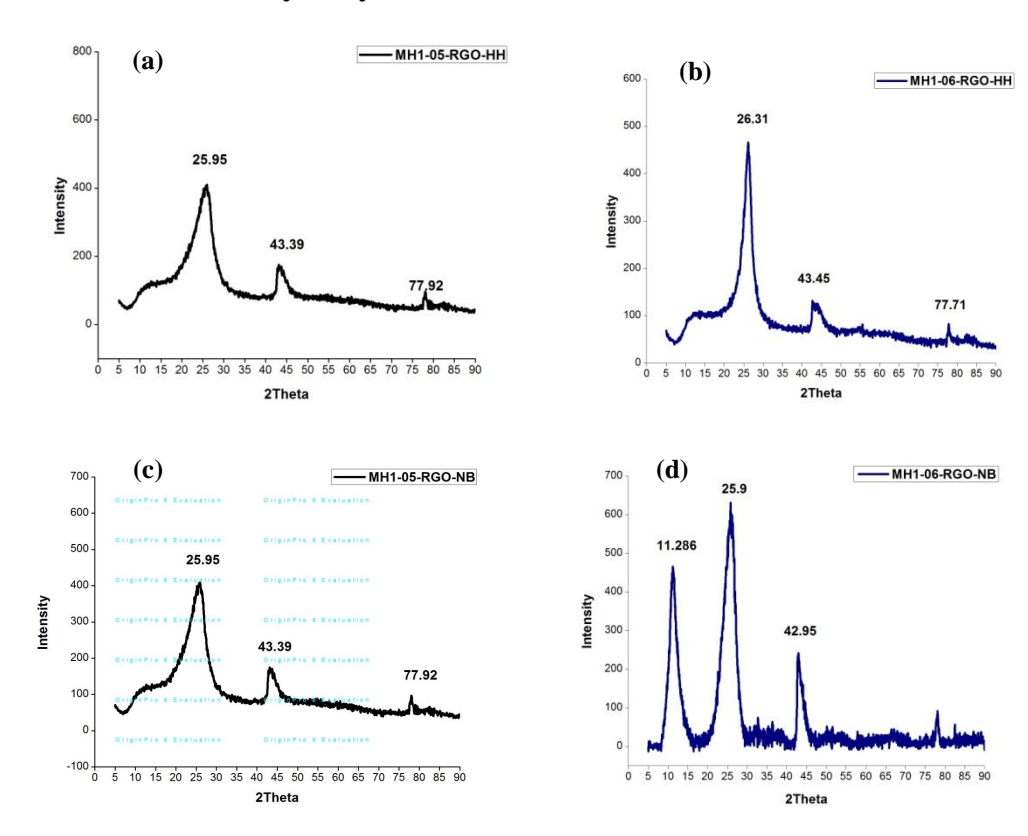


**Fig. 3.4.1** XRD analysis of rGO (a) MH1-05-RGO-HH and (b) MH1-06-RGO-HH (c) MH1-05-RGO-NB and (d) MH1-06-RGO-NB.

From the fig. 3.4.1 (a) and (b) shows acomplete decrease of graphene oxide synthesized in the presence of higher amount of sulphuric acid (H<sub>2</sub>SO<sub>4</sub>) where the reduced peak of MH1-05-RGO-HH retained at 25.95°. Higher the extent of oxidation implies lowers the reduction ratio and obtained with complete reduction and from the Fig. 3.4.1 (a), the broad peak upon reduction results the amorphous structure. In comparison to the synthesis of GO with lower sulphuric acid content observed from the fig. 3.4.1 (b), the reduction of

MH1-06-RGO-HH by hydrazine hydrate found with the peak at 26.31° where the completely reduced product with increased crystalline nature of reduced graphene oxide compound is obtained.

#### 3.4.2. FT-IR analysis

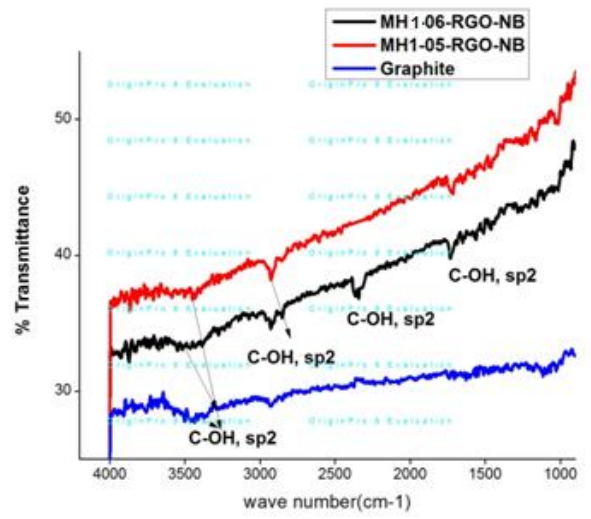
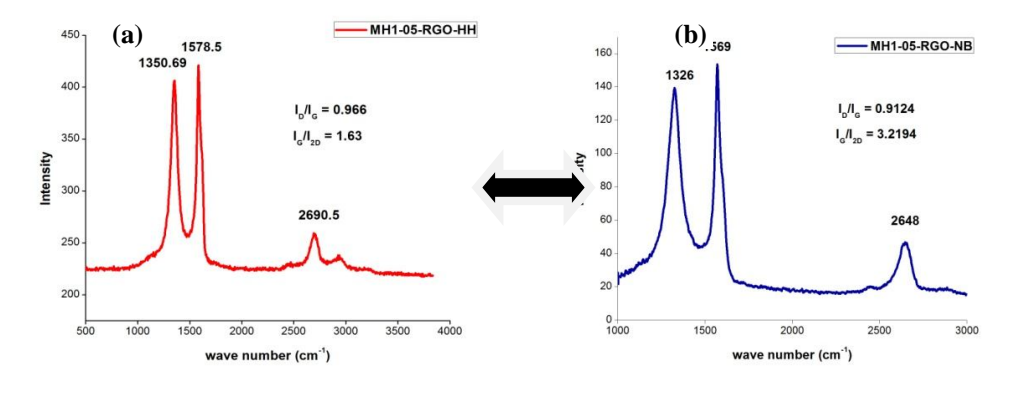
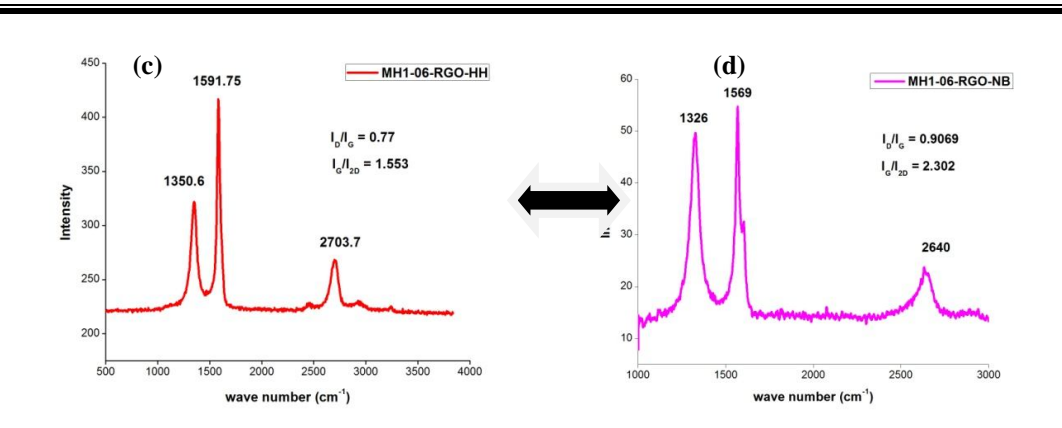


Fig. 3.4.2 Comparison plot of FT-IR data analysis of MH1-05-RGO-NB and MH1-06-RGO-NB.

From the Fig. 3.4.2, it is shown that comparison plot of MH1-05-rGO-NB and MH1-06-rGO-NB with different functional groups after reduction.

#### 3.4.3. Raman analysis



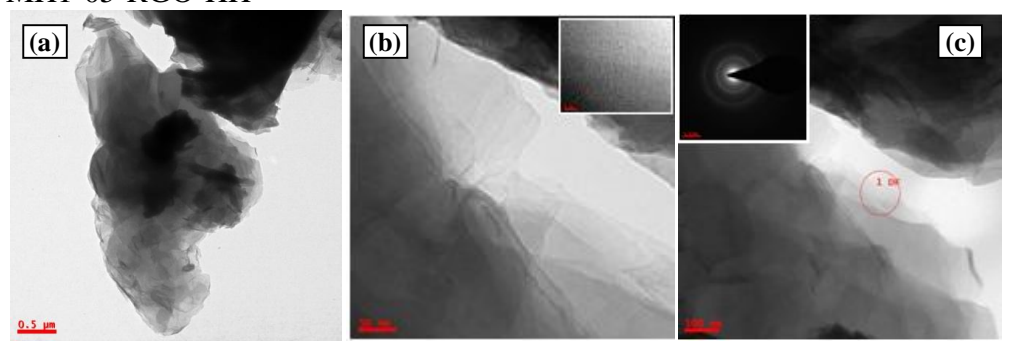


**Fig. 3.4.3** Raman data analysis of (a) MH1-05-RGO-HH (b) MH1-05-RGO-NB (c) MH1-05-RGO-HH and (d) MH1-06-RGO-NB.

From the above Raman analysis, Fig. 3.4.3 (a) and (b) results that reduction of MH1-05-GO using NaBH<sub>4</sub> and NH<sub>2</sub>-NH<sub>2</sub>.H<sub>2</sub>O observed with low I<sub>D</sub>/I<sub>G</sub> ratios of 0.966 & 0.9124 respectively. The reduction of GO by using hydrazine hydrate in presence of lower acid (H<sub>2</sub>SO<sub>4</sub>) ratios when compared with the higher amount of acid conditions we observed from the Fig. 3.4.3 (a & c) with the lower I<sub>D</sub>/I<sub>G</sub> ratios of 0.77 for the sample MH1-06-RGO-HH and 0.966 for MH1-05-RGO-HH respectively whereas the IG/I2D ratios for the samples from the Fig. 3.4.3 (a-d) found to be 1.63, 3.2194, 1.553 and 2.302 respectively.

#### 3.4.4. TEM analysis





MH1-06-RGO-HH

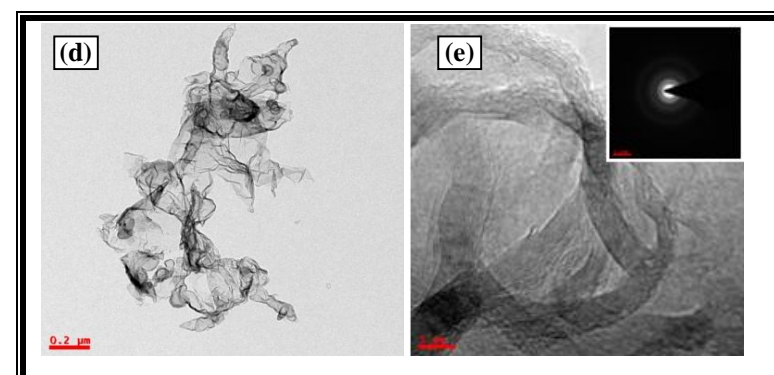
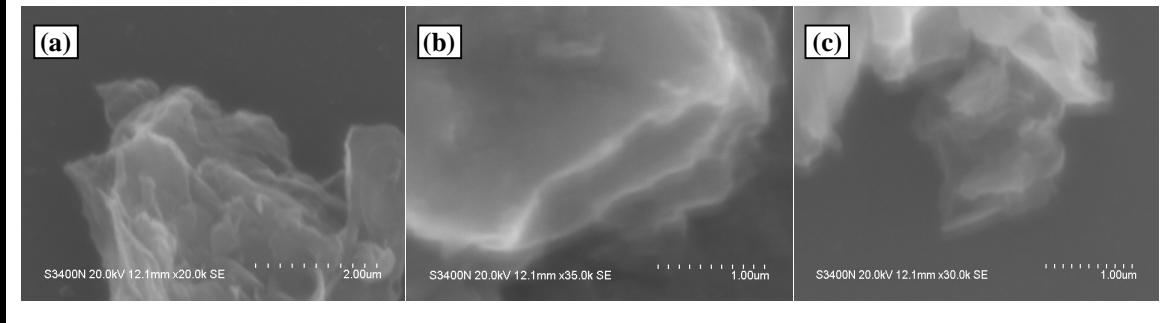


Fig.3.4.4 TEM analysis of (a, b, c) MH1-05-RGO-HH and (d, e) MH1-06-RGO-HH.

Fig. 3.4.4 (a), (b) and (c), TEM image analysis for the reduced samples of MH1-05-RGO-HH observed with highly transparent rGOnanosheets with amorphous structure since the GO obtained from modified Hummer's method shows the defects formation as confirmed from the Fig. 3.4.3 (a) Raman analysis. Whereas the sample MH1-06-RGO-HH observed with the wrinkled structure and morphology, transparent sheets and obtained with multi to few-layered reduced graphenenanosheets with amorphous structure from the Fig. 3.4.4 (d)& (e) SED pattern as observed from the TEM analysis.

#### 3.4.5. SEM analysis

#### MH1-05-RGO-NB

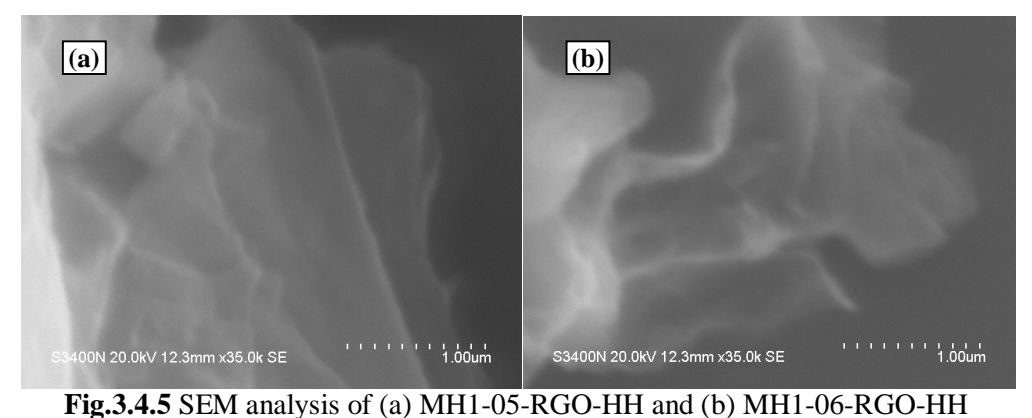


From the above Fig. 3.4.5 (a-c) of MH1-05-RGO-NB, the reduction of GO by using sodium borohydride observe with the layered by layer structure and morphology from the Fig. 3.4.5 SEM analysis. The exfoliation of graphenenanosheets with

thewrinkledstructuree due to the higher oxidation reactions with therise in temperatures (i.e., >150°C) observed and confirmed by the experimental results.

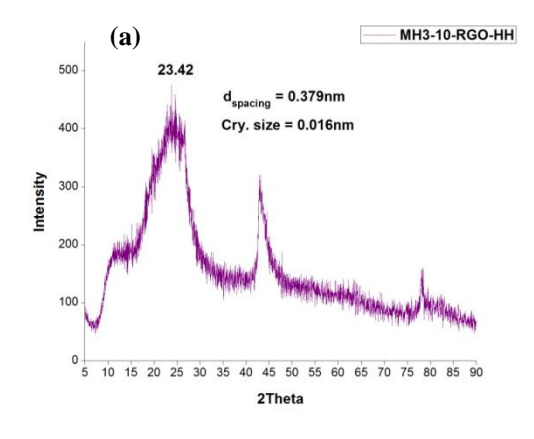
#### MH1-06-RGO-NB

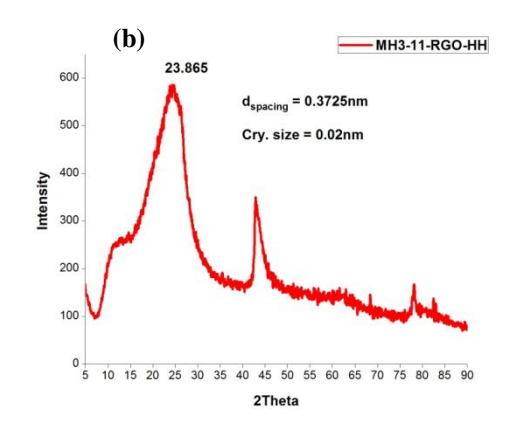
We can observe from the Fig. 3.4.5 (b) SEM analysis, the reduction of GO by sodium borohydride in presence of low sulphuric acid contents shows the largely reduced graphene oxide nanosheets with alayered structure and wrinkled morphology.

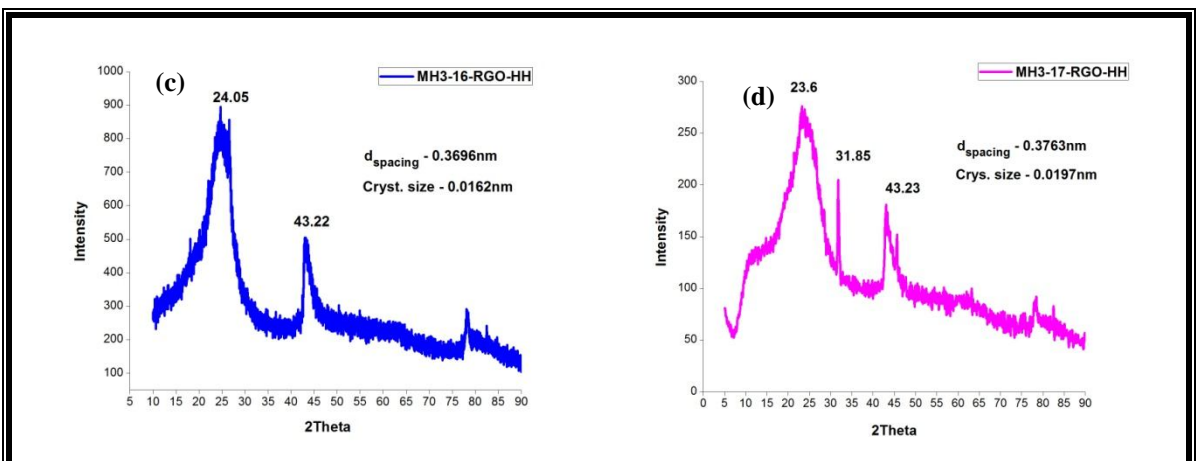


3.5. Reduction of GO synthesized by Volumetric Titration-Modified Hummer's method using hydrazine monohydrate

#### 3.5.1. XRD analysis



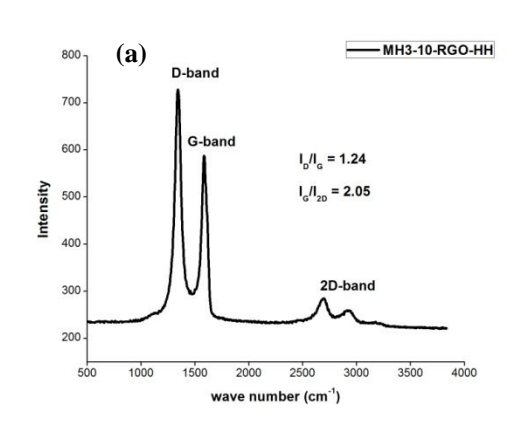




**Fig. 3.5.1** XRD analysis of RGO samples of Volumetric Titration -MHM method (a) MH3-10-RGO-HH (b) MH3-11-RGO-HH (c) MH3-16-RGO-HH (d) MH3-17-RGO-HH.

From the Fig. 3.5.1 XRD analysis, the reduction of GO synthesized by Volumetric Titration-Modified Hummer's method (VT-MHM) with varying mole ratios of KMnO<sub>4</sub> i.e., 0.2, 0.24, 0.3 and 0.5. We observe that with an increase in the mole ratio of GO synthesis and trailed by the complete decrease of GO using hydrazine monohydrate as a reducing agent found that there is not much difference in the d-spacing and the crystallite size is decreased when compared with the existing Hummer's method. We can observe the complete reduction of GO for the sample MH3-16-RGO-HH from the Fig. 3.5.1 (c) such that the ratio of sulphuric acid to oxidizing agent favors complete oxidation and reduction to obtain stable reduced graphene oxide.

#### 3.5.2. Raman analysis



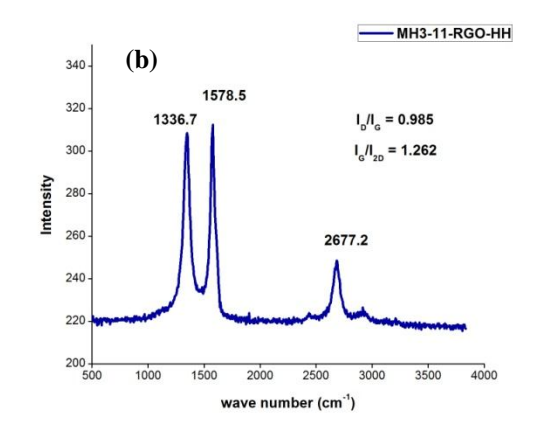


**Fig. 3.5.2** Ramandataof RGO samples by Volumetric Titration-MHM method (a) MH3-10-RGO-HH (b) MH3-11-RGO-HH.

From the Fig. 3.5.2 (a) and (b) shows the Raman analysis for the reduced samples of MH3-10-RGO-HH and MH3-11-RGO-HH. We infer that the I<sub>D</sub>/I<sub>G</sub>& I<sub>G</sub>/I<sub>2D</sub> ratios are at 1.24 & 2.05 respectively for the sample MH3-10-RGO-HH such that the rise in D-band intensity implies with the increase in the number of sp<sup>2</sup> domains indicates the increase in the 2D-band. The decrease in the G-band intensity infers the partial reduction as confirmed from the above Fig. 3.5.2 (a) XRD analysis. Similarly, as observed from the above Fig. 3.5.1 (a) Fig. 3.5.1 (b) little hump due to the partial reduction observed from the XRD analysis. Fig. 3.5.2 (b) infers the D & G-bands at 1336.7cm<sup>-1</sup>& 1578.5cm<sup>-1</sup> with a sharp 2D-band obtained at 2677.2cm<sup>-1</sup> because of the sp<sup>2</sup> bonded reduced graphene oxide obtained by the reduction using hydrazine monohydrate as a reducing agent. As observed that the ratios of  $I_D/I_G\& I_G/I_{2D}$  from the Fig. 3.5.2 (b) we infer the few layered reduced graphene structure is obtained.

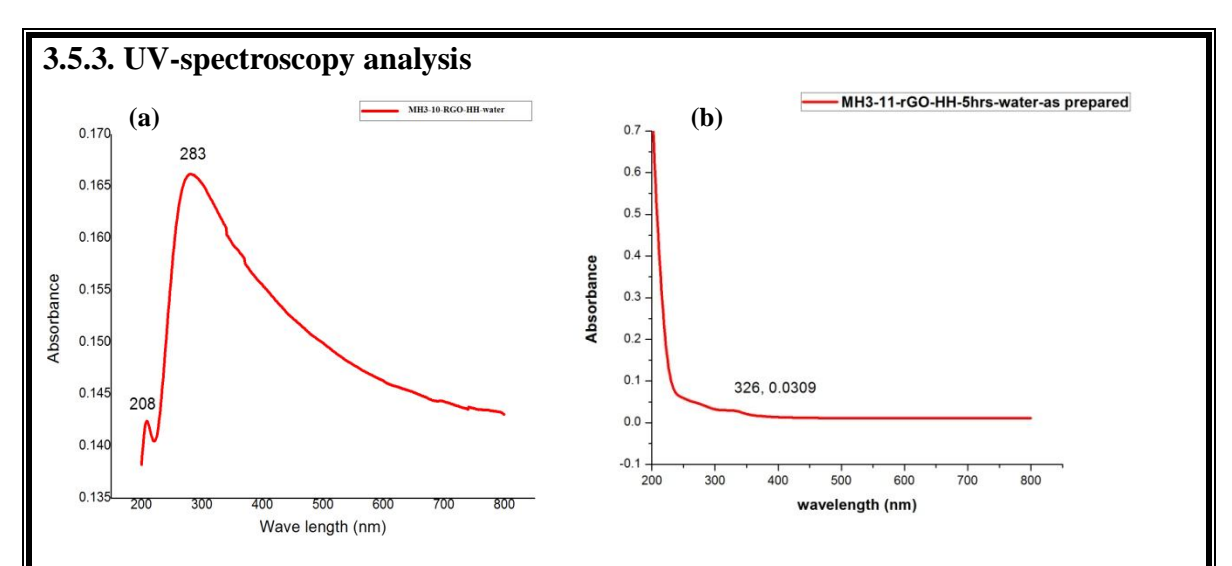


**Fig. 3.5.3** UV-spectroscopy of RGO samples in aqueous dispersion (a) MH3-10-RGO-HH (b) MH3-11-RGO-HH.

Fig. 3.5.3 (a) and (b) show UV spectroscopy of MH3-10-RGO-HH and MH3-11-RGO-HH. We can observe the two peaks where n to  $\pi$  and  $\pi$  to  $\pi^*$  transitions at 208nm and 283nm respectively from the Fig. 3.5.3 (a) in aqueous solution whereas Fig. 3.5.3 (b) we found the peak at 326nm with  $\pi$  to  $\pi^*$  transitions. We observed the highly transparent and large size reduced graphene oxide nanosheets.

#### 3.6. Conclusions

Reduction of GO synthesized by Hummer's method and modified Hummer's method. Here, the samples obtained from different synthesis methods are subjected to the reduction process by using different reducing agents like Hydrazine hydrate and sodium borohydride by varying the parameters such as temperature and the ratio of GO to the reducing agent. Characterization study of samples by using XRD, FT-IR, Raman spectroscopy and studied the structure, functionality, disorder/defect ratio i.e.,  $I_D/I_G$  and  $I_G/I_{2D}$ . Out of all the samples, GO synthesized by using novel approach subjected to reduction by hydrazine monohydrate and characterization of these samples with less

disordered structure by using Raman analysis. Finally, the rGO sample obtained by
disordered structure by using Raman analysis. I many, the 100 sample obtained by
reduction of GO synthesized by volumetric titration method dispersed in aqueous
solution was analyzed with the help of UV-spectroscopy to study absorbance of rGO in
aqueous solution.

## **Chapter-4**

## **Fabrication of PDMS and PDMS-rGONanocomposites**

#### 4.1. Introduction

Out of several polymers, PDMS (Polydimethylsiloxane), a silicone-based elastomer possesses excellent properties such as flexibility, biocompatibility, thermal steadiness, optical transparency, low price, low permeability, low flexibility and easy in micropatterning due to low glass transition temperature. Therefore, PDMS is generally used in microfluidic MEMS and bio-medical applications. Moreover, PDMS is also most commonly used for microfluidic device and bio-medical applications due to its optical transparent properties. However, the wide applications of PDMS are restricted due to its limiting electrical properties and mechanical durability; hence it is not widely applied in several device applications like MEMS, Sensors and Biomedical devices.

Anotherapproach is the addition of filler materials such as nanoparticles, carbon-based nanostructure materials e.g., graphene, graphenenanoribbons and other chemically modified carbon nanomaterials. Recently several reported work has been mentioned that CNT/graphenenanoplatelets and metal oxide can be used as filler materials for fabrication of nanocomposites because of their remarkable properties. In this chapter, graphene-based PDMS nanocomposites fabricated by mold casting process is described. The first part mainly deals with neat PDMS samples and second part involves the fabrication and characterization of rGO-PDMS nanocomposites.

## 4.2. Fabrication of Flexible PDMS material

#### **4.2.1.** Experimental procedure

Poly dimethyl Silicon Elastomer (PDMS) substrates of different thickness of 500, 1250, 2000 and 4000µm samples are prepared by mold casting. Silicon elastomer of 0.002056gms was taken in the plastic beaker (100ml) followed by the slow addition of hardener 0.0002056gms in the ratio of 1:10 such that 0.002056gms (Si. Elastomer: hardener = 1:10) mixed thoroughly by mechanical stirring for 40min and then poured into a Teflon mould of (2cm x 2cm) dimensions and thickness of 500um was prepared. Similarly 1250, 2000 and 4000µm thickness of pure flexible PDMS substrates were fabricated and the list of samples are shown in the Table. 4.2.1 below.

**Table: 4.2.1** List of pure flexible PDMS samples of different thickness

Sl.No.	Wt. of (Si. Elastomer + hardener) (gms)	Ratio of (Elastomer + hardener)	Thickness (µm)	Curing Temperature (°C)
1.	0.002056	1:10	500	80
2.	0.00514	1:10	1250	80
3.	0.00822	1:10	2000	80
4.	0.016448	1:10	4000	80

#### **Experimental work**



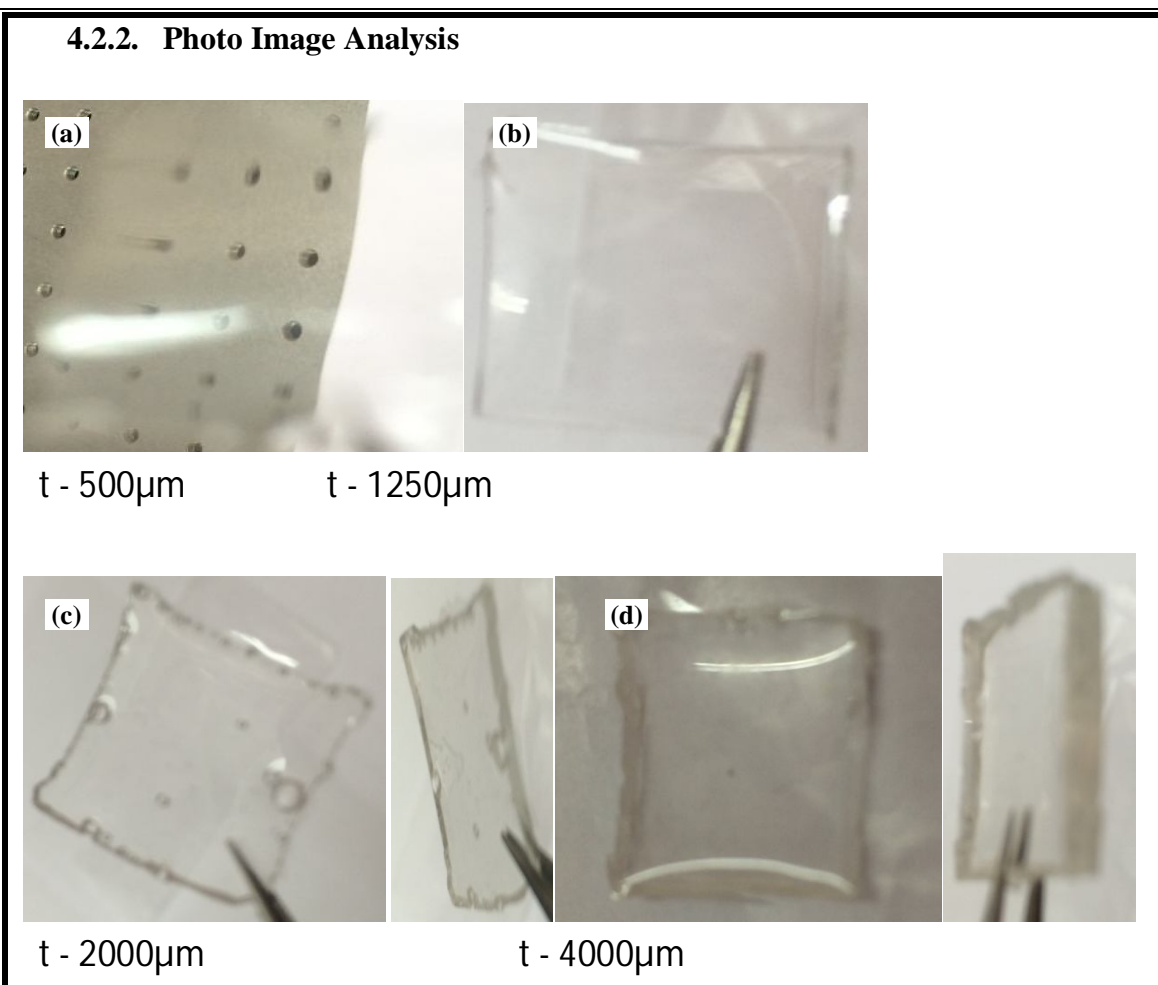


**Fig. 4.2.2** Photographimages of pure flexible PDMS substrates of different thickness of 500μm, 1250μm and 2000μm, and 4000μm respectively.

From the above image analysis, we can observe the highly transparent PDMS substrates of different thickness. The degree transparency decreases with an increase in the thickness and the bubbling obtained during fabrication. Fig. 4.2.2 (c) and (d) pure PDMS of 2000µm and 4000µm thickness surface morphology, transparency and cross-sectional area observed with uniformly cured samples at a curing temperature of 80°C on a hot-plate. Fig. 4.2.2 (a-d) shows the comparison of transmittance wrt to the different thickness of PDMS samples.

#### 4.3. Characterization of flexible PDMS substrates

Flexible PDMS substrates are fabricated by using mold casting technique. The characterization analysis of these substrates is discussed by using XRD, FT-IR, Raman spectroscopy and UV-visible spectroscopy.

#### **Block Diagram for the Fabrication of Flexible PDMS material**

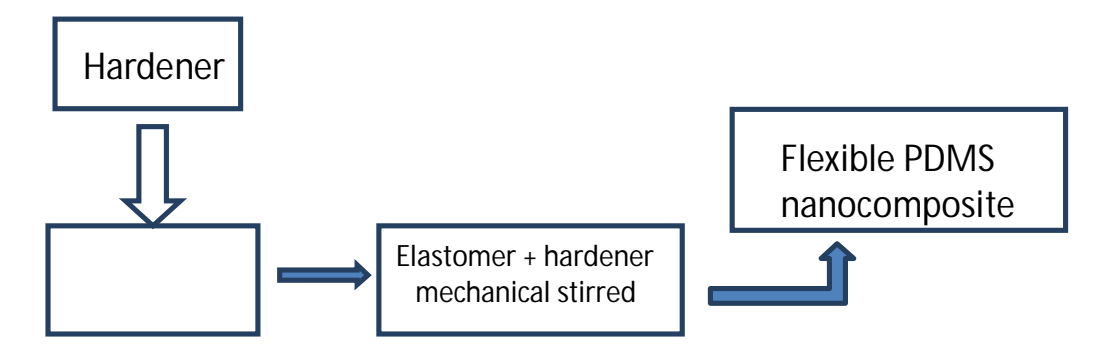


Fig. 4.3 Flow diagram used for the fabrication of Flexible PDMS material.

#### 4.3.1. Structural analysis by XRD

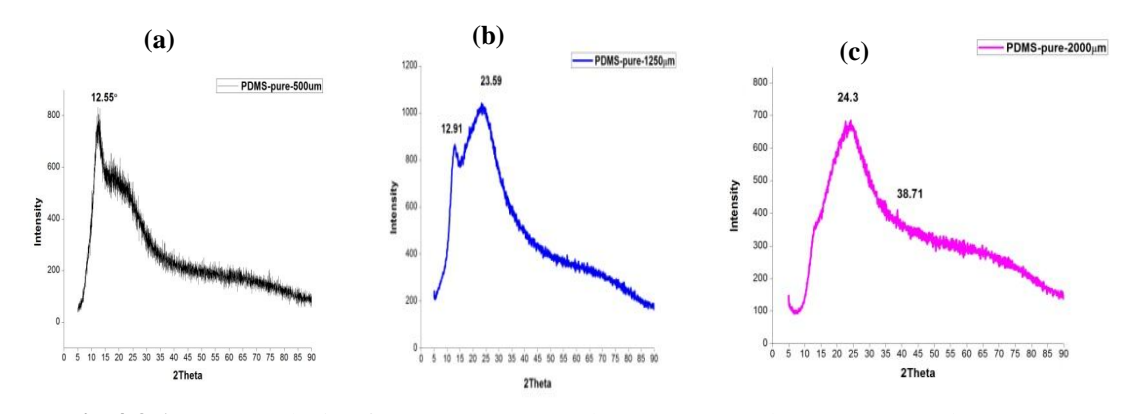


Fig.4.3.1 XRD analysis of pure PDMS samples (a)  $500\mu m$  (b)  $1250~\mu m$  and (c)  $2000\mu m$ .

From the Fig. 4.3.1 (a-c) shows the XRD analysis of pure PDMS substrates with 500um, 1250um and 2000um. The pure PDMS samples with peak positioned for 500um at 12.55°, 12.91° and 23.59° for PDMS thickness of 1250um whereasflexible PDMS 2000um material is found with 24.30% 38.71° respectively.

#### 4.3.2. Raman spectroscopy

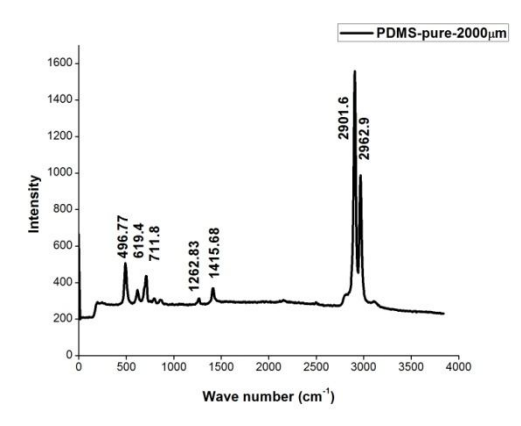


Fig.4.3.2 Raman spectroscopyof pure PDMS sample with 2000µm thickness.

Raman analysis from the above analysis shows the strong peak corresponding to the 2901.6cm<sup>-1</sup> and 2962.9cm<sup>-1</sup> from the pure PDMS material.

#### 4.4. Thickness-dependent properties of pure PDMS

#### 4.4.1. FTIR analysis

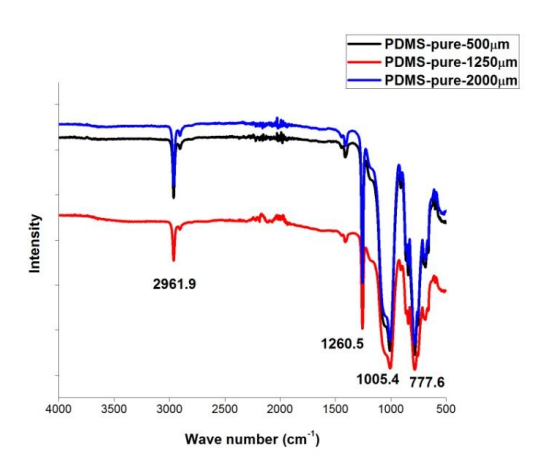
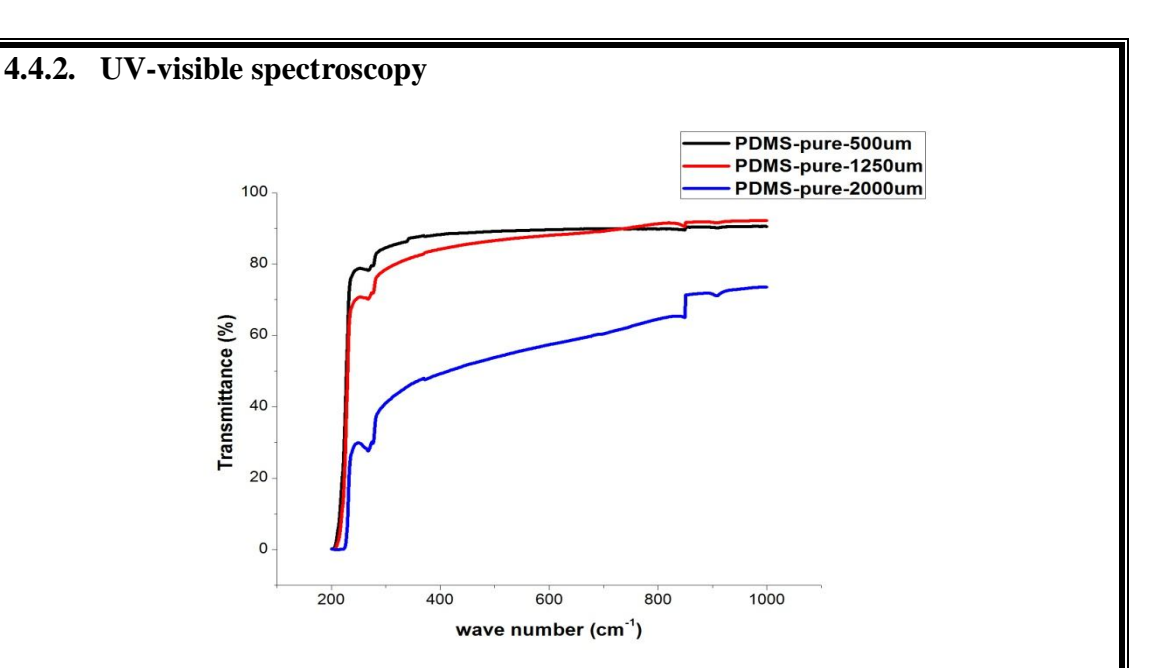


Fig.4.4.1 Comparison plot of FT-IR analysis of pure PDMS samples 500μm, 1250 μm and 2000μm.

From the above analysis, Fig. 4.4.1 displays FT-IR analysis of the pure PDMS samples of 500µm, 1250µm and 2000µm. The peak at 2961.9cm<sup>-1</sup> due to the C-H stretching of – CH<sub>3</sub>whereas the functional group of 1260.5cm<sup>-1</sup> because of the CH<sub>3</sub> symmetric deformation of Si-CH<sub>3</sub>; Si-O-Si stretching vibration gives a peak at 1005.4cm<sup>-1</sup> and 777.6cm<sup>-1</sup> due to the Si-C stretching and CH<sub>3</sub> rocking motion.



**Fig.4.4.2** UV-visible analysis of pure PDMS samples (a) 500μm (b) 1250 μm and (c) 2000μm.

From the above figure, UV-spectroscopy results in transparency in the range of ~96-98% with pure PDMS samples with the thickness of 500um and 1250um. We observe the transparency decrease with an increase in the thickness.

# **4.5.** Fabrication of PDMS-rGONanocomposites (without Chemical treatment)

#### 4.5.1. Experimental procedure

Silicon Elastomer (PDMS Sylgard 184) of 2.21665gms was taken in a (50ml, PP) beaker. Now then 0.00516gms of reduced GrapheneOxide(rGO) synthesized by Volumetric Titration-Modified Hummer's Method (VT-MHM) added to the elastomer and stirred for 45min and then followed by the addition of hardener to the above uniformly dispersed polymer mixture. Finally, the mixture stirred for 30min to obtain a homogenous viscous suspension and then poured into a Teflon mold (2cm x 2cm) dimensions with the

thickness of 500um, 1250um and 2000um. The PDMS-rGO based nanocomposites were placed under vacuum in a desiccator for 30min to remove bubbles and the curing temperature was maintained at 80°C for 40min. Finally, the cured rGO dispersed samples removed from the Teflon mold by using a sharp knife carefully and stored in a desiccator to remove traces of moisture content.

**Table 4.5.1** List of PDMS-rGO (0.23wt%) nanocompositesamples prepared without chemical treatment.

Sl.No.	Weight (%)	Wt. of rGO (gms)	Wt. of Si. Elastomer (gms)	Wt. of Hardener (gms)	Thickness (µm)
1.	0.23	0.00516	2.0353	0.18135	500 1250
					2000
	0.13	0.000478	0.18495	0.02055	500
2.	0.13		0110 170	0.02000	1250
					2000

Table 4.5.1 shows the list of samples of PDMS based rGOnanocomposites fabrication by using solid phase dispersion in silicon elastomer with different weight percentage (%).

# Photo-image analysis of PDMS-rGO nanocomposites (a) (b) (c)

**Fig 4.5.1** Photo image analysis of PDMS-rGO samples with a surface cross-sectional area of thickness (a & b) 1250um and (c & d) 2000um.

From the above Fig. 4.5.1, we can observe that the rGO nanoparticles are distributed randomly in the PDMS matrix and very few small air-bubbles are generated during the fabrication process can be seen in the surface morphology of from the above Fig. 4.5.1 (a) and (c) respectively. We can infer that rGO with 0.23wt% is distributed in the polymer matrix and the cross-sectional view of different thickness is shown from the Fig. 4.5.1 (b) and (d) respectively.

#### 4.5.2. Structural analysis by XRD

#### 4.5.2.1. Weight percentage (0.23%)

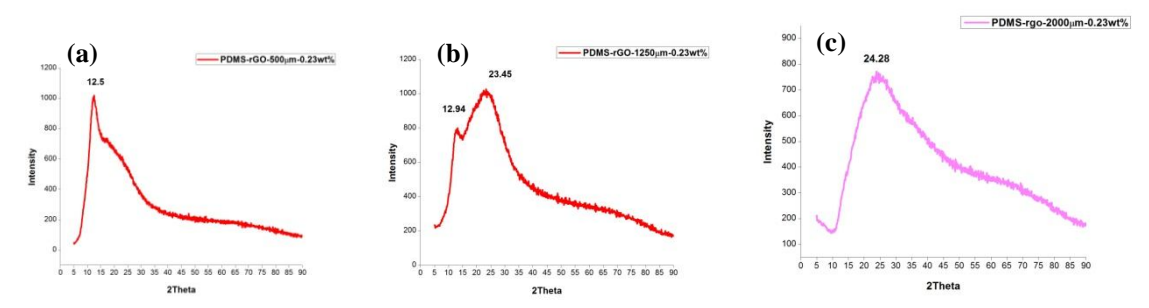


**Fig.4.5.2.1** XRD analysis of PDMS-rGOnanocomposites with 0.23wt% (a)  $500\mu m$  (b)  $1250 \mu m$  and (c)  $2000\mu m$ .

The Fig. 4.5.2.1 shows the XRD analysis of PDMS-rGO based nanocomposites of 0.23wt% with adifferent thickness of 500um, 1250um and 2000um respectively. Fig. 4.5.2.1 (a) observed that the peak value 2□ at 12.5° corresponds to the PDMS and the fig. 4.5.2.1 (b) infers we could observe the peak shift towards right and found that there is an increase in the 2□ value from 23.59° to 26.33° for the PDMS-rGOnanocomposite as compared to pure PDMS of 1250um thickness and the distribution of rGO confirmed that the bonding between the rGO and PDMS and the peaks at 29.06 ° & 38.98° shows the composite formation wrt pure PDMS. We can observe the 2□ peak at 24.28° from the Fig. 4.5.2.1 (c) the broadened in comparison to PDMS-rGO-1250um nanocomposite.

#### **4.5.2.2.** Weight percentage (0.13%)

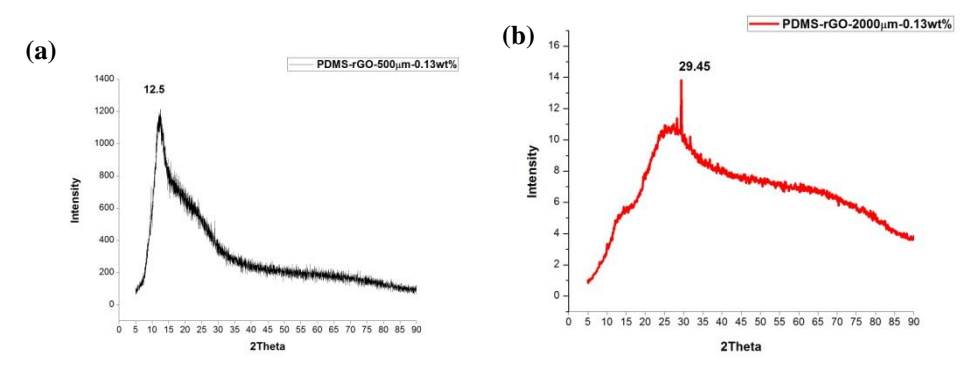
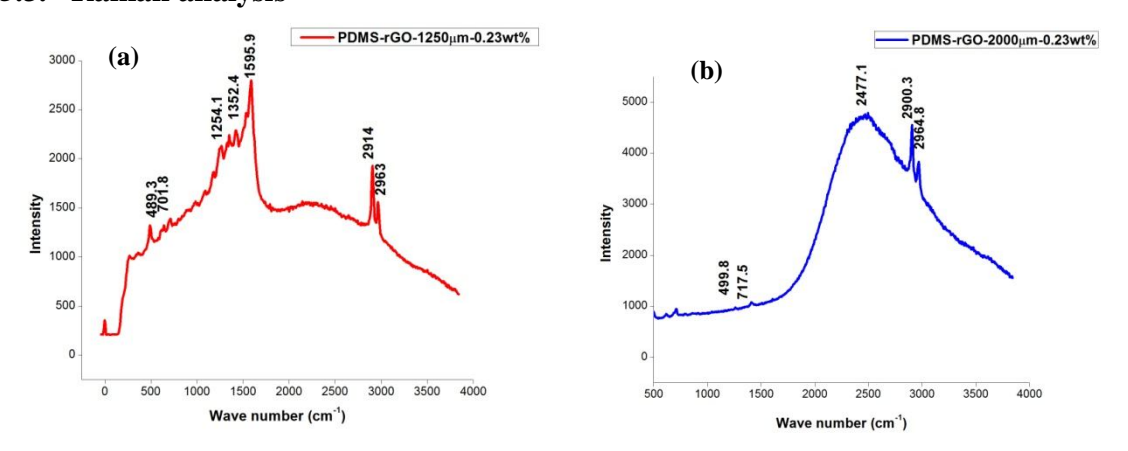


Fig.4.5.2.2 XRD analysis of PDMS-rGOnanocomposites with 0.13wt% (a) 500µm (b) 2000µm.

The above XRD analysis from the Fig. 4.5.2.2 (a) &(b) shows the PDMS-rGO with 0.13wt% of rGO in PDMS matrix of different thickness 500um and 2000um respectively. The PDMS-rGO for 500um thickness observed with neither shift and no additional peaks are found when compared to pure PDMS nanocomposite since the thin samples prepared to contain 0.13weight% of rGO is too small for the composite formation. The Fig. 4.5.2.2 (b) infers the composite formation with the peak at 29.45° where the shift in thepeak when compared to pure PDMS nanocomposite for 2000um.

#### 4.5.3. Raman analysis



**Fig.4.5.3** *Raman* analysis of PDMS-rGOnanocomposites with 0.23wt% for (a)  $1250\mu$ m and (b)  $2000 \mu$ m thickness.

Raman spectroscopy from the above analysis results the peak corresponding to 489.3cm<sup>-1</sup> where as 701.8cm<sup>-1</sup>, 1254.1cm<sup>-1</sup>, 1352.4cm<sup>-1</sup>, 1595.9cm<sup>-1</sup>, 2914cm<sup>-1</sup> and 2963cm<sup>-1</sup> respectively for 1250µm in Fig. 4.5.3 (a). The peak at 499.8cm<sup>-1</sup>; 717.5cm<sup>-1</sup>; 2471.1cm<sup>-1</sup>; 2900.3cm<sup>-1</sup> and 2964.8cm<sup>-1</sup> for the PDMS-rGO thickness of 2000µm in Fig. 4.5.3 (b) respectively.

## 4.6. Thickness-dependent properties of PDMS-rGOnanocomposite

#### 4.6.1. FTIR analysis

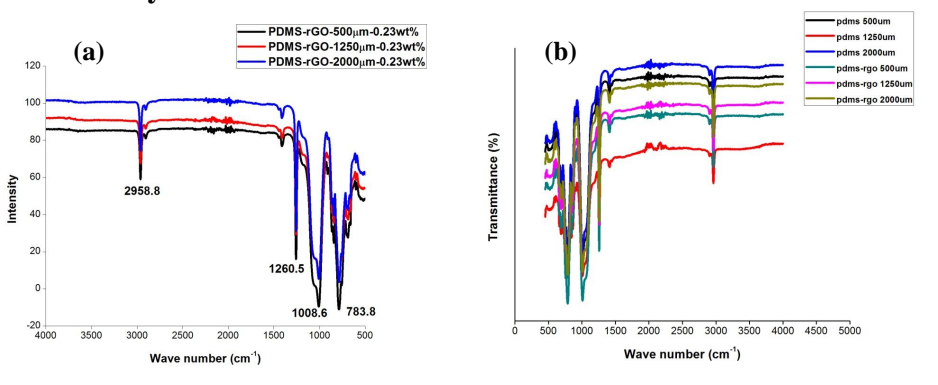


**Fig.4.6.1** *FT-IR* analysis with 0.23wt% of varying thickness i.e., 500μm, 1250μm and 2000μm (a) PDMS-rGOnanocomposites and (b) PDMS (pure) & PDMS-rGOnanocomposites samples.

PDMS-rGO without chemical treatment from the FT-IR spectroscopy analysis from the Fig. 4.6.1 shows a comparison of PDMS-rGOnanocomposites of different thickness 500µm, 1250µm and 2000µm respectively. The intensified peak at 2958.8cm<sup>-1</sup> due to the C-H stretching of –CH<sub>3</sub>; 1260.5cm<sup>-1</sup> functional group that corresponds to the CH<sub>3</sub> symmetric deformation of Si-CH<sub>3</sub> obtained from the pure PDMS material present without interacting the polymer and distributed rGO molecules whereas intensified peak at 1008.6cm<sup>-1</sup> shift in peak towards right when compared with pure PDMS samples from

the Fig. 4.6.1 because of the Si-O-Si stretching vibrations and 783.8cm<sup>-1</sup> from the Si-C stretching and CH<sub>3</sub> rocking motion in PDMS-rGOnanocomposites.

The FT-IR spectrum from the above analysis shows PDMS-rGOnanocomposites without chemical treatment that shows the peak at 2959cm<sup>-1</sup> is due to the C-H stretching of –CH<sub>3</sub> and aromatic C=C gives a peak at 1613cm<sup>-1</sup>, CH<sub>3</sub> asymmetric deformation of Si-CH<sub>3</sub> gives a peak at 1414cm<sup>-1</sup>; the peak at 1260cm<sup>-1</sup> is due to the CH<sub>3</sub> symmetric deformation of Si-CH<sub>3</sub>; Si-O-Si stretching vibration gives peak at 1030cm<sup>-1</sup> which is highly intense peak. Peak at 782cm<sup>-1</sup> is due to Si-C stretching and CH<sub>3</sub> rocking motion. There is no peak corresponding to C=O indicating the absence of DMF solvent. Hence, it is confirmed that DMF is completely evaporated when the sample is post cured at 150°C for 4hrs.

#### 4.6.2. UV-spectroscopy

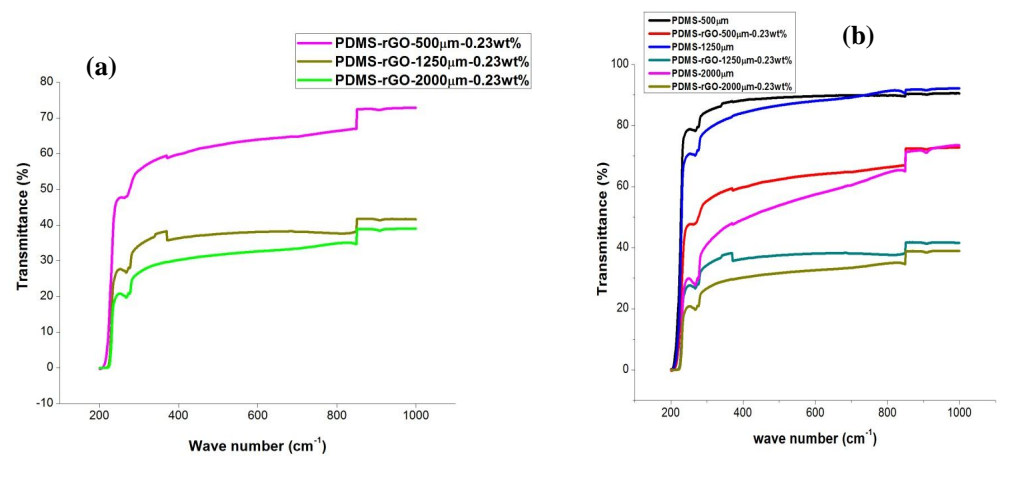


**Fig. 4.6.2**UV-spectroscopyComparison of Transmittance with different thickness i.e., 500um, 1250um and 2000um (a) PDMS-rGO samples (b) comparison of PDMS (pure) and PDMS-rGO samples.

From the above Figure, the Transmittance (%) of the PDMS and PDMS-rGO samples observed that the decrease in transparency of PDMS-rGOwrt to pure PDMS nanocomposite because of the dispersion of the filler material i.e., rGO in the polymer

matrix. We can infer that the (%) transmittance even reduced with a rise in the thickness of PDMS nanocomposites since the bending of the rays due to the filler material or may be due to the size of the filler i.e, may be an agglomeration of the particles in the matrix. It is found from the above figure, UV-spectroscopy results the PDMS-rGO shows ~80%, 42% & ~38% transmittance with a thickness of 500um, 1250um and 2000um of PDMS-rGO samples respectively.

#### 4.6.3. Dielectric properties

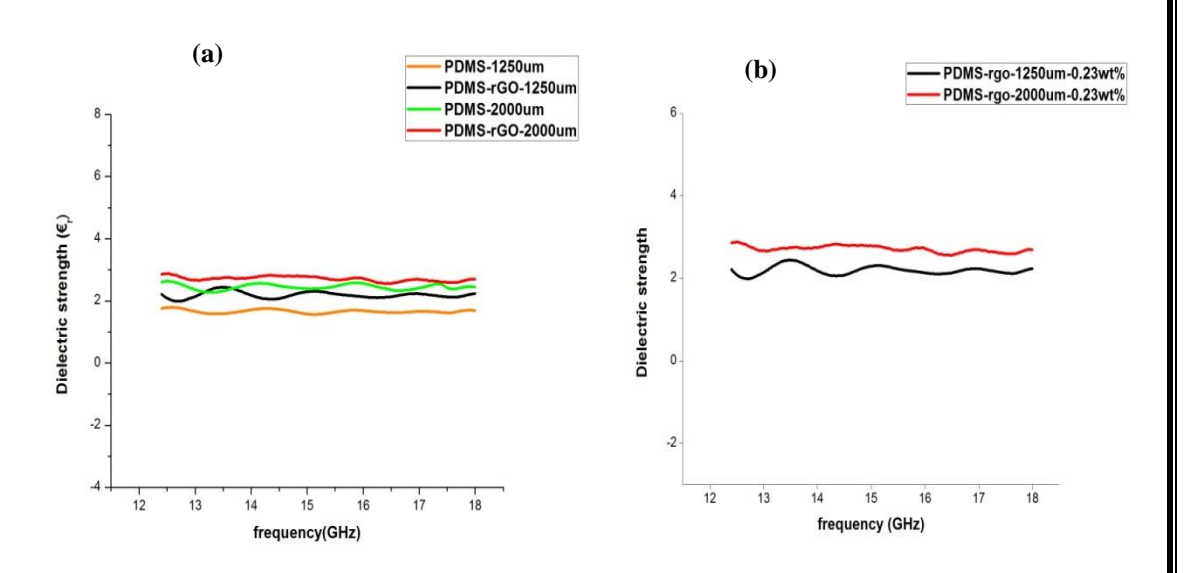


**Fig. 4.6.3** Comparison plot represents the Dielectric constant of PDMS, PDMS-rGO samples with different thickness i.e., 1250um and 2000um.

From the above figure, the PDMS and PDMS-rGO samples of 1250um thickness were compared. We observe the rise in dielectric constant with the addition of rGO as filler material of 0.23wt% which is synthesized by volumetric method.

#### 4.7. Conclusions

Flexible PDMS and PDMS-rGO samples were fabricated by using mould casting technique. Here, the fabrication of rGO synthesized by the Volumetric Titration method used as the filler material in the PDMS polymer matrix. The PDMS-rGO samples are prepared by the solid phase dispersal of the rGO nanoparticles in the PDMS matrix and characterized by FT-IR, XRD, Raman examination and studied the corresponding structural, bonding and defects/disordered structure. The PDMS-rGOnanocomposite optical properties by using UV-spectroscopy and finally, the dielectric properties are studied for both neat PDMS and PDMS-rGOnanocomposites.

## **Chapter-5**

# Fabrication of Chemically treated PDMS-1, 4-D-rGO Nanocomposites

#### 5.6. Introduction

Electrically conductive polymer composites have shown a lot of attention in recently and some progress has been achieved by the accumulation of conductive fillers like carbon black and carbon nanotubes (CNTs) into non-conductive polymer matrices for enhancing the electrical conductivity of the host polymer material. Further, due to cost-effective in the production of chemically modified graphene, it has been applied for fabrication of composites for electronic, photovoltaic solar cells and field effect transistors. Similarly, graphene-based compounds have also been examined for energy storage, chemical and biochemical sensing applications. A substantial number of reports have been also indicated that the thermal stability of polymers can be enhanced by using graphite nanoparticles (GNPs) and various CMGs as filler; even graphene oxide (GO) has the ability to improve the total composite thermal stability in comparison to the neat polymer, despite being thermally unbalanced itself.

Therefore, the current trend as per recently reported work has suggested that the solution-phase process has the ability to produce higher yield exfoliated graphene sheets with minimal defects for fabricating of PDMS based nanocomposites for flexible optical and electronic applications[14, 47, 90-92].

The fabrication process of 1,4-Dioxane chemically treated rGO-PDMS based nanocomposites

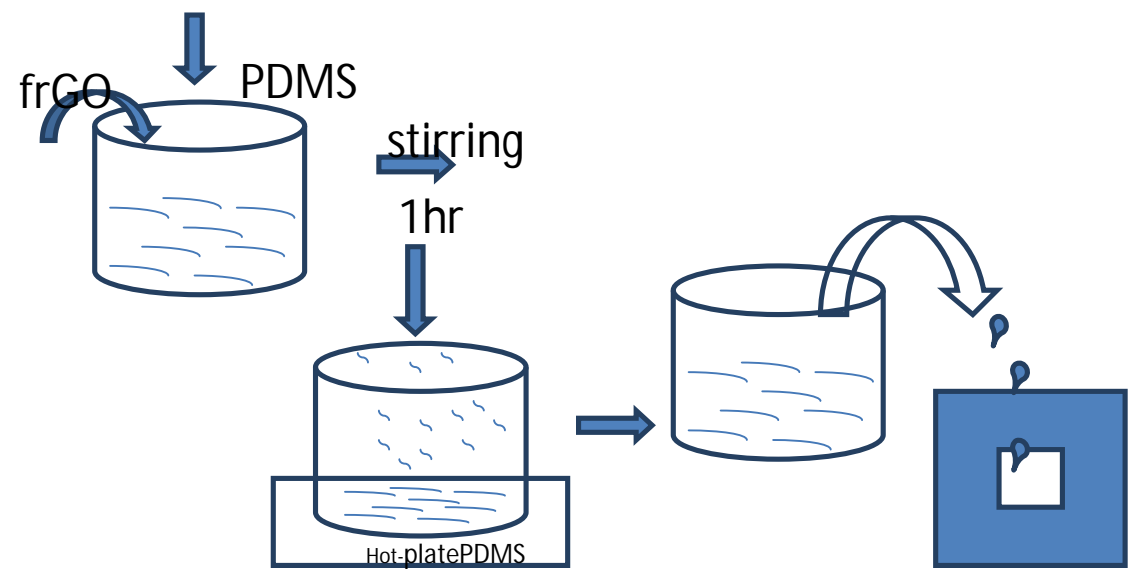


**Fig. 5.1.1**Schematic diagram represents the preparation of PDMS-1,4-D-rGO treated nanocomposites.

# 5.7. Study the dispersion behavior of chemically treated rGO in different solvent system

#### 5.7.1. Experimental procedure

Different solvents were used and studied the ultrasonication for uniform dispersion of rGO in the solvent system. The solvent (10ml) was taken in a beaker (100ml) with the addition of 0.5mgs/ml of rGO and subjected to ultrasonication for 1hour for homogeneous dispersion of solution. Similarly, dispersion behavior of rGO was studied by using different solvents. i.e.,

**Assumption:** 0.5mg/ml of rGO in solvents

- 1. Cyclohexane
- 2. Diethyl ether
- 3. 1,4-Dioxane
- 4. N-methyl-2-pyrollidine
- 5. Ethanol

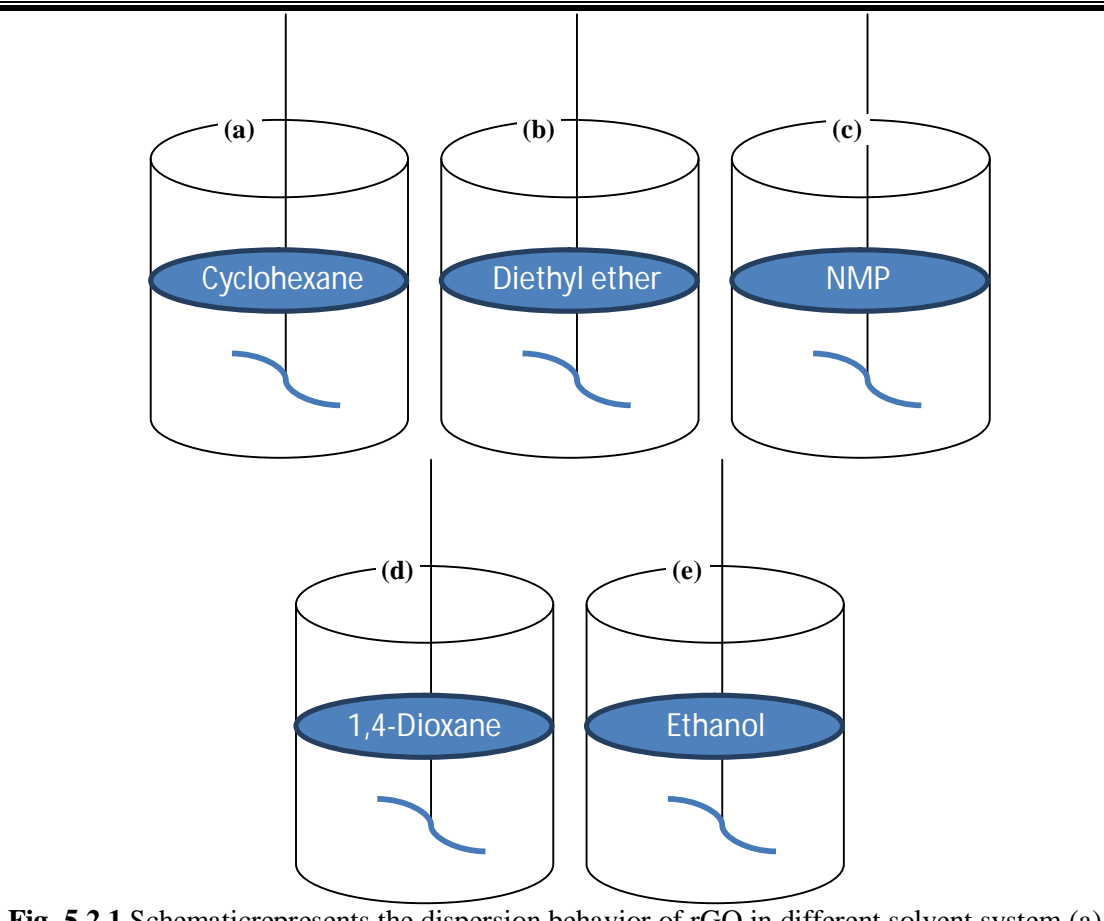
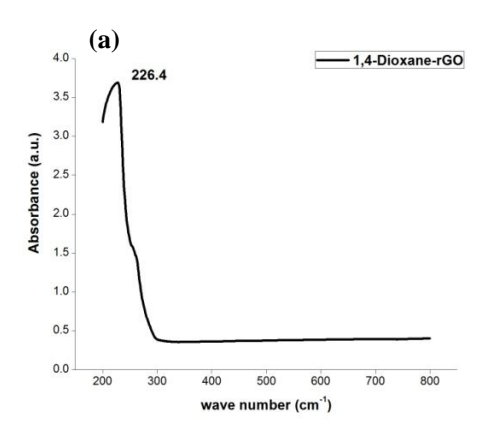


**Fig. 5.2.1** Schematicrepresents the dispersion behavior of rGO in different solvent system (a) cyclohexane (b) Diethyl ether (c) NMP (d) 1,4-Dioxane and (e) Ethanol.

The above Fig. 5.2.1 shows the schematic for the dispersion behavior of rGOin a different solvent systems such as Cyclohexane, diethyl ether, 1, 4-Dioxane, NMP and Ethanol. From the above experimental results we observed the evaporation of solvent upon sonication for an hour. The homogenous dispersion of solution used for the fabrication of PDMS based chemically treated rGO to obtain uniform nanocomposites for optoelectronic device applications.

#### 5.7.2. UV-spectroscopy

From the Fig. 5.2.2, the schematic shows the samples of rGO in 1,4-Dioxane and rGO-NMP solvents and these are subjected to characterization and the dispersion behavior of rGO synthesized by volumetric titration–MHM method are studied by using UV-spectroscopy.



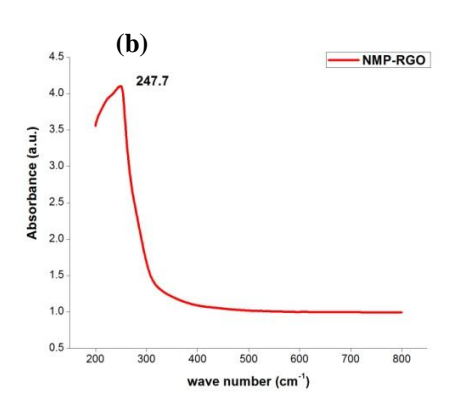


**Fig. 5.2.2**UV-spectroscopyrepresents the dispersion behavior of rGO in solvents (a)1, 4-Dioxane and (b) NMP.

From the above fig. 5.2.2 shows UV-spectroscopy of rGO in different solvents i.e., 1, 4-Dioxane and NMP. We observe the peak at 226.4cm<sup>-1</sup> and 247.7cm<sup>-1</sup> for the samples 4.3.1 (a) and 4.3.1 (b) respectively.

#### 5.7.3. FT-IR spectroscopy

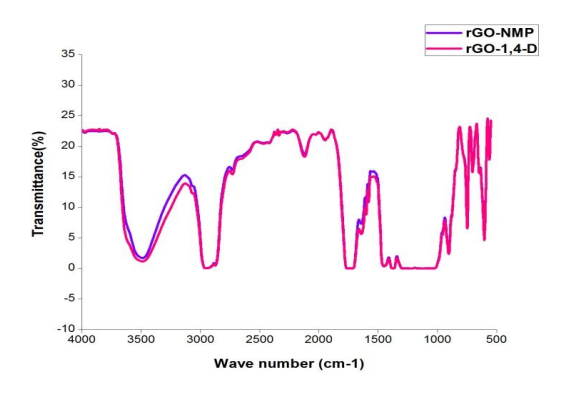


Fig. 5.2.3 FT-IR spectroscopy of dispersion rGO NMP and 1,4-Dioxane.

From the above figure analysis, there is no change in the chemical structure but there is a homogenous dispersion of the reduced graphene oxide (rGO) in different solvent systems i.e., NMP and 1,4-Dioxane.

# **5.3.** Fabrication of 1,4-Dioxane treated PDMS-rGONanocomposites

#### **5.3.1.** Experimental procedure

Pre-calculated amount of reduced Graphene oxide (rGO) was added to 1, 4-Dioxane in the ratio of (0.5mg/1ml) and then sonicated by using an ultrasonication bath (Branson 40 KHz) for 1h at 30°C at low amplitude to avoid the breakage of reduced graphene oxide sheets and heat generation during the sonication process. In order to uniformly disperse rGO in PDMS matrix, the above RGO dispersed in 1,4-D solution was added dropwise to the 10 parts of the poly-dimethyl silicon elastomer. Finally, 1 part of hardener was added to the above solution mixture and mechanical mixing was carried out to obtain a uniform frGO PDMS composite. Once, the uniform distribution of fRGo was achieved, the above solution was poured into a Teflon mold having 2x2cm<sup>2</sup> in size and kept in a desiccator for 30min in order to remove moisture and bubbling from the nanocomposite. Finally, it was cured at 80°C for 1h to obtain the functionalized-rGO-PDMS nanocomposite. The curing temperature was maintained at 80°C for better bonding between the PDMS matrix and filler material (RGO) and also for enhancing the flexibility of the nanocomposite. The final cured frGO-PDMS composite was removed by using a tweezer from the mold. The lateral dimension and thickness were measured by using a Verniercalliper which confirmed 2cm in length and 2cm in width. The thickness of the sample was estimated

and found to be  $\sim 1250 \mu m$ . The low-cost fabrication process for formation of the nanocomposite was graphically illustrated in the schematic below. COOF Hydrazine Reduction Oxidation Graphene Oxide(RGO) Graphene Oxide (GO) Chemically treated with 1,4 Dioxane Mechanical and Sonication mixing F With PDMS 1,4-Dioxane treated Reduced 1,4-D treated rGO-PDMS GrapheneOxide(rGO) nanocomposite

**Fig. 5.3.1** Schematic shows the flow process for the fabrication of PDMS-1,4-D treated – rGO based nanocomposites.

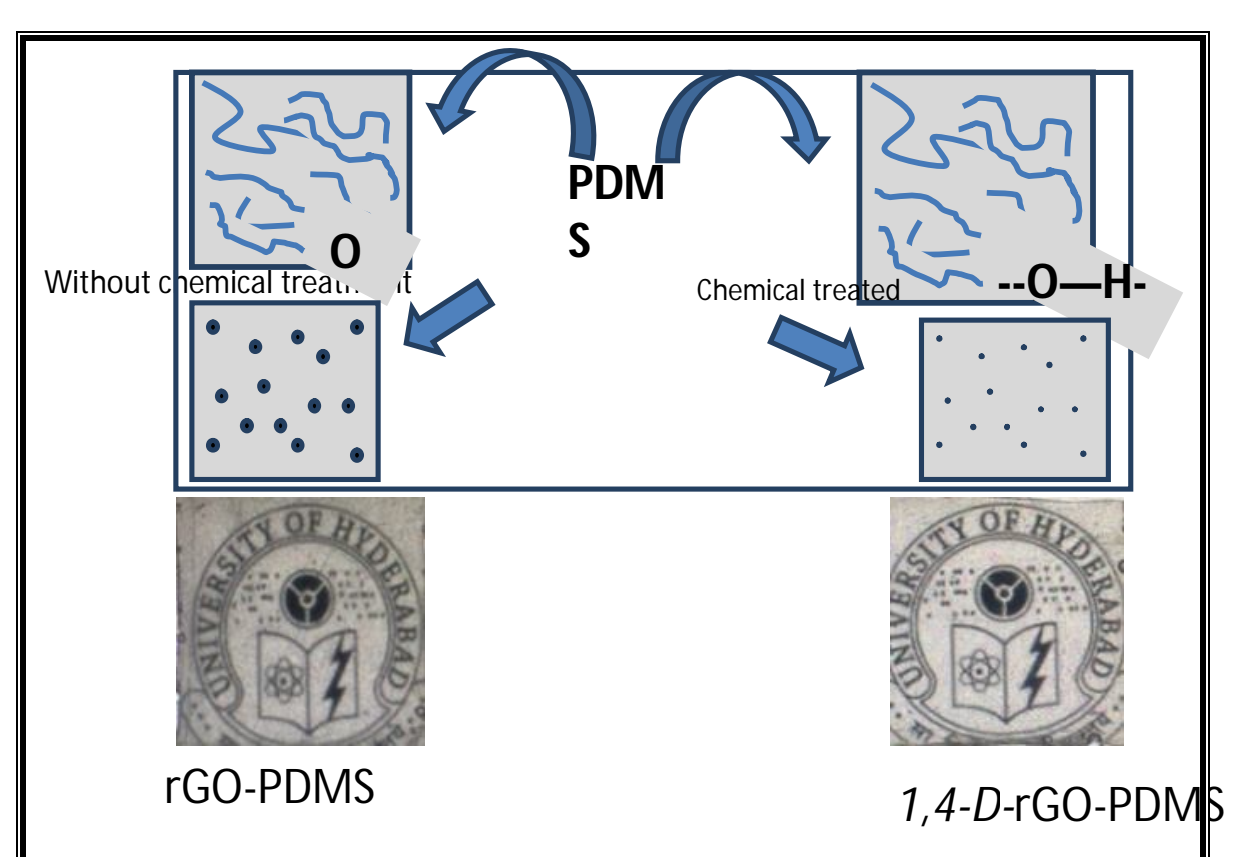
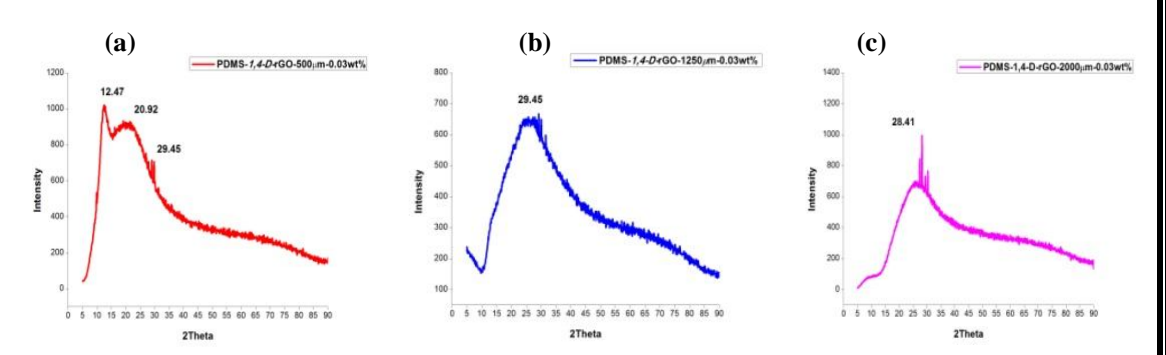


Fig. 5.3.1.2 represents the PDMS-rGO and PDMS-1,4-D-chemically treated rGOnanocomposites

#### **5.3.2.** X-ray Diffraction Analysis



**Fig. 5.3.2** XRD analysis of PDMS-1,4-D-rGO samples with 0.03wt% (a)  $500\mu m$  (b)  $1250~\mu m$  and (c)  $2000\mu m$ .

From the above Fig. 5.3.2, XRD analysis shows 1,4-Dioxane treated rGO-PDMS nanocomposites with 0.03wt% by means of liquid phase dispersion of different thickness i.e., 500um, 1250um and 2000um. The PDMS based 1,4-Dioxane treated rGO from the Fig. 5.3.2 (a) 500um infers the uniform dispersion of rGO by physicochemical

interactions and bonding characteristics with the lower weight (%) such that the diffraction peaks are found with the  $2\square$  values at  $12.47^{\circ}$  corresponds to the PDMS matrix and the broad peak  $20.92^{\circ}$  where as  $29.45^{\circ}$  due to the PDMS-rGO composite formation because of the interactions between rGO and polymer matrix. The PDMS-rGOnanocomposite with 0.03% for 1250um thickness in comparison to 500um XRD analysis is observed with the broad peak at  $29.45^{\circ}$  whereas 2000um from the Fig. 5.3.2 (c) shows the diffraction peak at  $28.41^{\circ}$  because of the homogenous dispersion implies with an increase in the distribution of rGO and polymer molecules interactions.

#### 5.3.3. Raman spectroscopy

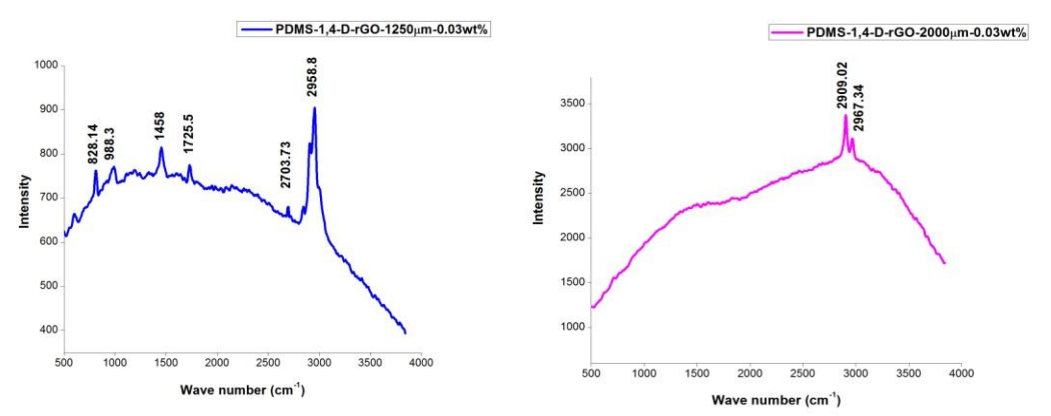


**Fig.5.3.3** Raman analysis comparison plot of PDMS-1,4-D treated rGOnanocomposite with 0.03wt% of 500μm, 1250μm and 2000μm.

Raman analysis shows the PDMS-1,4-D treated rGOnanocomposites with the major sharp peak associated with PDMS (pure) flexible nanocomposite. From the above figure, we can observe the shift in peak because of the chemically treated rGO dispersion in the polymer nanocomposite.

#### 5.3.4. Scanning Electron Microscopy

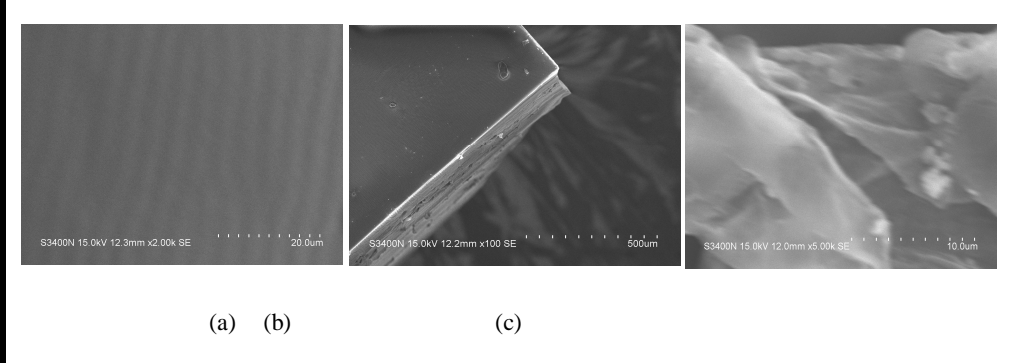
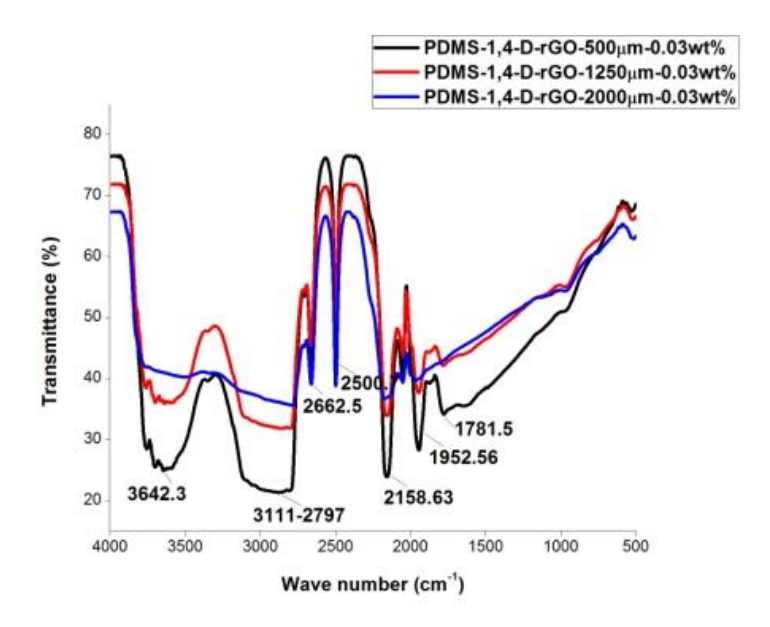


Fig.5.3.4 Scanning electron Microscopy (SEM) analysis (a & b) PDMS and (c) PDMS-rGOnanocomposites.

From the above figure (a & b), the SEM analysis shows the PDMS (pure) flexible nanocomposite with a layered structure. Fig. 4.3.4 (c), shows the rGO distributed in the PDMS matrix. The morphology observed with the rGO agglomerated in the polymer matrix.

## 5.4. Thickness-dependent properties of PDMS-1,4-Dioxane treated rGOnanocomposite

#### 5.4.1. Fourier-Transform Infrared spectroscopy



**Fig.5.4.1** FT-IR analysis comparison of PDMS-1,4-D treated rGOnanocomposite with 0.03wt% of 500μm, 1250μm and 2000μm.

The above Fig. 5.4.1 FT-IR analysis shows PDMS-1,4-Dioxane treated rGO based nanocomposites with the hydroxyl group at 3642.3cm<sup>-1</sup> and thebroad peak at 3111cm<sup>-1</sup> - 2797cm<sup>-1</sup> corresponds the functional group 2662.5cm<sup>-1</sup>; 2500cm<sup>-1</sup>; 2158.63cm<sup>-1</sup>; 1952.56cm<sup>-1</sup> and 1781.5cm<sup>-1</sup>.

#### **5.4.2.** UV-visible spectroscopy

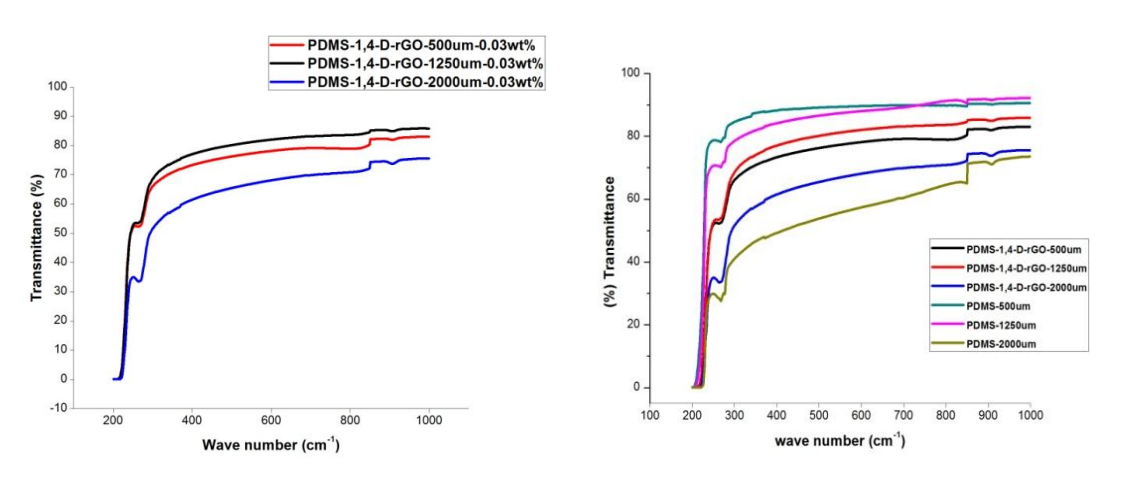


**Fig. 5.4.2** UV-visible spectroscopy of PDMS-1,4-Dioxane chemically treated rGO (a & b) PDMS and (c) PDMS-rGOnanocomposites.

UV-visible spectroscopy of PDMS-1,4-D chemically treated rGOnanocomposite with 0.03wt% with different thickness i.e., 500um, 1250um and 2000um respectively. We observe that there is an increase in the transmittance of 1,4-D chemically treated rGO distribution in the PDMS matrix when compared with the rGO (without chemically treated) distribution in the polymer matrix.

#### 5.5. Conclusion

PDMS-1,4-Dioxane nanocomposites are fabricated by using mold casting technique of different thickness i.e., 500um, 1250um and 2000um. Here, in this chapter the detailed fabrication of chemically treated nanocomposites are discussed in detail. The dispersion behavior of rGO in the different solvent system is studied and then the homogenous dispersion of solution obtained studied by UV-spectroscopy. The fabrication of chemically treated rGO based PDMS nanocomposites and characterization of the samples using XRD, Raman-spectroscopy, FT-IR analysis. Therefore, studied the dielectric and optical properties. transmittance PDMS-1,4-D chemically The of treated rGOnanocomposites of different thickness i.e., 500um, 1250um and 2000um are compared by using UV-spectroscopy. The neat PDMS shows highly transparent (98%) and decreases in (%) transmittance with the accumulation of rGO as filler nanomaterial in the PDMS matrix and transmittance reduced with a rise in the thickness due to the incorporation of rGO filler material in PDMS-rGO based nanocomposites. Moreover, the uniform dispersal of the rGO filler material in the polymer matrix is obtained and thickness dependent optical properties are studied by using UV-spectroscopy analysis.

#### **Chapter-6**

# Comparative study of PDMS-rGO based Nanocomposites (without and with chemical treatment using 1,4-Dioxane)

#### 6.1. Introduction

The fabrication of PDMS (pure) and PDMS-rGO without chemical technique by using mould casting prepared samples in the chapter-4 were compared with PDMS-1,4-Dioxane chemically treated rGO based nanocomposite of 1250um from the chapter-5 and analyzed by using XRD, Raman, FT-IR, UV-spectroscopy, dielectric and IV-analysis.

## **6.2.** Characterization of rGO-PDMS composite and 1,4-D-rGO-PDMS composite

#### 6.2.1. Structural analysis by XRD analysis

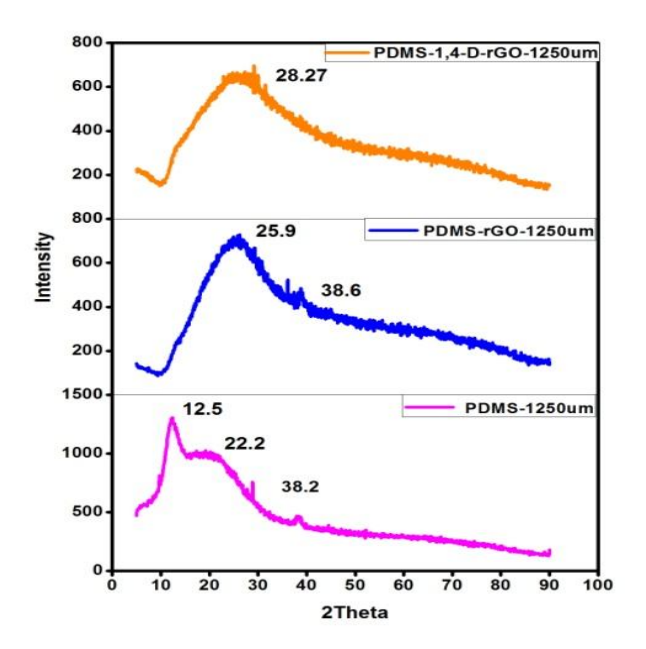


Fig. 6.2.1 XRD analysis shows comparison plot of PDMS (pure), PDMS-rGO and PDMS-1,4-D-rGO.

Fig. 6.2.1 shows the XRD patterns of PDMS, PDMS-rGO and PDMS-1,4-D-rGOnanocomposites respectively. As shown in Fig. 5.5.1, (for the PDMS XRD pattern), the corresponding 2□ values are at 12.5°, 22.2° and 38.2° which are same as reported earlier for the PDMS<sup>40</sup>. For PDMS-rGO, the corresponding 2□ values are at 25.9° and 38.6° respectively. As shown from the above Fig. 5.5.1, there is a shifting in peak position from 22.2° to 25.9° occurs for PDMS-rGO which is owing to the incorporation of rGOnanosheets in the polymer matrix. For PDMS-1,4-D-rGO, the corresponding 2□ value is at 28.27° and only one peak is seen, the possible reason is due to the cross-linking bond formation between the filler and PDMS matrix.

#### **6.2.2.** Raman spectroscopy

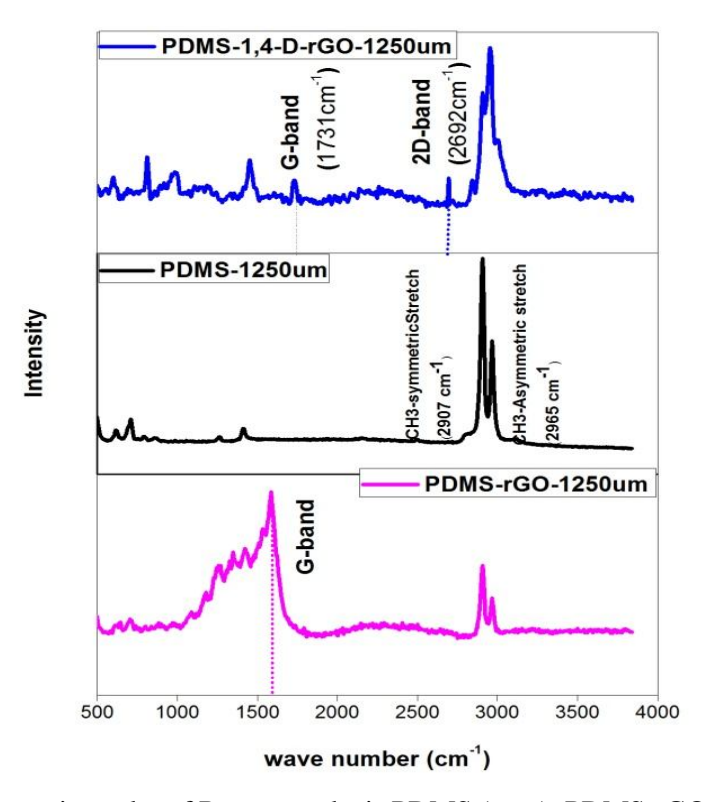


Fig. 6.2.2 Comparison plot of Raman analysis PDMS (pure), PDMS-rGO and PDMS-1,4-D-rGO.

Raman spectroscopy of PDMS, PDMS-rGO and PDMS-1,4-D-rGO nanocomposites are shown in Fig. 6.2.2. For the spectrum PDMS-1,4-D-rGO, the predominant peaks at 1731cm<sup>-1</sup>& 2692cm<sup>-1</sup> correspond to the G and 2D band of the reduced graphene oxide(rGO). As shown in the above figure, the G band moved to the higher wave number side after 1,4-D-rGO dispersed in PDMS while 2D band position remains unchanged. The blue shift of the G band occurs mainly because of charge doping with electron-withdrawing components of PDMS. The other peaks correspond to the PDMS polymer matrix nanocomposite as shown in Figure 4b ( themiddle figure is one for PDMS ref[93-95].

#### **6.2.3.** Fourier Transform-Infrared spectroscopy (*FT-IR*)

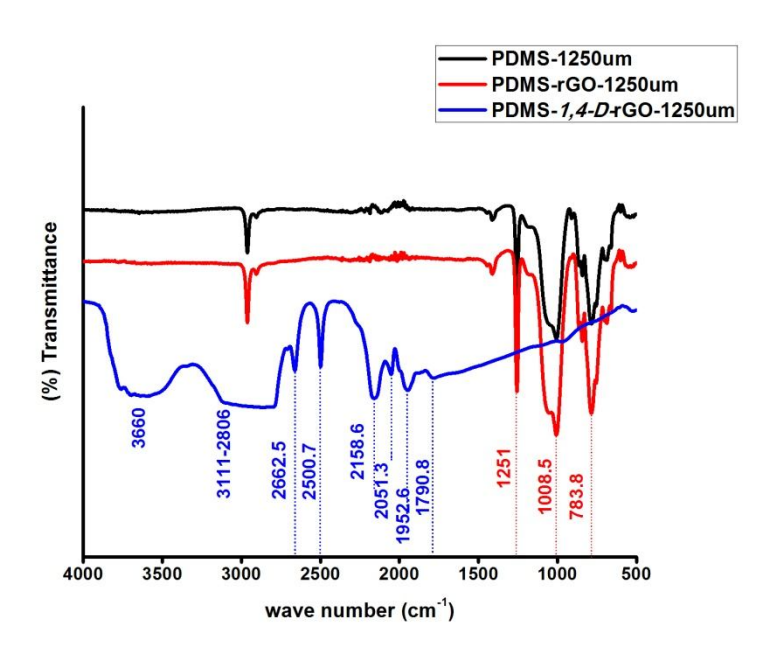
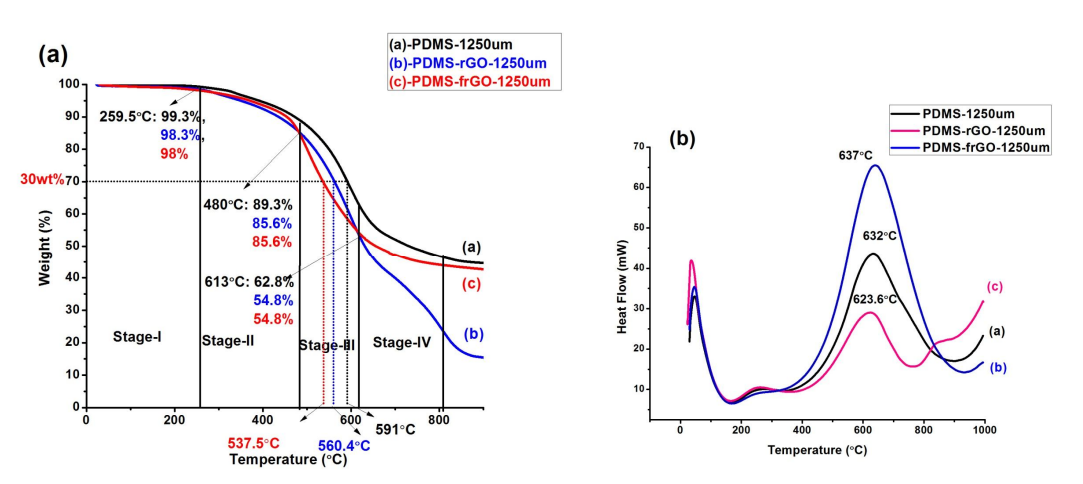


Fig.6.2.3 FT-IR study comparison plot of PDMS (pure), PDMS-rGO and PDMS-1,4-D-rGO.

Fig. 6.2.3 depicts the FTIR spectra of rGO, PDMS-rGO and PDMS-1,4-D-rGO nanocomposites respectively. The broadband appears at 3660cm<sup>-1</sup> for PDMS-1,4-D-rGO mainly due to the vibrations of Si-OH groups that is because of the hydroxyl groups

absorption, the band Si-H group peak appears at 2158.6cm<sup>-1</sup> which confirms the hydrosilanes groups present in the sample further indicating the bond formation between PDMS base and 1,4-D-rGO and acts as a crosslinker. The peak appears at 1790cm<sup>-1</sup> corresponds to C=C aromatic stretching between 1,4-D-GO and PDMS due to Si(OOR) stretching in functional polymers and further it may increase the orientation of filler in the composite to enhance the properties of the material. Moreover, the Si-O-Si stretching at 1008cm<sup>-1</sup> and C-H stretching shakings in the range 2500cm<sup>-1</sup> to 2662cm<sup>-1</sup> arealso found in the 1,4-D-rGO-PDMS nanocomposites. Thus, from the FT IR analysis we conclude that the filler along with solvent (1,4-D) characteristic interactions modify the surface bonding of the molecular structure whichenhances the nanocomposite flexibility because of weak cross-linking regions. Therefore, both FT-IR and Raman outcomes clearly indicate the sturdy interaction between the chemically treated 1,4-D-reduced grapheneoxide(1,4-D-rGO) and PDMS matrix[96, 97].

#### 6.2.4. Thermo gravimetric (TGA) analysis



**Fig. 6.2.4** (a & b) TGA analysis of PDMS-ref, PDMS-rGO and PDMS-1,4-D treated *rGO*nanocomposites.

Thermogravimetric study was done to understand the weight loss of the nanocomposites with variation in the temperature at the heating rate of 10°C/min by using a Perkin Elmer instrument (SDT Q600 V20.9 Build 20) and the corresponding percentage (%) weight loss of the cured PDMS, PDMS-rGO and PDMS-1,4-D-rGO nanocomposite are plotted with temperature as shown in Fig.6.2.4 (a). As shown in Fig 6.2.4 (a), the nanocomposites decomposition occur primarily in four different stages such as in the temperature range 25°C-259°C for stage-I, 259°C-480°C for stage-II, 480°C-613°C for stage-III and 613°C-800°C for stage-IV respectively. The degradation starts in the first stage due to the homolytic scission of chemical bonds in the network for PDMS-rGO and PDMS-1,4-DrGO samples respectively with a maximum weight loss of 2-3% in the stage-I<sup>45</sup>. In stage II, only 15% weight loss occurs because of the elimination of water molecules and the bonding between the PDMS matrix and carbonyl (C=O) groups of the rGO due to the chemical treatment by dispersion process. In stage-III, the region (480°C-613°C) where both the PDMS-rGO and PDMS-1,4-D-rGO loss weight linearly and a maximum 45% weight loss is seen at 613°C. In the last stage (4<sup>th</sup> stage > 613°C), one interesting phenomenon is occurring (as shown in Fig. 6.2.4 (a) for the PDMS-1,4-D-rGO nanocomposite in comparison to the PDMS-rGO that the weight loss is very rapid for the PDMS-rGO and a maximum weight loss of 75% occurs at 800°C. In contrast to this only 55% of weight loss occurs for the PDMS-1,4-D-rGO nanocomposite at the same 800°C. Moreover, the weight loss is saturated beyond 800°C for the PDMS-1,4-DrGOnanocomposite whereas still weight loss is happening for the PDMSrGOnanocomposite[41, 42, 98].

It is also seen that from the Fig. 6.2.4 (a), both PDMS host and 1,4-D-rGO-PDMS nanocomposite are following the similar decomposition pattern with a maximum weight loss of 50-55% at high temperature. Our experimental results from TGA analysis indicated that a higher thermal stability PDMS-1,4-D-rGO nanocomposite is obtained by chemical treatment of rGO with 1,4-Dioxane. Further, it suggested that a robust interfacial bonding between the filler material and polymer matrix owing to the uniform distribution of 1,4-D-rGO in the PDMS matrix by the chemicaltreatment is mainly responsible for the enhancement in the thermal stability of 1,4-D-rGO-PDMS nanocomposites, same results are also reported earlier from TGA analysis.

Therefore, PDMS-1,4-D-rGO nanocomposite is more thermally stable at high temperature and don't degrade much at high temperature. The possible reason for this unique behavior of 1,4-D-rGO-PDMSnanocomposite is owing to the solid interaction between the filler material and PDMS matrix as confirmed from the FTIR results (Fig. 6.2.3) and also due to the uniform distribution of 1,4-D-rGO in the polymer matrix as a result of chemical treatment by dispersion technique.

To understand more details about the thermal properties heat flow analysis was performed for PDMS, PDMS-rGO and PDMS-1,4-D-rGO cured nanocomposites and shown in Fig. 6.2.4 (b). As shown in Fig.6.2.4 (b), PDMS-1,4-D-rGO shows higher stability in comparison to rGO-PDMS nanocomposite. A peak shift towards high temperature by 5°C is noticed for 1,4-D-rGO-PDMS from the PDMS host whereas a peak shift towards lower temperature by 8.4°C is seen for PDMS-rGO sample from the host PDMS. In case of PDMS-1,4-D-rGO, a segmental movement of the constrained polymer chains occurs because of the global network structure between the filler and the PDMS

matrix due to uniform distribution of the 1,4-D-rGO in PDMS matrix, thus there is an increase in the thermal stability. On the other side, in the case of PDMS-rGOnanocomposite, we observed less thermal stability because of the relative immobilization of the remaining amorphous PDMS segments between the rigid crystalline lamellae, the peak deviates and the relaxation is broadened significantly[45, 99, 100].

#### **6.2.5.** Dielectric properties

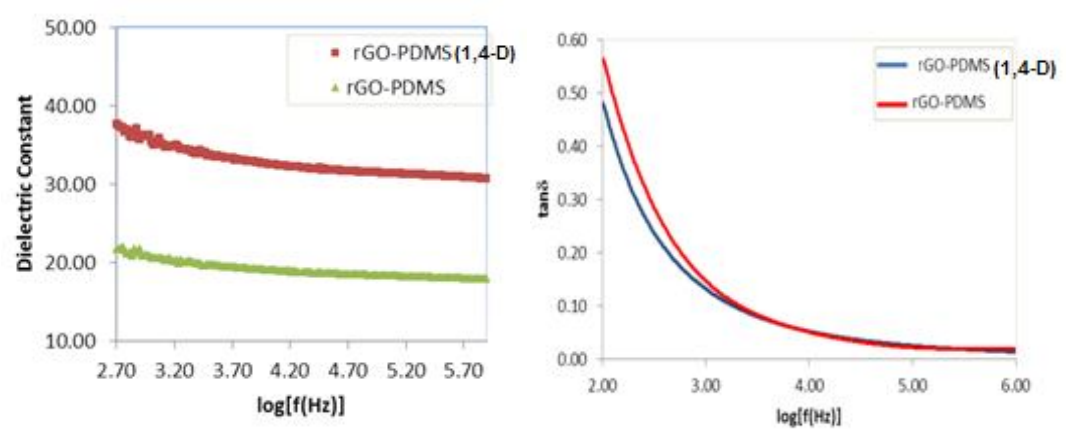


**Fig. 6.2.5**Comparison plot represents the Dielectric constant of PDMS-rGO and PDMS-1,4-D-rGO samples with a thickness 1250um.

Further, to understand the electrical properties of nanocomposites, electrical testing was performed and variation of the dielectric constant with frequency for the fabricated rGO-PDMS and 1,4-D-rGO-PDMSnanocomposites is shown in Fig. 6.2.5 (a) and variation of loss factor ( $\tan \delta$ ) with frequency is shown in Fig. 6.2.5 (b). A common trend that can be noticed for both the rGO-PDMS and 1,4-D-rGO-PDMS samples in Fig. 6.2.5 (a) by the addition of rGO or 1,4-D-rGO in PDMS matrix and the dielectric constant increases dramatically to that of the host PDMS(dielectric constant in the range of 2.32-2.40) which is consistent with the earlier reported results. Further, compared with the rGO-PDMS nanocomposite(22), a relatively high dielectric constant(38) is achieved

in 1,4-D-rGO-PDMS nanocomposite even at very low vol. % of the filler which is remarkably lower than the percolation threshold as reported earlier. The improvement in the dielectric constant for 1,4-D-rGO-PDMS nanocomposite is mainly attributed to the identical distribution of the rGO in PDMS matrix after chemical treatment with 1,4,D. Secondly, the surface adsorption process has a tendency to make the rGO slightly more nonconductive which can prevent some extent to form the continuous conductive path in the PDMS matrix as a result dielectric constant increases. Thirdly, due to the establishment of microcapacitor networks in the PDMS which consisting of nanoplatelets detached by a thin insulating PDMS layer, the dielectric constant increases drastically in case of 1,4-D-rGO-PDMS nanocomposite. On the other hand, the above-mentioned phenomena are not happening in case of the rGO-PDMSnanocomposite, moreover due to the agglomeration of the rGO in PDMS matrix, the properties of the rGO are not anymore retained like individual rGO sheet in the PDMS matrix. Hence, certainly the dielectric constant of rGO-PDMS is lower than that of the 1,4-D-rGO-PDMSnanocomposite. However, compared to the host PDMS, the dielectric constant is significantly higher for even rGO-PDMS nanocomposite. In addition to this, it is also seen from the Fig. 6.2.5 (a) that dielectric constant of the rGO-PDMS and 1,4-D-rGO-PDMS decreases with a rise in frequency at low frequency range (< 10<sup>4</sup> Hz) whereas it remains stable and becomes constant once frequency increases beyond 10<sup>4</sup>Hz indicating the dielectric constant are nearly independent of frequency and attain a constant value. The frequency dependence of dielectric constant at low frequency can be explained on the basis of Maxwell-Wanger-Sillars(MWS) polarization or interfacial polarization, which occurs due to the addition of charge carriers at an interface between two materials. Though, we have

employed conductive 1,4-D-rGO as filler materials for formation of the nanocomposite, due to very low vol. % of the filler material they never touch to each other as a result insulating spacer layer can exist between them in the PDMS matrix[101-103].

Indeed, due to this reason, the free charges present in graphene pile up at the interface between graphene and space layer which in returns provides strong MWS polarization. Furthermore, chemical treatment by dispersion of rGOin 1,4-Dioxane solvent improves the dissemination of filler in the PDMS matrix which further increases the interface area between 1,4-D-rGO and PDMS and correspondingly enhances the interfacial polarization. Thus the dielectric constant of the fabricated 1,4-D-rGO-PDMS is always higher at low-frequency range in comparison to that of rGO-PDMS nanocomposite as shown in Fig. 6.2.5 (a). In addition to this unusual dielectric response at lower frequency range, it is also seen from the Fig. 6.2.5 (a) that dielectric constant gradually decreases for both the nanocomposites as the frequency increases and becomes stable beyond 10<sup>4</sup> Hz. However, one interesting point to mention here that, the dielectric constant of the 1,4-D-rGO-PDMSnanocomposite is always higher that of rGO-PDMS nanocomposite whether at low or high-frequency range indicating that not only the interfacial polarization but also existence of the spacer layer between the filler and PDMS matrix is responsible for enhancing the dielectric constant in the 1,4-D-rGO-PDMSnanocomposite. This characteristic of nanocomposite may be useful while fabricating capacitance based MEMS and sensors devices [3, 68, 70].

To clearly understand the conductivity of the nanocomposites, four-point probe method was performed at room temperature for both 1,4-D-rGO-PDMS and rGO-PDMS nanocomposites. As expected from the dielectric analysis results, it was found that the

conductivities of the two samples are very low (  $\sigma_{rGO-PDMS} = 5.8 \times 10^{-9} \text{Sm}^{-1}$  and  $\sigma_{1.4-D-rGO-PDMS} = 5.8 \times 10^{-9} \text{Sm}^{-1}$  $PDMS = 8.0 \times 10^{-9} \text{ Sm}^{-1}$ ). Thus, it is apparently understandable from these results that there is a slight enhancement in the electrical conductivity of the 1,4-D-rGO-PDMS nanocomposite that is good deal with the dielectric analysis outcomes as discussed earlier. However, there is a significant progress in the electrical conductivity in comparison to the host PDMS( $\sigma_{PDMS} \sim 10^{-14}~Sm^{-1}$ ). The low conductivity of the 1,4-DrGO-PDMS nanocomposite is found mainly owing to the nonexistence of the conductive path in the insulating PDMS matrix because of very low vol. % of the filler(1,4-D-rGO) was employed in PDMS matrix, which is very lower than the threshold value as reported earlier in the PDMS matrix. The primary intention of choosing very low vol. % of the filler was to retain the mechanical durability and flexibility of the fabricated nanocomposites as a result the electrical conductivity has to be compromised in return. Therefore the overall summary of our work, chemical treatment of rGO with 1,4-Dioxane promoted the uniform distribution of the reduced graphene oxide in the PDMS matrix and also improved the cross-linking bond between the filler and PDMS matrix. Further, due to this uniform distribution of the 1,4-D-rGO in PDMX matrix the fabricated nanocomposites show higher optical transparency, higher thermal stability at high temperature and improved electrical properties. Therefore our experimental work demonstrated a novel optoelectronic nanocomposite material with higher thermally stability at a higher temperature for several applications like Micro-fluidic devices, sensors, actuators, bio-medical devices and Optical-MEMS[9, 13, 104, 105].

#### 6.2.6. I-V analysis

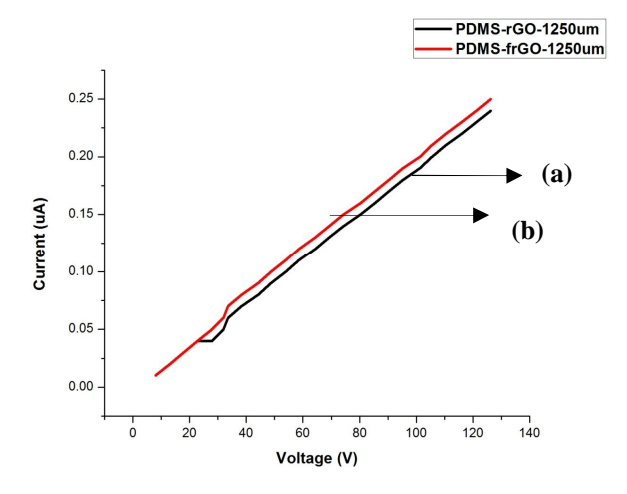


**Fig.6.2.6** IV-analysis shows the (a) PDMS-rGO and (b) PDMS-1,4-Dioxane chemically treated rGOnanocomposites.

From the above figure, IV-analysis shows the PDMS-rGO and PDMS-1,4-Dioxane treated rGO based nanocomposites. We observe the linear curve with voltage (V) vs current ( $\mu Amps$ ).

#### **6.2.7.** UV-visible spectroscopy

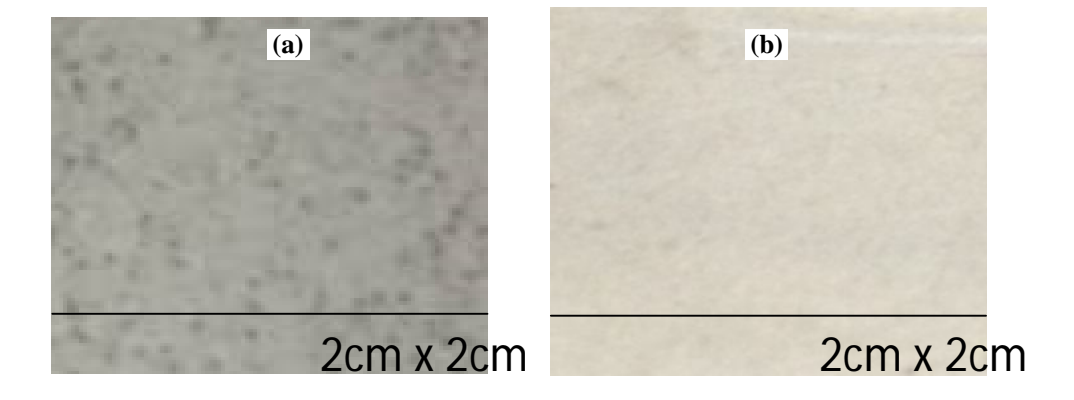
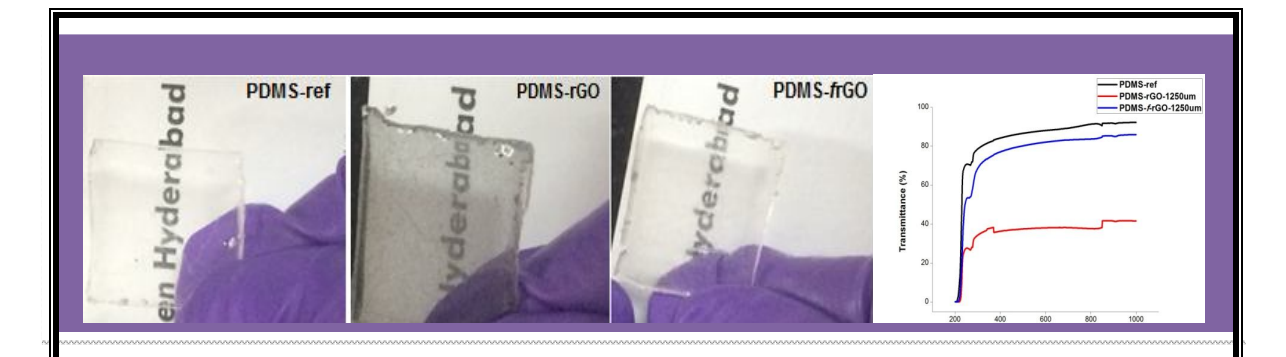


Fig. 6.2.7 Photo image analysis of PDMS-rGO and PDMS-1,4-D-rGO nanocomposites.



**Fig. 6.2.7** Photography images of (a) PDMS-ref (b) PDMS-rGO and (c) PDMS-1,4-D-rGO and (d) UV-visible spectra of PDMS-ref, PDMS-rGO and PDMS-1,4-D-rGOnanocomposites.

Fig. 6.2.7 (a-c) show the photographic images of the PDMS, PDMS-rGO and PDMS-1,4-D-rGO respectively. As shown in Figure 6a-c, the 1, 4-D-rGO based PDMS shows better transparency due to uniform distribution of the 1,4-D-rGO in the polymer matrix. Further, UV-analysis (as shown in Fig. 6.2.7 (d) indicates that 1,4-D-rGO-PDMS nanocomposite shows 82% of optical transparency. The rGO-PDMS nanocomposite shows only ~42% optical transparency. As per existing reported work and as per our knowledge based on the current literature, we have first time reported a PDMS based nanocomposite with 82% optical transparency by incorporating very low vol. % of chemically treated rGO as filler in PDMS matrix [43, 106-109].

#### 6.2.8. Conclusion

In summary, we have demonstrated an optically transparent, thermally stable at a higher temperature and improved electrical properties nanocomposites first time by dispersing uniformly very low vol. % (very lower than percolation threshold) chemically treated reduced graphene(1,4-D-rGO) in silicon elastomer (PDMS). Synthesis of Graphene Oxide (GO) was done by using modified Hummer's method and hydrazine monohydrate was used to reduce GO to reduced graphene oxide. Uniform distribution of the reduced Graphene Oxide(rGO) in PDMS matrix was obtained by chemical treatment with 1,4-

Dioxane, Further, hydroxyl groups those are present after the solvent dispersion process is more responsible for the cross-linking bond between rGO and PDMS matrix as confirmed by FT IR analysis. FT IR, TGA and Raman analysis confirmed the nanocomposite formation successfully. At 0.018 vol. % loading of 1,4-D treated rGO as filler, UV spectroscopy showed 82% optical transparency of the 1,4-D-rGO-PDMS nanocomposites. In addition to this, improved thermal stability at high temperature is achieved for 1,4-D-rGO-PDMS nanocomposite which was confirmed by the TGA analysis. Moreover, 1,4-D-rGO-PDMS nanocomposites exhibited very high-value of dielectric constant (dielectric constant = 38), which 16 times higher than of host PDMS and 1.7 times higher than rGO-PDMS nanocomposites. Furthermore, electrical conductivity studied through the four-point probe and it showed very low conductivity of the 1,4-D-rGO-PDMS nanocomposites. Though, electrical conductivity the fabricated 1,4-D-rGO-PDMS nanocomposite is very low, an improvement in the order of 10<sup>5</sup> as compared to host PDMS is achieved. Therefore, our experimental results indicate that 1-4-D chemical treatment solvent dispersion process improves the uniform distribution of the filler-RGO material in the silicon elastomer and also enhances the cross-linking bond between the filler and PDMS matrix. As a result, the thermal stability and dielectric properties of the nanocomposites can be enhanced to higher order even if at very low vol.% of filler when compared to that of host PDMS material. In addition to this, fabricated nanocomposites showed 82% optical transparency. We believe that our this low cost and facile approach to fabricate these optoelectric nanocomposites can be useful for potential applications in flexible and wearable electronic devices, optical MEMS, sensors, energy storage devices and biomedical devices.

#### **Chapter-7**

#### **Summary and Conclusions**

Studies on the synthesis of GO as reported in the recent literature is that GO is synthesized from the graphite as source material where the oxidation of graphite to graphene oxide is carried out in a consistent process by using Hummers and Modified Hummers method. It has been reported that the GO is the promising material for several applications and a source material to produce the reduced Graphene Oxide (rGO), hence, it is easy and faster to obtain than graphene. In this thesis work, we have studied the preparation of GO by different chemical approaches with a novel improved Hummers method, where no toxic chemicals such as NaNO<sub>2</sub> or NaNO<sub>3</sub> were involved. Moreover, we have established a new facile, cost-effective, commercially viable novel approach of volumetric titration-modified Hummer's method, which is more assuring for the development of Graphene Oxide and subsequently graphene-based composite materials. Our approach indicated that fully oxidized and 2-3 layers graphene oxide can be obtained which is confirmed from the HRTEM, XRD, Raman and UV spectroscopy analysis.

The second part of the thesis, we have studied the dispersion behavior and stability of the GO synthesized by our approach to the fabrication of flexible PDMS based GO/rGO based nanocomposites. Here, the PDMS based flexible nanocomposites were developed by considering three different thicknesses i.e., 500um, 1250um and 2000um by using the mould-casting technique. Two approaches were investigated; firstly, as synthesized RGO was directly employed as filler material and secondly, chemically treated (1,4,D) RGO

was applied as filler materials. The structure and morphology determined by using XRD analysis and the functionality and bonding behavior studied from the FT-IR analysis, the defects or disordered structure determined using Raman analysis, structure and morphology studied from SEM shows the layered structure and TEM analysis results shows the thin graphene sheets obtained from the number of layers from the HR-TEM image analysis and the crystalline studied from the SED pattern of TEM analysis.

From our experimental results, we concluded that by treating RGO with 1,4,D, more uniform distribution of the RGO in PDMS matrix can be obtained with almost 88% as compared to the pure PDMS. Electrical testing results showed that all the samples are insulating in nature. Dielectric measurements results indicated that the dielectric constant can be improved by the addition of chemically treated RGO as compared to the PDMS

Therefore, these thesis research outcomes guided towards to synthesize significantly useful smart materials by incorporating carbon nanomaterials (Graphene) for several applications. However, more challenges are still required to overcome for utilization of these polymer composites for MEMS, sensors, and electronic applications.

host materials. Moreover, the thermal stability of the composite materials can be more

improved by the addition of RGO as confirmed from the thermal analysis results from

TGA.

#### References

- 1. Bokobza, L., Review Mechanical and Electrical Properties of Elastomer Nanocomposites Based on Different Carbon Nanomaterials. Carbon, 2017, 3(10) p. 1-22.
- 2. Masuelli, M.A., Introduction of Fibre-Reinforced Polymers Polymers and Composites: Concepts, Properties and Processes, in Chapter from the book Fiber Reinforced Polymers.
- 3. Castellino Micaela, Chiolerio Alessandro, Shahzad Muhammad Imran, Jagdale Pravin Vitthal, and T.A., Electrical conductivity phenomena in an epoxy resincarbon-based materials composite. Composites: Part A, 61, 2014. p. 108-114.
- 4. Huafeng Yang, Q.Z., Changsheng Shan, Fenghua Li, Dongxue Han, and Li Niu, Stable, Conductive Supramolecular Composite of Graphene Sheets with Conjugated Polyelectrolyte. Langmuir, 2010. 26(9) p. 6708-6712.
- 5. D.R. Paul, L.M. Robeson, Polymer nanotechnology: Nanocomposites. Polymer, 2008. 49 p. 3187-3204.
- 6. Gejo George a, S.B.S.a., Teenu Tomy a, Bincy Akkoli Pottammal a, V.S.a. Alaganandam Kumaran a, Rajmohan Gopimohan a,, and L.R.a. Swaminathan Sivaram b, Thermally conductive thin films derived from defect free graphenenatural rubber latex nanocomposite: Preparation and properties. Carbon, 2017. 119: p. 527-534.
- 7. Xinhong Xiong, Z.W., \* Jingjing Pan, Lulu Xue, Yajun Xu and Hong Chen, A facile approach to modify poly(dimethylsiloxane) surfaces via visible light-induced grafting polymerization. J. Mater. Chem. B, 2015. 3: p. 1-6.
- 8. Y.L.e., A new method for fabricating ultrathin metal films as scratch-resistant flexible transparent electrodes. Journal of Materiomics, 2015. 1: p. 52-59.
- 9. Rasheed Atif, I.S.a.F.I., Mechanical, Thermal, and Electrical Properties of Graphene-Epoxy Nanocomposites—A Review. Polymers, 2016. 8(281): p. 1-37.
- 10. Itoh, S.T.a.T., Novel MEMS Devices Based on Conductive Polymers. The Electrochemical Society Interface, 2012.
- 11. Sadanand Pandey a, b., \*, Highly sensitive and selective chemiresistor gas/vapor sensors based on polyaniline nanocomposite: A comprehensive review. Journal of Science: Advanced Materials and Devices, 2016. xxx: p. 1-23.
- 12. Heonjoo Ha, B.S.M.S., Functional Polymer/Graphene Oxide Composites Synthesis, Characterization and Applications, in Faculty of the Graduate School of The University of Texas at Austin. 2016, The University of Texas at Austin. p. 1-182.
- 13. Velram Balaji Mohan, K.J.D.B., Hybridization of graphene-reinforced two polymer nanocomposites. INTERNATIONAL JOURNAL OF SMART AND NANO MATERIALS, 2016. 7(3): p. 179-201.
- 14. WANG, X.a.S., M., Toughening of polymers by graphene. Nanomaterials and Energy, 2013. 2 (5): p. 265 278.
- 15. Hyunwoo Kim, A.A.A., ‡ and Christopher W. Macosko\*,†, Graphene/Polymer Nanocomposites. Macromolecules, 2010. 43: p. 6515-6530.
- al., D.e., Reduced graphene oxide: a promising electrode material for oxygen electrodes. Journal Of Nanostructure in Chemistry, 2013. 3(49): p. 5.

- 17. Viet Hung Pham, a.S.H.H., a Eui Jung Kim, a Bum Sung Kimb and J.S. Chung\*a, Highly efficient reduction of graphene oxide using ammonia borane†. Chem. Commun., 2013 49: p. 6665-6667.
- 18. Lua, Y.S.A.C., A facile method for the large-scale continuous synthesis of graphene sheets using a novel catalyst. 2013.
- •, M.Y.W.Z.Z.S., X.Z.X.Z.Y.Z. •, and S. Ma, Controllable functionalization and wettability transition of graphene-based films by an atomic oxygen strategy. J Nanopart Res, 2013. 15(1811): p. 14.
- 20. Sudhir Ravula, S.N.B., Ganesh Kamath and Gary A. Baker\*, Ionic liquid-assisted exfoliation and dispersion: stripping graphene and its two-dimensional layered inorganic counterparts of their inhibitions. Nanoscale 2015. 7: p. 4338–4353.
- 21. SURTI, B.A.a.F., Water Soluble Graphene Synthesis. Chem Sci Trans., 2012. 1(3): p. 500-507.
- 22. K.M. Mohsin, Y.M.B.a.A.S., Metallic Single-Walled Carbon Nanotube Temperature Sensor with Self Heating, in Nanosensors, Biosensors, and Info-Tech Sensors and Systems 2014. 2014: Published in SPIE Proceedings Vol. 9060. p. 7.
- 23. By Yanwu Zhu, S.M., Weiwei Cai, Xuesong Li, Ji Won Suk, Jeffrey R. Potts, and a.R.S.R. \*, Graphene and Graphene Oxide: Synthesis, Properties, and Applications. Adv. Mater., 2010. 22: p. 3906–3924.
- 24. Choudhuri, S., BULK SYNTHESIS OF GRAPHENE NANOSHEETS, in Department of Ceramic Engineering. 2012, NATIONAL INSTITUTE OF TECHNOLOGY ROURKELA. p. 35.
- 25. LEILA SHAHRIARY, A.A.A. and U.o.P. Department of Chemistry, Pune, Maharashtra-, Graphene Oxide Synthesized by using Modified Hummers Approach. International Journal of Renewable Energy and Environmental Engineering, 2014. 02(01): p. 58-63.
- 26. Grzegorz Sobon, \* Jaroslaw Sotor,1 Joanna Jagiello,2 Rafal Kozinski,2 Mariusz Zdrojek,3 Marcin Holdynski,4 and J.B. Piotr Paletko, 1 Ludwika Lipinska,2 and Krzysztof M. Abramski1, Graphene Oxide vs. Reduced Graphene Oxide as saturable absorbers for Er-doped passively mode-locked fiber laser. Opt Express, 2012. 20(17): p. 19463-73.
- 27. Tapas Kuilla a, S.B., Dahu Yaoa, Nam Hoon Kimc, and J.H.L. Saswata Bosed, d,\*, Recent advances in graphene based polymer composites. Progress in Polymer Science, 2010. 35: p. 1350-1375.
- 28. Syed Nasimul Alam, N.S., Lailesh Kumar, Synthesis of Graphene Oxide (GO) by Modified Hummers Method and Its Thermal Reduction to Obtain Reduced Graphene Oxide (rGO)\*. Graphene, 2017. 6: p. 1-18.
- 29. Samulski\*, Y.S.a.E.T., Synthesis of Water Soluble Graphene. Nano Lett., 2008. 8(6): p. 1679-1682.
- 30. Theodosis Skaltsas, a.N.K., a Hui-Juan Yan,b Chun-Ru Wang,b Stergios Pispas\*a and a.N. Tagmatarchis\*a, Graphene exfoliation in organic solvents and switching solubility in aqueous media with the aid of amphiphilic block copolymers†. J. Mater. Chem., 2012. 22: p. 21507–21512.
- 31. Vorrada Loryuenyong, 2 Krit Totepvimarn,1 Passakorn Eimburanapravat,1 and a.A.B. Wanchai Boonchompoo, 2, Preparation and Characterization of Reduced

- Graphene Oxide Sheets via Water-Based Exfoliation and Reduction Methods. Advances in Materials Science and Engineering, 2013: p. 5.
- **•**, P.D.M.H.D.A., S.S.G.V.M.S.T.P. •, and A.P.S.K. Das, Percolation network dynamicity and sheet dynamics governed viscous behavior of polydispersed graphene nanosheet suspensions. J Nanopart Res, 2013. 15(2095): p. 1-12.
- 33. Yun-Hong Zhao\*, Z.-K.W., Ya-Fei Zhang†, Shu-Lin Bai, THERMAL CONDUCTIVITY OF 3D GRAPHENE FILLED POLYMER COMPOSITE. 10th International Conference on Composite Science and Technology, 2015: p. 1-8.
- Olfa Kanoun, C.M., Abderahmane Benchiroif, Flexible Carbon Nanotube Films for High Performance Strain Sensors. Sensors, 2014. 14: p. 10042-10071.35. Jinhong Du, H.-M.C., The Fabrication, Properties, and Uses of Graphene/Polymer Composites. Macromol. Chem. Phys., 2012. 213: p. 1060-1077.
- 36. Prusty2, T.K.D.a.S., Graphene-Based Polymer Composites and Their Applications. Polymer-Plastics Technology and Engineering, 2013. 52: p. 319-331.
- 37. Jincheng Liu, Y.W., Shiping Xu, Darren Delai Sun\*, Synthesis of graphene soluble in organic solvents by simultaneous ether-functionalization with octadecane groups and reduction. Materials Letters, 2010. 64: p. 2236-2239.
- 38. Yang Liua, b., Cheng-Lu Lianga, Jing-jie Wub, Rui-Ying Baoa, Guo-Qiang Qia, Yu and W.Y. Wangc, a, Bang-Hu Xiea, and Ming-Bo Yanga, Solvent-Controlled Formation of Reduced Graphite Oxide gel via Hydrogen Bonding. Royal Society of Chemistry, 2016.
- 39. Siyuan Xie, 2 Bowu Zhang,1 ChunleiWang,1 ZiqiangWang,1 Linfan Li,1 and Jingye Li1, Building up Graphene-Based Conductive Polymer Composite Thin Films Using Reduced Graphene Oxide Prepared by The Scientific World Journal, 2013: p. 1-7.
- 40. Yang Qiua, F.C., Robert H. Hurta,b, and Indrek Külaotsa,b,\*, Thermochemistry and kinetics of graphite oxide exothermic decomposition for safety in large-scale storage and processing. Carbon N Y., 2016. 96: p. 20-28.
- 41. M. N. Muralidharan1, Seema Ansari1\*, Thermally reduced graphene oxide/thermoplastic polyurethane nanocomposites as photomechanical actuators. Adv. Mat. Lett., 2013. 4(12): p. 927-932.
- 42. Si Zhou1, A.B., Origin of the Chemical and Kinetic Stability of Graphene Oxide. Scientific reports, 2013. 3(2484): p. 1-7.
- 43. Baoqing Zhang, W.N., Jinming Zhang, Xin Qiao, and J.H. Jun Zhang, Chen-Yang Liu, Stable Dispersions of Reduced Graphene Oxide in Ionic Liquids. Journal of Materials Chemistry, 2010.
- 44. AL., D.G.E., Recent Advances in Fabrication and Characterization of Graphene-Polymer Nanocomposites. Graphene, 2012. 1: p. 30-49.
- 45. I. Tantis, G.C.P., D. Tasis, Functionalized graphene poly(vinyl alcohol) nanocomposites: Physical and dielectric properties. eXPRESS Polymer Letters, 2012. 6(4): p. 283-292.
- 46. Dimitrios G. Papageorgiou, I.A.K., Robert J. Young, Graphene/elastomer nanocomposites. Carbon, 2015. 95: p. 460-484.

- 47. D. Hoang Tien, J.P., Sang A Han, Muneer Ahmad and Yongho Seo, Electrical and Thermal Conductivities of Stycast 1266 Epoxy/Graphite Composites. Journal of the Korean Physical Society, 2011. 59(4): p. 2760-2764.
- 48. Jeffrey R. Potts a, D.R.D.b., Christopher W. Bielawski b, Rodney S. Ruoff a, Graphene-based polymer nanocomposites. Polymer, 2011. 52: p. 5-25.
- 49. Wayne E. Jones Jr. 1, Jasper Chiguma 2, Edwin Johnson 1, Ashok Pachamuthu 3 and and D.S. 3, Electrically and Thermally Conducting Nanocomposites for Electronic Applications. Materials, 2010. 3: p. 1478-1496.
- 50. 1Sangamesha, M.A., 1K. Pushpalatha and 2G.L. Shekar, STRUCTURAL AND OPTICAL STUDIES OF CONDUCTING PANI/Cus NANOCOMPOSITES ON NANOCRYSTALLINE ZINC-OXIDE THIN FILM. American Journal of Nanotechnology, 2014. 5(1): p. 3-11.
- 51. Sangamesha, M.A., K. Pushpalatha and G.L. Shekar, Structural and optical studies of conducting PANI/CuS Nanocomposites on Nanocrystalline Zinc-Oxide Thin film. American Journal of Nanotechnology, 2014. 5(1): p. 3-11.
- 52. P. Noorunnisa Khanam, D.P.a.M.A.A.-M. and Springer, Electrical Properties of Graphene Polymer Nanocomposites, in Graphene-Based Polymer Nanocomposites in Electronics, K.K.S.e. al., Editor. 2015, Springer International Publishing Switzerland. p. 1-24.
- 53. Making flexible molds with PDMS.
- 54. Jingjing Wang, X.N., Boyi Jiang, Bin Huang, Jun Wang, Weinan Li, Hui Zhou, Hui Li, Fangmin Sun, and G.Z. Jinyong Zhang, Jinhui Li, Tianzhun Wu, Yan Chen\*, Lei Wang\*, Development of CNT/Graphene/PDMS Stretchable and Conductive Electrode for Wearable ECG Monitoring.
- 55. Dongzhi Chen a, Fengxiang Chen a, b, Xiaoyun Hu c, Hongwei Zhang a, Xianze Yin a, and Y.Z. a, Thermal stability, mechanical and optical properties of novel addition cured PDMS composites with nano-silica sol and MQ silicone resin. Composites Science and Technology, 2015. 117: p. 307-314.
- 56. Nicolas Tiercelin1, Philippe Coquet1,3, Ronan Sauleau2, and a.H.F. Vincent Senez1, Polydimethylsiloxane membranes for millimeter-wave planar ultra flexible antennas. J. Micromech. Microeng., 2006. 16: p. 2389–2395.
- 57. Josef Osicka 1, M.I.c., Miroslav Mrlik 1, Antonín Mina rík 1, Vladimir Pavlinek 1 and and Jaroslav Mosná cek 2, The Impact of Polymer Grafting from a Graphene Oxide Surface on Its Compatibility with a PDMS Matrix and the Light-Induced Actuation of the Composites. Polymers, 2017. 9(264): p. 1-14.
- 58. Neng-Jian Huang, a.J.Z., a Guo-Dong Zhang,\*a Li-Zhi Guan,a Shi-Neng Li,ab and L.Z.a.L.-C.T. \*a, Efficient interfacial interaction for improving mechanical properties of polydimethylsiloxane nanocomposites filled with low content of graphene oxide nanoribbons†. RSC Adv.,, 2017. 7: p. 22045-22053.
- 59. Luiz G. P. Martinsa, Yi Songb,1, Tingying Zengb, Mildred S. Dresselhausb,c, Jing Kongb,2, and Paulo T. Araujob,d,2, Direct transfer of graphene onto flexible substrates. PNAS Early Edition: p. 1-6.
- 60. David W. Johnson, B.P.D., Karl S. Coleman □, A manufacturing perspective on graphene dispersions. Current Opinion in Colloid & Interface Science, 2015. 20: p. 367–382.

- 61. Technology, t.I.C.o.C.S.a., Nanoparticle doped Electrically-conducting Polymers for Flexible Nano-Micro Systems 10th International Conference on Composite Science and Technology, 2012.
- 62. Le Cai, J.L., Pingshan Luan, Haibo Dong, Duan Zhao, Qiang Zhang, Xiao Zhang, Min Tu, Qingsheng Zeng, Weiya Zhou, Sishen Xie., Highly Transparent and Conductive Stretchable Conductors Based on Hierarchical Reticulate Single-Walled Carbon Nanotube Architecture. Advanced functional materials, 2012. 22: p. 5238-5244.
- 63. Sungjin Park, J.A., Inhwa Jung, Richard D. Piner, Sung and X.L. Jin An, Aruna Velamakanni, and Rodney S. Ruoff, Colloidal Suspensions of Highly Reduced Graphene Oxide in a Wide Variety of Organic Solvents. Nano Lett., 2009. 9(4): p. 1593-1597.
- 64. Chiara Acquarelli 1, \*, Licia Paliotta 1,2, Alessio Tamburrano 1,2, Giovanni De Bellis 1,2 and and Maria Sabrina Sarto 1, Electro-Mechanical Properties of Multilayer Graphene-Based Polymeric Composite Obtained through a Capillary Rise Method. Sensors, 2016. 16(1780): p. 1-15.
- 65. Dilini Galpaya, M.W., Meinan Liu, Nunzio Motta, Eric Waclawik, Cheng Yan\*, Recent Advances in Fabrication and Characterization of Graphene-Polymer Nanocomposites. Graphene, 2012. 1: p. 30-49.
- 66. KUO, A.C.M., Poly(dimethylsiloxane). 1999, Polymer Data Handbook: Oxford University Press. p. 411-435.
- 67. Viet Hung Pham, T.V.C., Seung Hyun Hur, Eun Woo Shin, Jae Seong Kim, and E.J.K. Jin Suk Chung \*, Fast and simple fabrication of a large transparent chemically-converted graphene film by spray-coating. Carbon, 2010. 48: p. 19 4 5 –1 9 5 1.
- 68. Peixuan Wu, M.Z., Han Wang, Hui Tang, Patrick Bass, and Lin Zhang, Effect of coupling agents on the dielectric properties and energy storage of Ba0.5Sr0.5TiO3/P(VDF-CTFE) nanocomposites. AIP Advances, 2017. 7(075210): p. 1-9.
- 69. Ping Du, X.L., and Xin Zhang, DIELECTRIC CONSTANTS OF PDMS NANOCOMPOSITES USING CONDUCTING POLYMER NANOWIRES. IEEE, 2011.
- 70. Shail K. Gupta, K.N.P., Vishal Verma, Smita Mathur, and and V. Kumar\*, Dielectric Properties of Polymethylmethacrylate/Barium Titanate (PMMA/BaTiO3) Nanocomposites. Applied Polymer Composites, 2013. 1(1): p. 47-56.
- 71. I. Latif, T.B.A., Ammar H. Al-Dujaili\*, Low Frequency Dielectric Study of PAPA-PVA-GR Nanocomposites. Nanoscience and Nanotechnology, 2012. 2(6): p. 190-200.
- 72. Highly Conductive and Stretchable Polymer Composites Based on Graphene/MWCNT Network. The Royal Society of Chemistry, 2013.
- 73. Cheol-Hwan Park, 2, \* Feliciano Giustino†,1, 2 Marvin L. Cohen,1, 2 and Steven G. Louie1, 2, Electron-Phonon Interactions in Graphene, Bilayer Graphene, and Graphite. Nano Lett., 2008. 8: p. 6.
- 74. C. N. R. Rao, U.M., and H. S. S. Ramakrishna Matte, Synthesis, Characterization, and Selected Properties of Graphene. 2013: p. 1-48.

- 75. Clinton Young, L.D., MEMS Graphene Strain Sensor, in Department of Electrical and Computer Engineering. Iowa State University: Ames, IA. p. 1-28.
- 76. Swisher, S.L., Synthesis, Characterization, and Applications of Solution-processed Nanomaterials: From Thin-film Transistors to Flexible "Smart Bandages", in Engineering Electrical Engineering and Computer Sciences. 2016, University of California: Berkeley.
- 77. Wang, N., Functionalization and Characterization of Carbon-based Nanomaterials, in Department of Microtechnology and Nanoscience (MC2). 2015, CHALMERS UNIVERSITY OF TECHNOLOGY: BioNano Systems Laboratory. p. 1-58.
- 78. Seema Ansari , C.R.M.N.M., Photomechanical Characteristics of Thermally Reduced Graphene Oxide Polydimethylsiloxane Nanocomposites. Polymer-Plastics Technology and Engineering, 2013. 52: p. 1604–1610.
- 79. Zarandi, H.A.B.a.M.B., Effects of Annealing and Thickness on the Structural and Optical Properties of Crystalline ZnS Thin Films Prepared by PVD Method. International Journal of Optics and Photonics (IJOP), 2011. 5(2): p. 1-8.
- 80. N C S Vieira1, J Borme1, G Machado Jr.1, F Cerqueira2, P P Freitas1, V Zucolotto3, N M R Peres2 and P Alpuim1,2, Graphene field-effect transistor array with integrated electrolytic gates scaled to 200 mm.
- 81. James P. Lewicki1\*, P.W.B., Mathew W. C. Robinson2 and Robert S. Maxwell1, A Dielectric Relaxometry Study of Segmental Dynamics in PDMS/Boron Composite and Hybrid Elastomers, in polymer. 2013, LAWRENCE LIVERMORE NATIONAL LABORATORY.
- 82. Shuying Wu, R.B.L., † Jin Zhang,‡ Kamran Ghorbani,† Xuehua Zhang,§ Adrian P. Mouritz,† 4 Anthony J. Kinloch,⊥ and Chun H. Wang†\*, Strain Sensors with Adjustable Sensitivity by Tailoring the Microstructure of 2 Graphene Aerogel/PDMS Nanocomposites. ACS Applied Materials and Interfaces, 2016.
- 83. Edreese H. Alsharaeh 1, Ali A. Othman 1 and Mohammad A. Aldosari 2, Microwave Irradiation Effect on the Dispersion and Thermal Stability of RGO Nanosheets within a Polystyrene Matrix. Materials, 2014: p. 5212-5224.
- 84. Hong Yan, a.H.Z., a Qun Ye,a Xiaobai Wang,a Ching Mui Cho,a and A.Y.X.T.a.J. Xu\*ab, Engineering polydimethylsiloxane with twodimensional graphene oxide for an extremely durable superhydrophobic fabric coating†. RSC Adv., 2016. 6: p. 66834–66840.
- 85. Iti Srivastava, R.J.M., 1 Zhong-Zhen Yu,3 Linda Schadler,1,a and and a. Nikhil Koratkar2, Raman study of interfacial load transfer in graphene nanocomposites. APPLIED PHYSICS LETTERS, 2011. 98(063102): p. 1-4.vand Candido Fabrizio Pirri1,2, Evaluation of different conductive nanostructured particles as filler in smart piezoresistive composites. Nanoscale Research Letters, 2012. 7(327): p. 1-5.
- 87. Laura J Romasanta, M.H., Miguel A López-Manchado and Raquel Verdejo\*, Functionalised graphene sheets as effective high dielectric constant fillers. Nanoscale Research Letters, 2011. 6(508): p. 6.
- 88. Gregory J. Silverberg, P.P., †,‡ and Chad D. Vecitis\*,†, Controlling Self-Assembly of Reduced Graphene Oxide at the Air- Water Interface: Quantitative

- Evidence for Long-Range Attractive and Many-Body Interactions. ACS Appl. Mater. Interfaces, 2015. 7: p. 3807-3815.
- 89. Ye Ji Noh1, H.-I.J., Jaesang Yu1, Soon Hyoun Hwang2, Sungho Lee1, Cheol Ho Lee1, Seong Yun Kim1,3\* and J.R. Youn2\*, Ultra-high dispersion of graphene in polymer composite via solvent free fabrication and functionalization. 2015. p. 1-7.
- 90. Eda, G.C., M., Graphene-based Composite Thin Films for Electronics. J. of Nano Letters, 2009. 9: p. 814–818.
- 91. Terzopoulou, Z.K.G.Z.B., D.N. , Recent Advances in Nanocomposite Materials of Graphene Derivatives with Polysaccharides. Materials,, 2015. 8(2): p. 652–683.
- 92. Zhang, W.L.P., B.J.; Choi,H.J., Colloidal Graphene Oxide/Polyaniline Nanocomposite and Its Electrorheology. . Chem. Comm., 2010. 46(30): p. 5596-8.
- 93. John S. F. Barrett, A.A.A.a.F.S., Poly(hydroxyalkanoate) Elastomers and Their GrapheneNanocomposites. Macromolecules, 2014. 47: p. 3926-3941.
- 94. Kim, I.H.J., Y.G. J. , Polylactide/exfoliated Graphite Nanocomposites with Enhanced Thermal Stability, Mechanical Modulus, and Electrical Conductivity. Polym. Sci. Part B Polym. Phys., , 2010. 48: p. 850.
- 95. Dong Seok Shin, a.H.G.K., ‡b Ho Seon Ahn,‡c Hu Young Jeong,d, e.D.O. Youn-Jung Kim, a N. Tsogbadrakh,f Han-Bo-Ram Lee\*b, and a.B.H. Kim\*a, Distribution of oxygen functional groups of graphene oxide obtained from low-temperature atomic layer deposition of titanium oxide†. RSC Adv.,, 2017. 7(13979): p. 1-6.
- 96. Xu, Z.G., C., In Situ Polymerization Approach of Graphene-Reinforced Nylon-6 Composites. Macromolecules, 2010. 43(16): p. 6716-23.
- 97. Xingcheng Xiao, a.T.X.a.a.Y.-T.C., Self-healable graphene polymer composites†. J. Mater. Chem., , 2010. 20: p. 3508–3514.
- 98. B'elanger, B.D.O.a.D., Synthesis and characterization of sulfophenylfunctionalized reduced graphene oxide sheets†. RSC Adv.,, 2017. 7: p. 27224–27234.
- 99. Nantao Hu, R.G., Yanyan Wang, Yanfang Wang, Jing Chai, and E.S.-W.K. Zhi Yang\*, and Yafei Zhang\*, The Preparation and Characterization of Non-Covalently Functionalized Graphene. J. Nanosci. Nanotechnol., 2012. 12 (1): p. 99–104.
- 100. Yuxi Xu, H.B., Gewu Lu, Chun Li,\* and Gaoquan Shi\*, Flexible Graphene Films via the Filtration of Water-Soluble Noncovalent Functionalized Graphene Sheets. J. AM. CHEM. SOC. , 2008. 130: p. 5856–5857.
- 101. Dang, Z.M.W., L.;Yin,Y.;Zhang, Q.; Lei, Q., Giant Dielectric Permittivities in Functionalized Carbon-Nanotube/Electroactive-Polymer Nanocomposites. Adv. Mater., 2007. 19: p. 852-857.
- 102. Das, B.V., R.;Rout, C.S.; Rao., Changes in the Electronic Structure and Properties of Graphene Induced by Molecular Charge-transfer. Chemm. Commun., 2008: p. 5155-5157.
- 103. Virendra Singh, Daeha Joung, Lei Zhai, Soumen Das, and Saiful I. Khondaker, Sudipta Seal, Graphene based materials: Past, present and future. Progress in Materials Science 2011 [cited 56; 1178-1271].

- Muhammad Taha Jilani, M.Z.u.R., Abid Muhammad Khan, and S.M.A. Muhammad Talha Khan, A Brief Review of Measuring Techniques for Characterization of Dielectric Materials. International Journal of Information Technology and Electrical Engineering, 2012. 1(1): p. 1-5.
- I. Latif, T.B.A., Ammar H. Al-Dujaili, Low Frequency Dielectric Study of PAPA-PVA-GR Nanocomposites. Nanoscience and Nanotechnology, 2012. 2(6): p. 190-200.
- 106. Brahim Aïssa 1, Nasir K. Memon 1, Adnan Ali 1 and Marwan K. Khraisheh 1, Recent progress in the growth and applications of graphene as a smart material: a review. Front. Mater., 2015: p. 1-19.
- 107. Héctor A. Becerril, J.M., Zunfeng Liu, Randall M. Stoltenberg, Zhenan Bao, and Yongsheng Chen, Evaluation of Solution-Processed Reduced Graphene Oxide Films as Transparent Conductors. ACS Nano., 2008. 2(3): p. 463–470.
- 108. Sasha Stankovich a, D.A.D.a., Richard D. Piner a, Kevin A. Kohlhaas a,, Y.J.c. Alfred Kleinhammes c, Yue Wu c,, and SonBinh T. Nguyen b, Rodney S. Ruoff a, Synthesis of graphene-based nanosheets via chemical reduction of exfoliated graphite oxide. Carbon, 2007. 45 p. 1558–1565.
- 109. F. Bonaccorso, z.S., t. Hasan and a. C. Ferrari, graphene photonics and optoelectronics. nature photonics, 2010. 4: p. 611-622.

# Synthesis and Characterization of Graphene oxide by a Novel Approach (Volumetric Titration Method) and Fabrication of GO/rGO-PDMS Nanocomposite for Flexible Sensors

by Gunda Rajitha

**Submission date:** 21-Mar-2018 04:39PM (UTC+0530)

**Submission ID: 933766380** 

File name: Rajitha\_PhD\_Thesis\_16MAR18.pdf (14.22M)

Word count: 18605 Character count: 98896 Synthesis and Characterization of Graphene oxide by a Novel Approach (Volumetric Titration Method) and Fabrication of GO/rGO-PDMS Nanocomposite for Flexible Sensors

#### ORIGINALITY REPORT

SIMILARITY INDEX

INTERNET SOURCES

 $\mathbf{Q}_{\%}$ 

**PUBLICATIONS** 

STUDENT PAPERS

#### **PRIMARY SOURCES**

Peixuan Wu, Min Zhang, Han Wang, Hui Tang, Patrick Bass, Lin Zhang. "Effect of coupling agents on the dielectric properties and energy storage of Ba Sr TiO /P(VDF-CTFE) nanocomposites ", AIP Advances, 2017

Publication

www.mdpi.com Internet Source

1%

Rajitha Gunda, Buchi Suresh Madireddy, Raj Kishora Dash. "Synthesis of graphene oxide and reduced graphene oxide using volumetric method by a novel approach without NaNO2 or NaNO3", Applied Nanoscience, 2018 Publication

Cai, Le, Jinzhu Li, Pingshan Luan, Haibo Dong, Duan Zhao, Qiang Zhang, Xiao Zhang, Min Tu, Qingsheng Zeng, Weiya Zhou, and Sishen Xie. "Highly Transparent and Conductive Stretchable Conductors Based on Hierarchical

%

# Reticulate Single-Walled Carbon Nanotube Architecture", Advanced Functional Materials, 2012.

Publication

5	thescipub.com Internet Source	<1%
6	Skaltsas, Theodosis, Nikolaos Karousis, Hui- Juan Yan, Chun-Ru Wang, Stergios Pispas, and Nikos Tagmatarchis. "Graphene exfoliation in organic solvents and switching solubility in aqueous media with the aid of amphiphilic block copolymers", Journal of Materials Chemistry, 2012.	<1%
7	www.nature.com Internet Source	<1%
8	Potts, J.R "Graphene-based polymer nanocomposites", Polymer, 20110107  Publication	<1%
9	Submitted to Deakin University Student Paper	<1%
10	Pham, V.H "Fast and simple fabrication of a large transparent chemically-converted graphene film by spray-coating", Carbon, 201006  Publication	<1%

11	Shuying Wu, Raj B. Ladani, Jin Zhang, Kamran Ghorbani, Xuehua Zhang, Adrian P. Mouritz, Anthony J. Kinloch, Chun H. Wang. "Strain Sensors with Adjustable Sensitivity by Tailoring the Microstructure of Graphene Aerogel/PDMS Nanocomposites", ACS Applied Materials & Interfaces, 2016 Publication	<1%
12	Papageorgiou, Dimitrios G., Ian A. Kinloch, and Robert J. Young. "Graphene/elastomer nanocomposites", Carbon, 2015.  Publication	<1%
13	www.nano.if.pw.edu.pl Internet Source	<1%
14	mnm.embs.org Internet Source	<1%
15	Noh, Ye Ji, Han-Ik Joh, Jaesang Yu, Soon Hyoun Hwang, Sungho Lee, Cheol Ho Lee, Seong Yun Kim, and Jae Ryoun Youn. "Ultra- high dispersion of graphene in polymer composite via solvent free fabrication and functionalization", Scientific Reports, 2015. Publication	<1%
16	Flavio Pendolino, Emilio Parisini, Sergio Lo	_11

Flavio Pendolino, Emilio Parisini, Sergio Lo Russo. "Time-Dependent Structure and Solubilization Kinetics of Graphene Oxide in

<1%

#### Methanol and Water Dispersions", The Journal of Physical Chemistry C, 2014

Publication

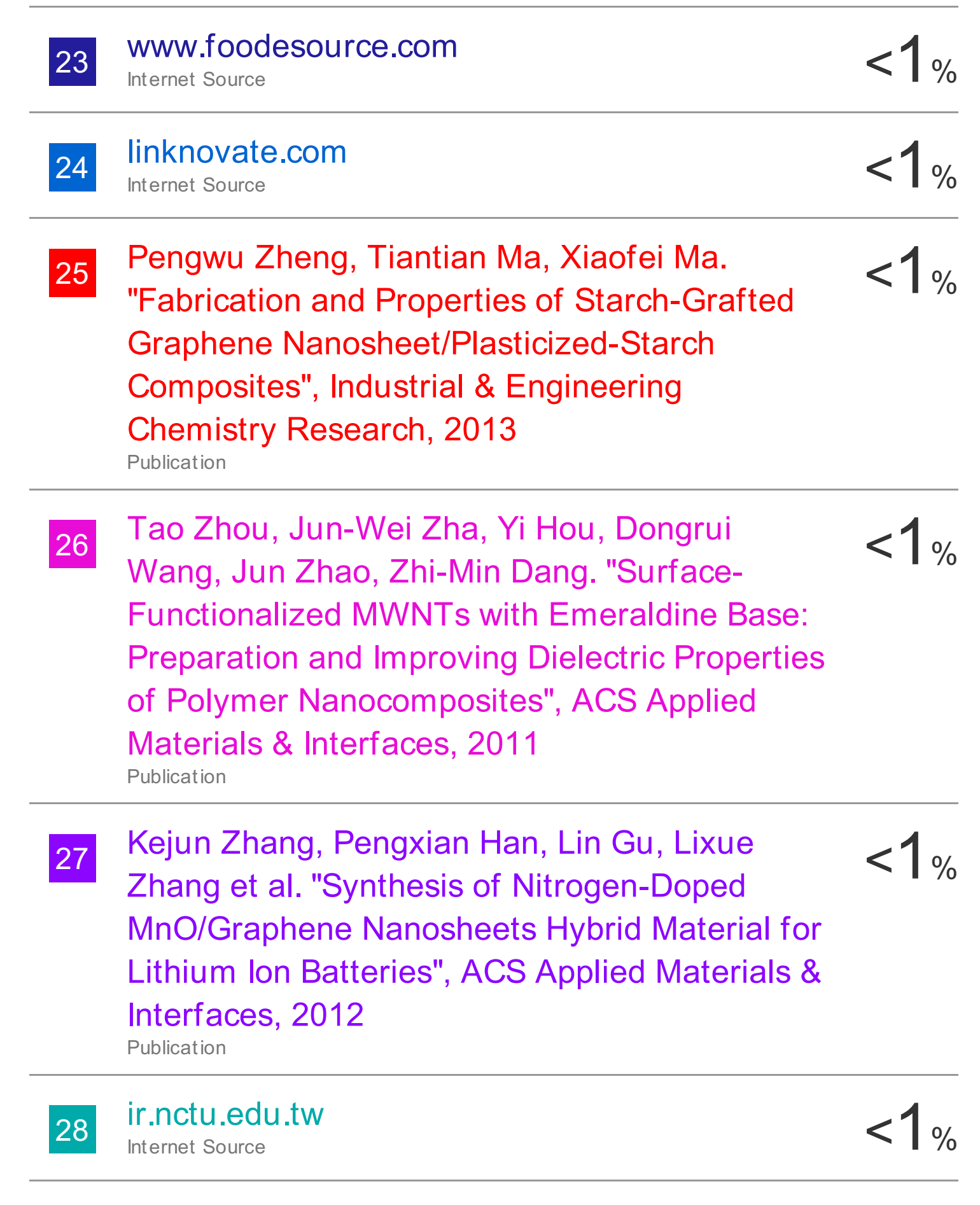
Zheng Li, Zheng Liu, Haiyan Sun, Chao Gao. <1% 17 "Superstructured Assembly of Nanocarbons: Fullerenes, Nanotubes, and Graphene", Chemical Reviews, 2015 Publication <1% Carotenuto, G, V Romeo, I Cannavaro, D 18 Roncato, B Martorana, and M Gosso. "Graphene-polymer composites", IOP Conference Series Materials Science and Engineering, 2012. Publication www.askiitians.com <1% 19 Internet Source <1% Pedro Ruiz-Compean, Joanne Ellis, João 20 Cúrdia, Richard Payumo, Ute Langner, Burton Jones, Susana Carvalho. "Baseline evaluation of sediment contamination in the shallow coastal areas of Saudi Arabian Red Sea",

Publication

www.academicconcepts.net Internet Source

Marine Pollution Bulletin, 2017

Environmental Science and Engineering, 2014. **Publication** 



29	PEDOT: PSS/ graphene oxide nanocomposites for perovskit", Polymer Engineering and Science, June 2017 Issue	<1%
30	Zhou, Wenying, Ying Gong, Litao Tu, Li Xu, Wei Zhao, Jiangtao Cai, Yating Zhang, and Anning Zhou. "Dielectric properties and thermal conductivity of core-shell structured Ni@NiO/poly(vinylidene fluoride) composites", Journal of Alloys and Compounds, 2017. Publication	<1%
31	"Recent Trends in Materials Science and Applications", Springer Nature, 2017 Publication	<1%
32	Submitted to Mahidol University Student Paper	<1%
33	Yongzheng Pan, Hongqian Bao, Lin Li. "Noncovalently Functionalized Multiwalled Carbon Nanotubes by Chitosan-Grafted Reduced Graphene Oxide and Their Synergistic Reinforcing Effects in Chitosan Films", ACS Applied Materials & Interfaces, 2011 Publication	<1%
34	Yuan, J "Preparation and properties of Nafion^(R)/hollow silica spheres composite	<1%

#### membranes", Journal of Membrane Science, 20081201

Publication

Shuying Wu, Jin Zhang, Raj B. Ladani, Anil R. <1% 35 Ravindran, Adrian P. Mouritz, Anthony J. Kinloch, Chun H. Wang. "Novel Electrically Conductive Porous PDMS/Carbon Nanofiber Composites for Deformable Strain Sensors and Conductors", ACS Applied Materials & Interfaces, 2017 Publication Submitted to University of Pune <1% 36 Student Paper www.godac.jamstec.go.jp 37 Internet Source <1% Elham Ghavidel, Amir Hossein Sari, Davoud 38 Dorranian. "Experimental investigation of the effects of different liquid environments on the graphene oxide produced by laser ablation method", Optics & Laser Technology, 2018 Publication A. Pricilla Jeyakumari, S. Manivannan, S. Dhanuskodi. "Spectral and optical studies of 2-

A semiorganic nonlinear optical material",

Spectrochimica Acta Part A: Molecular and

Biomolecular Spectroscopy, 2007

amino-5-nitropyridinium dihydrogen phosphate:

40	"Research Data from UGC DAE Consortium of Scientific Research Update Understanding of Molecular Struc", Science Letter, April 15 2016 Issue Publication	<1%
41	www.lacie.com Internet Source	<1%
42	Rao, C N R, K S Subrahmanyam, H S S Ramakrishna Matte, B Abdulhakeem, A Govindaraj, Barun Das, Prashant Kumar, Anupama Ghosh, and Dattatray J Late. "A study of the synthetic methods and properties of graphenes", Science and Technology of Advanced Materials, 2010.  Publication	<1%
43	www.ise.ufl.edu Internet Source	<1%
44	repositorium.sdum.uminho.pt Internet Source	<1%
45	Sunghun Cho, Jun Seop Lee, Jyongsik Jang. " Poly(vinylidene fluoride)/NH -Treated Graphene Nanodot/Reduced Graphene Oxide Nanocomposites with Enhanced Dielectric Performance for Ultrahigh Energy Density Capacitor ", ACS Applied Materials &	<1%

Publication

46	Yu, R. Spiesz, P. Brouwers, H.J.H  "Development of ultra-high performance fibre reinforced concrete (UHPFRC): Towards an efficient utili", Construction and Building Materials, March 15 2015 Issue  Publication	<1%
47	railwayengineering.in Internet Source	<1%
48	nssdcftp.gsfc.nasa.gov Internet Source	<1%
49	koreancircj.kr Internet Source	<1%
50	Singh, V "Graphene based materials: Past, present and future", Progress in Materials Science, 201110  Publication	<1%
51	Jindu Huang, Qianqiu Tang, Weibin Liao, Gengchao Wang, Wei Wei, Chunzhong Li. "Green Preparation of Expandable Graphite and Its Application in Flame-Resistance Polymer Elastomer", Industrial & Engineering Chemistry Research, 2017 Publication	<1%

53

Paul M. Dinakaran and S. Kalainathan.
"Nucleation Kinetics, Chemical Etching, Sem,
Edax And Mechanical Studies Of 3-Methyl 4Methoxy 4-Nitrostilbene (MMONS): A Potential
Nonlinear Optical Crystal", International Journal
of ChemTech Research, 2013.

< 1 %

Publication

54

Taichi Matsumoto. "Synthesis of Rhodamine B-Doped and Monodispersed Spherical Particles of Polyorganosiloxane Using a W/O Emulsion", Journal of the American Ceramic Society, 12/2005

<1%

Publication

55

YinHua Lei. "Hybrid microsystem with functionalized silicon substrate and PDMS sample operating microchannel: A reconfigurable microfluidics scheme", Science China Technological Sciences, 08/2010

<1%

56

Lyaysan Amirova, Albina Surnova, Dinar Balkaev, Delus Musin, Rustem Amirov, Ayrat M. Dimiev. "Homogeneous Liquid Phase Transfer of Graphene Oxide into Epoxy Resins", ACS Applied Materials & Interfaces, 2017

<1%

<1% Mandal, Tapas K., and Deepak Kunzru. 57 "Catalytic gasification of coke during the pyrolysis of n-hexane", Industrial & Engineering Chemistry Process Design and Development, 1986. Publication festvox.org <1% 58 Internet Source S. Takamatsu, T. Itoh. "Novel MEMS Devices 59 Based on Conductive Polymers", Interface magazine, 2012 Publication Larisika, Melanie, Jingfeng Huang, Alfred Tok, <1% 60 Wolfgang Knoll, and Christoph Nowak. "An improved synthesis route to graphene for molecular sensor applications", Materials Chemistry and Physics, 2012. Publication Gokulakrishnan, N.. "Effective uptake of <1% 61 decontaminating agent (citric acid) from aqueous solution by mesoporous and microporous materials: An adsorption process", Chemosphere, 200604 Publication

McVeigh, C.. "An interactive micro-void shear localization mechanism in high strength steels",

# Journal of the Mechanics and Physics of Solids, 200702

Publication

63	NAUMAN ALI. "EFFECTS OF THE REDUCING AGENTS ON MORPHOLOGIES OF GOLD NANOPARTICLES IN POLY(STYRENE-B-4-VINYLPYRIDINE) MICELLES", International Journal of Modern Physics B, 2010 Publication	<1%
64	Dimiev, Ayrat M., and James M. Tour. "Mechanism of Graphene Oxide Formation", ACS Nano, 2014. Publication	<1%
65	Jong Hun Kang, Taehoon Kim, Jaeyoo Choi, Jisoo Park et al. "Hidden Second Oxidation Step of Hummers Method", Chemistry of Materials, 2016 Publication	<1%
66	Varrla Eswaraiah, Venkataraman Sankaranarayanan, Sundara Ramaprabhu. "Graphene-Based Engine Oil Nanofluids for Tribological Applications", ACS Applied Materials & Interfaces, 2011 Publication	<1%

Exclude quotes On Exclude matches < 5 words

Exclude bibliography On